Research Report
KTC-99-17

Seismic Evaluation of the US41 Southbound Bridge over the Ohio River at Henderson, KY
(KYSPR 96-173)

by

Issam E. Harik
Professor of Civil Engineering and Head, Structures Section,
Kentucky Transportation Center

K. Vasudevan
Visiting Professor, Kentucky Transportation Center

Chelliah Madasamy
Visiting Professor, Kentucky Transportation Center

Denglin Chen
Research Assistant, Dept. of Civil Engineering

Leonong Zhou
Formerly Visiting Professor, Kentucky Transportation Center

Kevin Sutterer
Assistant Professor, Department of Civil Engineering

Ron Street
Assistant Professor, Department of Geological Sciences

and

David L. Allen
Transportation Engineer, Kentucky Transportation Center

Kentucky Transportation Center
College of Engineering, University of Kentucky

in cooperation with

Transportation Cabinet
Commonwealth of Kentucky

and

Federal Highway Administration
U.S. Department of Transportation

November 1999

Commonwealth of Kentucky
Transportation Cabinet
Frankfort, Kentucky 40622

James C. Codell, III
Secretary of Transportation

E. Jeffrey Mosley
Deputy Secretary

Paul E. Patton
Governor

December 20, 2000

Mr. Jose M. Sepulveda
Division Administrator
Federal Highway Administration
330 West Broadway
Frankfort, KY 40601

Subject:
- Implementation Statement for Final Report entitled "Seismic Evaluation of the US41 Southbound bridge over the Ohio River at Henderson, KY"
- Study number: KYSPR 96-173
- Study title: "Seismic Rating and Evaluation of Highway Structures"

Dear Mr. Sepulveda:

This study was conducted to seismically evaluate the US41 Southbound bridge over the Ohio River at Henderson, KY for a projected 50-year earthquake event. The objective set forth has been achieved by conducting field testing, computer modeling, and dynamic analysis.

The results of this study show that the superstructure of the main bridge will withstand the 50-year earthquake event without any damage. All supports on the piers of the main bridge, and ten out of twelve supports having fixed bearings on the approach spans require retrofit. This retrofit can be provided by additional anchor bolts in order to prevent shear failure of the existing anchor bolts, or by replacing those bearings with seismic isolation bearings. Potential loss of span exists at three out of twenty-five supports having expansion bearings on the approach spans, and the loss of span can be prevented by providing cable restrainers or replacing the existing expansion bearings with elastomeric bearings.

Sincerely,

J. M Yowell, P.E.
State Highway Engineer

JMY/JLC/dp

c: John Carr

EDUCATION PAYS

Technical Report Documentation Page

1. Report No.	2. Government Accession No.	3. Recipient's Catalog No.
KTC-99-17		

4. Title and Subtitle

SEISMIC EVALUATION OF THE US41 SOUTHBOUND BRIDGE OVER THE OHIO RIVER AT HENDERSON, KY

(KYSPR 96-173)

5. Report Date
November 1999

6. Performing Organization Code

7. Author(s): I.E. Harik, K. Vasudevan, C.M. Madasamy, D. Chen, L. Zhou, K. Sutterer, R. Street and D. Allen

8. Performing Organization Report No.
KTC-99-17

9. Performing Organization Name and Address

Kentucky Transportation Center
College of Engineering
University of Kentucky
Lexington, Kentucky 40506-0281

10. Work Unit No. (TRAIS)

11. Contract or Grant No.
KYSPR 96-173

13. Type of Report and Period Covered
Final

12. Sponsoring Agency Name and Address

Kentucky Transportation Cabinet
State Office Building
Frankfort, Kentucky 40622

14. Sponsoring Agency Code

15. Supplementary Notes
Prepared in cooperation with the Kentucky Transportation Cabinet and the U.S. Department of Transportation, Federal Highway Administration.

16. Abstract

This report presents the seismic evaluation of the US41 Southbound bridge over the Ohio River connecting Evansville, Indiana and Henderson, Kentucky. The main bridge is a four-span cantilever through-truss type. The approach bridge has 9 spans on the Evansville, IN side and 20 spans on the Henderson, KY side. Although this bridge has not yet been subjected to a moderate or major earthquake, it is situated within the influence of the New Madrid and Wabash Valley Seismic Zones.

The seismic evaluation program consisted of field testing and seismic response analysis. The modal properties of the main bridge were determined through field testing, and were used to calibrate a three dimensional finite element model. The finite element model was then subjected to the acceleration time histories of the 50-year earthquake event. Stresses and displacements due to projected earthquakes are found to be very low. Analytical results indicate that the main bridge superstructure will survive the projected 50-year earthquake without any damage and no loss-of-span. However, all the supports on the piers of the main bridge require additional anchor bolts or seismic isolation bearings.

The Kentucky and Indiana approach spans are analyzed using the response spectrum method with simplified single-degree-of-freedom models. Ten out of twelve supports having fixed bearings on both the approach spans require additional anchor bolts or seismic isolation bearings. At three out of twenty-five supports having expansion bearings, the existing rocker bearings need to be replaced with elastomeric bearings or cable restrainers need to be provided to avoid loss-of-span.

17. Key Words
Seismic Evaluation, Time-History, US41 Southbound Bridge, Field Testing, Finite Element Model, Response Spectra

18. Distribution Statement
Unlimited with approval of Kentucky Transportation Cabinet

19. Security Classif. (of this report)	20. Security Classif. (of this page)	21. No. of Pages	22. Price
Unclassified	Unclassified	165	

Executive Summary

Research Objectives

The objective of this investigation is to assess the structural integrity of the Ohio River bridge on US41 Southbound at Henderson, Kentucky (Figures E-1 through E-3), when subjected to a projected 50-year earthquake. The investigation considers the main bridge and the approach spans. To achieve the objective, the work was divided into the following four tasks: 1) Field testing of the main bridge; 2) Finite element modeling and calibration of the main bridge; 3) Time-history seismic response analysis of the main bridge; and 4) Seismic response of the approach bridges using the response spectrum method.

Background

The need for evaluating the seismic adequacy of the existing infrastructure has come into focus following the damage and collapse of numerous bridge structures due to recent earthquakes. For example, the 1989 Loma Prieta earthquake and the 1994 Northridge earthquake brought to the attention of the public the seismic risk to bridges and elevated freeway structures. In particular, the seismic rehabilitation of older bridges in regions of high seismicity, which were designed prior to the advent of modern seismic design codes, is a matter of growing concern. The US41 Southbound bridge at Henderson, KY was built in accordance with the earlier codes that had minimal provisions for earthquake loading.

Field Testing of the Main Bridge

The ambient vibration properties of the main bridge were obtained from field testing under traffic- and wind-induced excitations in order to determine the natural frequencies and their associated mode shapes. These vibration properties were subsequently used as a basis for calibrating the finite element model for seismic response analysis.

Finite Element Modeling of the Main Bridge

A three dimensional finite element model of the main bridge was used for free vibration and seismic response analyses. The model was calibrated by comparing the free vibration analysis results with the ambient vibration properties obtained from

field testing. After calibration, the model was used for seismic response analysis. The three dimensional model of the main bridge was subjected to the time histories of the projected 50-year earthquake to determine maximum displacements at joints, stresses in members, and forces on bearings.

Approach Spans

The approach spans were modeled using simplified single-degree-of-freedom systems. The seismic response was analyzed in the longitudinal direction using the response spectrum method.

Recommendations

The seismic analysis indicates that the main bridge can resist the 50-year earthquake event without yielding or buckling of truss members, and loss-of-span at supports. The analysis indicates a possibility for anchor bolt shear failure at all pier bearings. In order to avoid anchor bolt shear failure at all pier bearings, additional anchor bolts are required, or replacement of the existing bearings with seismic isolation bearings is suggested (Figure E-4). Chapter 5 presents the details for the proposed retrofit measures (Figures 5.9 through 5.13 and Table 5.16) for the main bridge.

The approach spans on the Henderson, KY side have the potential for anchor bolt shear failure due to longitudinal seismic forces at all six supports having fixed bearings. Therefore, retrofitting of the fixed bearings, at those six supports on the approach spans, with additional anchor bolts, or replacing the existing bearings with seismic isolation bearings is suggested (Figure E-5). Furthermore, one support out of nineteen supports having expansion bearings (rocker bearings) on the approach spans has the potential for loss of span. Therefore, it is recommended to replace those expansion bearings with elastomeric bearings or provide cable restrainers (Figure E-6).

Similarly, the approach spans on the Evansville, IN side have the potential for anchor bolt shear failure due to longitudinal seismic forces at four out of six supports having fixed bearings. Therefore, retrofitting of the fixed bearings, at those four supports on the approach spans, with additional anchor bolts, or replacing the existing bearings with seismic isolation bearings is recommended (Figure E-7). Also, two out of six supports having expansion bearings (rocker bearings) on the approach spans have the potential for loss of span. Therefore, it is recommended to replace those expansion bearings with elastomeric bearings or provide cable restrainers (Figure E-8). Chapter 6 depicts the details of the analysis and the proposed retrofit measures (Figures 6.7 through 6.19, and Tables 6.4 through 6.7) for both the approach spans.

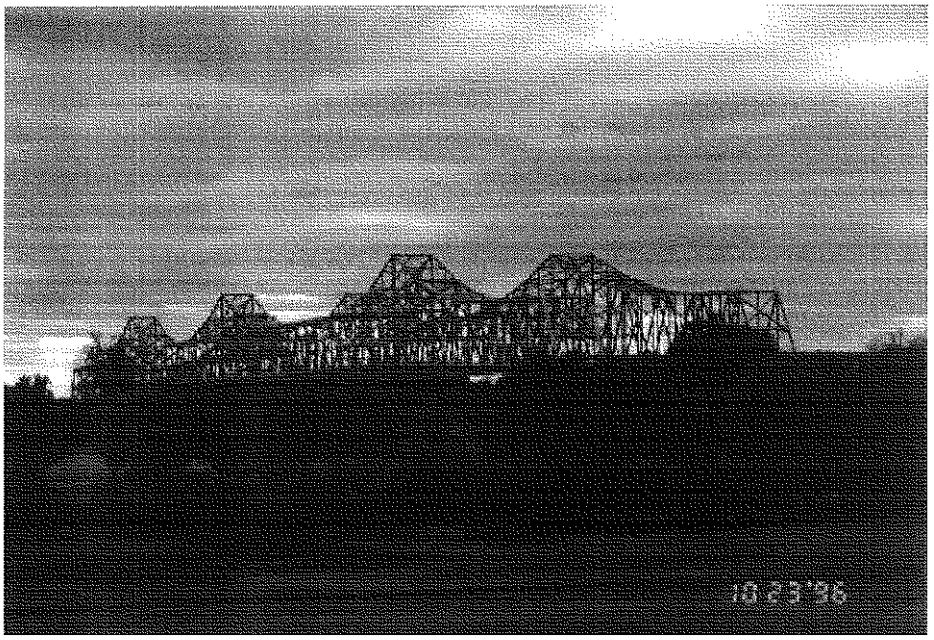

Figure E-1 US41 Bridges over the Ohio River at Henderson, KY

Figure E-2 The US41 Southbound Approach Spans at Henderson, KY

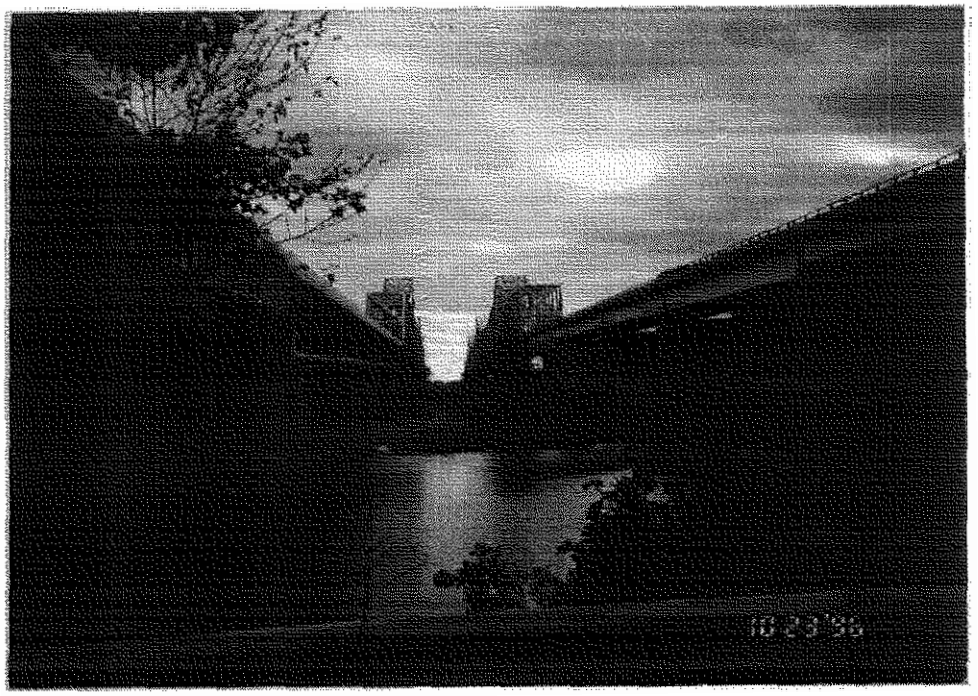

Figure E-3 The US 41 Southbound Approach Spans at Evansville, IN (Southbound on Right Side)

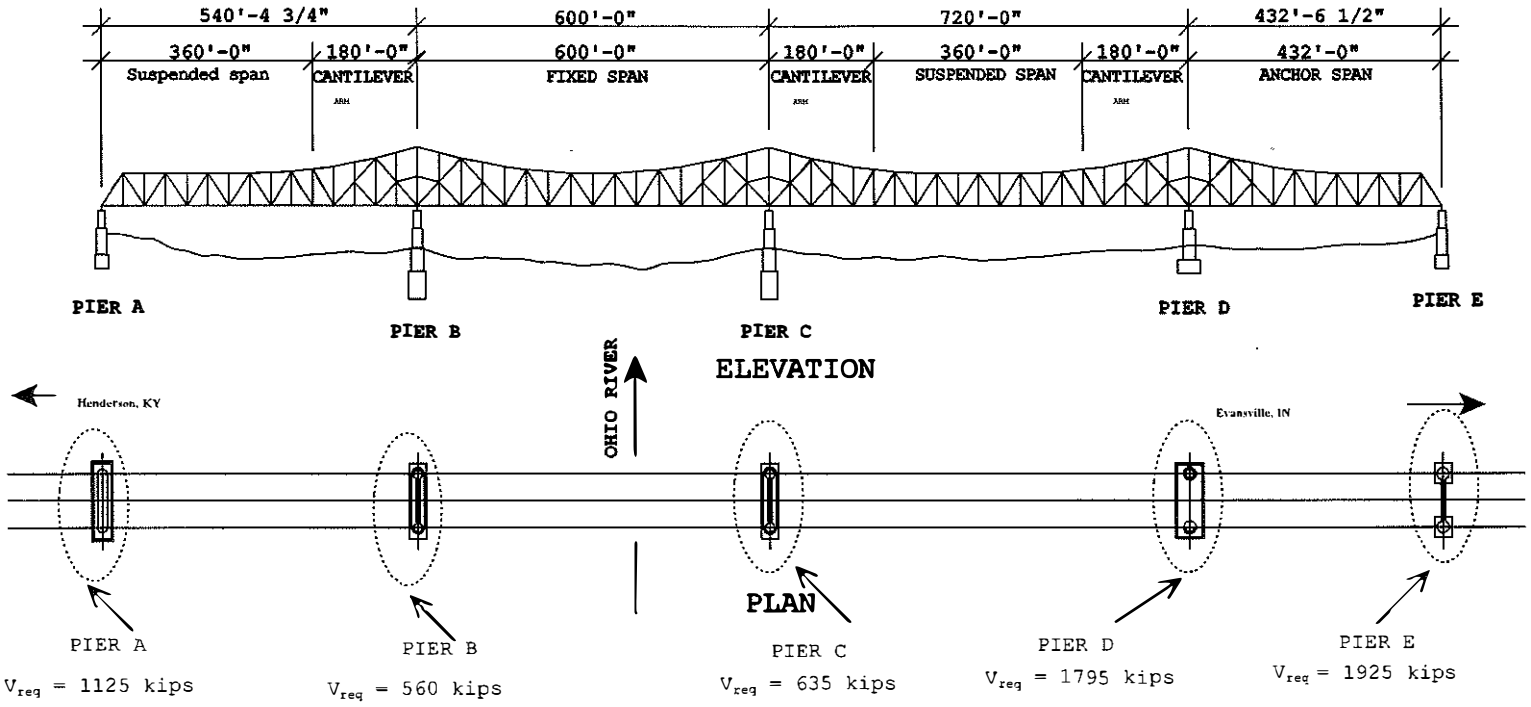

Figure E-4 Minimum Required Shear Capacity (Vreq) to be Provided by Additional Anchor Bolts at Bridge Piers for the US 41 Southbound Main Bridge

Note: Refer Figures 5.9 through 5.13 for the proposed retrofit details. Alternate retrofit would be to replace the existing fixed bearings with seismic isolation bearings.

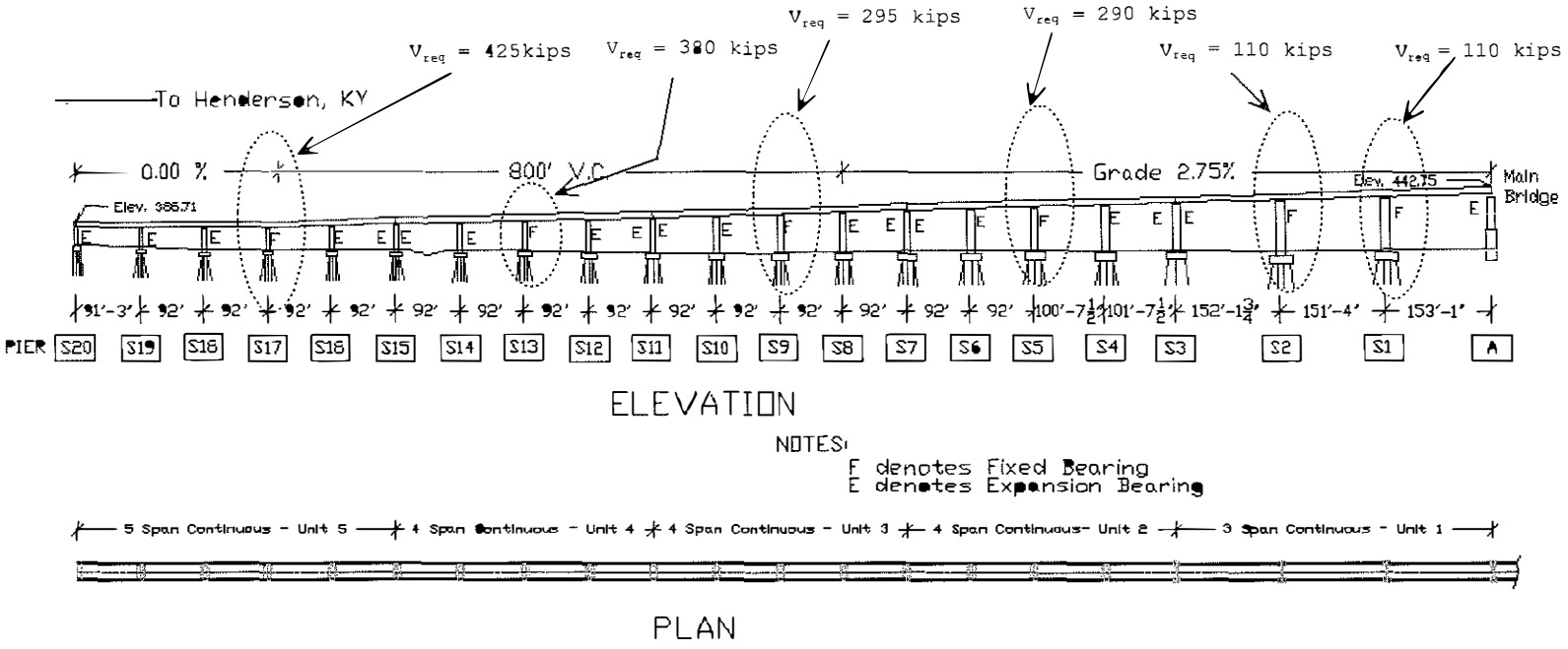

Figure E-5 Minimum Required Shear Capacity (V_{req}) to be Provided by Additional Anchor Bolts at Fixed Bearings on the Henderson, KY Approach on the US41 Southbound Bridge

Note: Refer Figures 6.13 through 6.18 for the proposed retrofit details. Alternate retrofit would be to replace the existing fixed bearings with seismic isolation bearings.

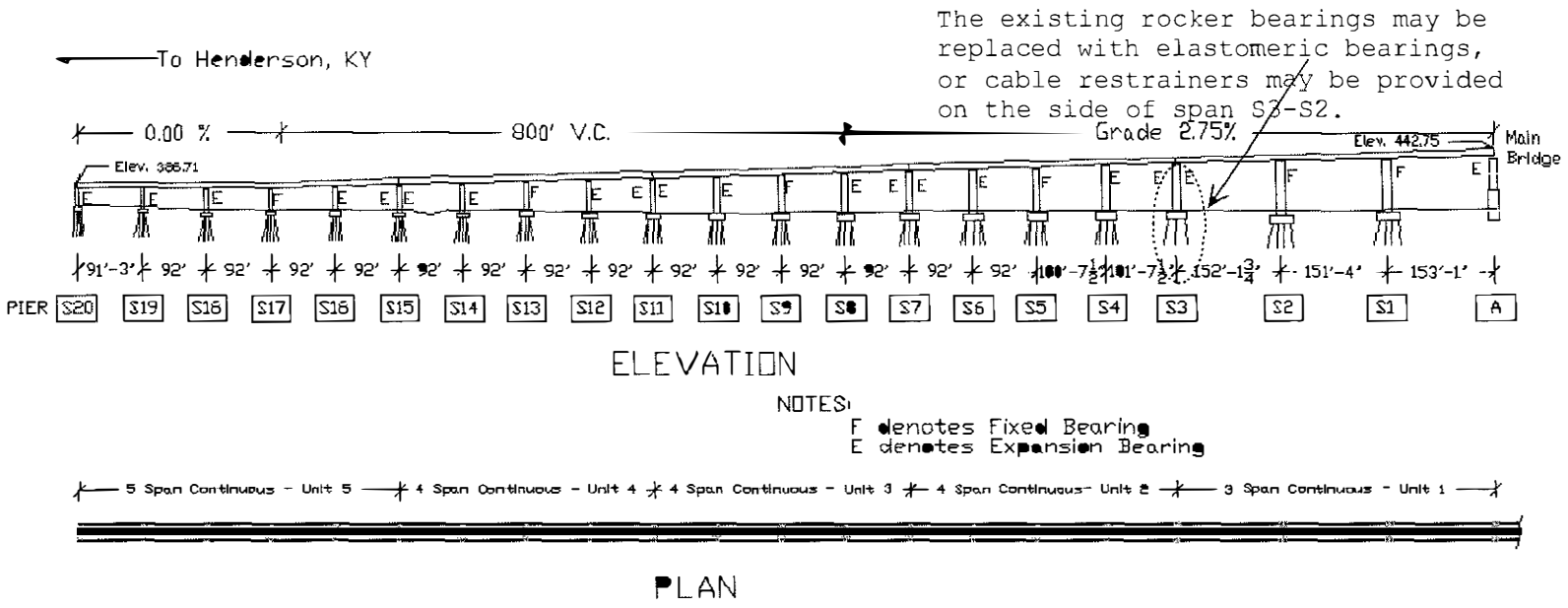

Figure E-6 Proposed Retrofit Measures for the Expansion Bearings on the Henderson, KY Approach, US41 Southbound Bridge

Note: Refer Figure 6.19 for more retrofit details

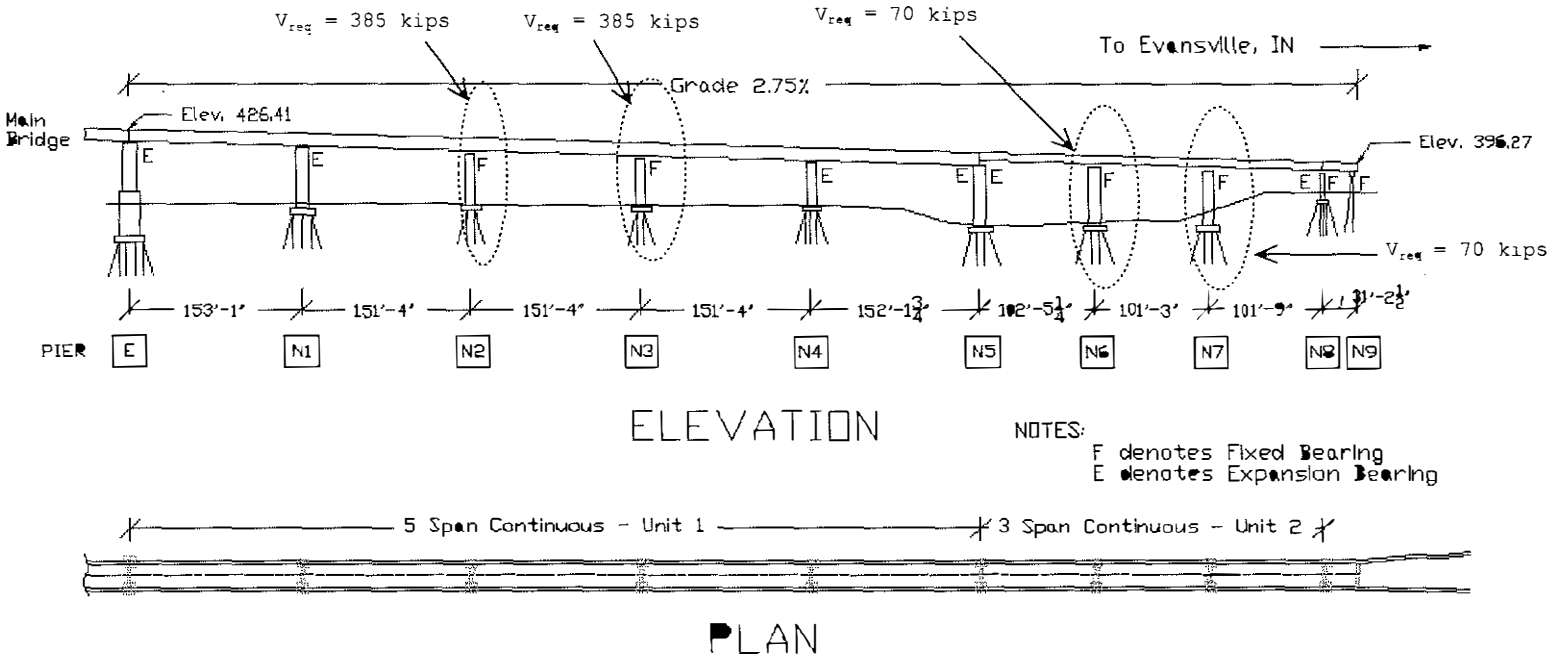

Figure E-7 Minimum Required Shear Capacity (V_{req}) to be Provided by Additional Anchor Bolts at Fixed Bearings on the Evansville, IN Approach on the US41 Southbound Bridge

Note: Refer Figures 6.7 through 6.10 for the proposed retrofit details. Alternate retrofit would be to replace the existing fixed bearings with seismic isolation bearings.

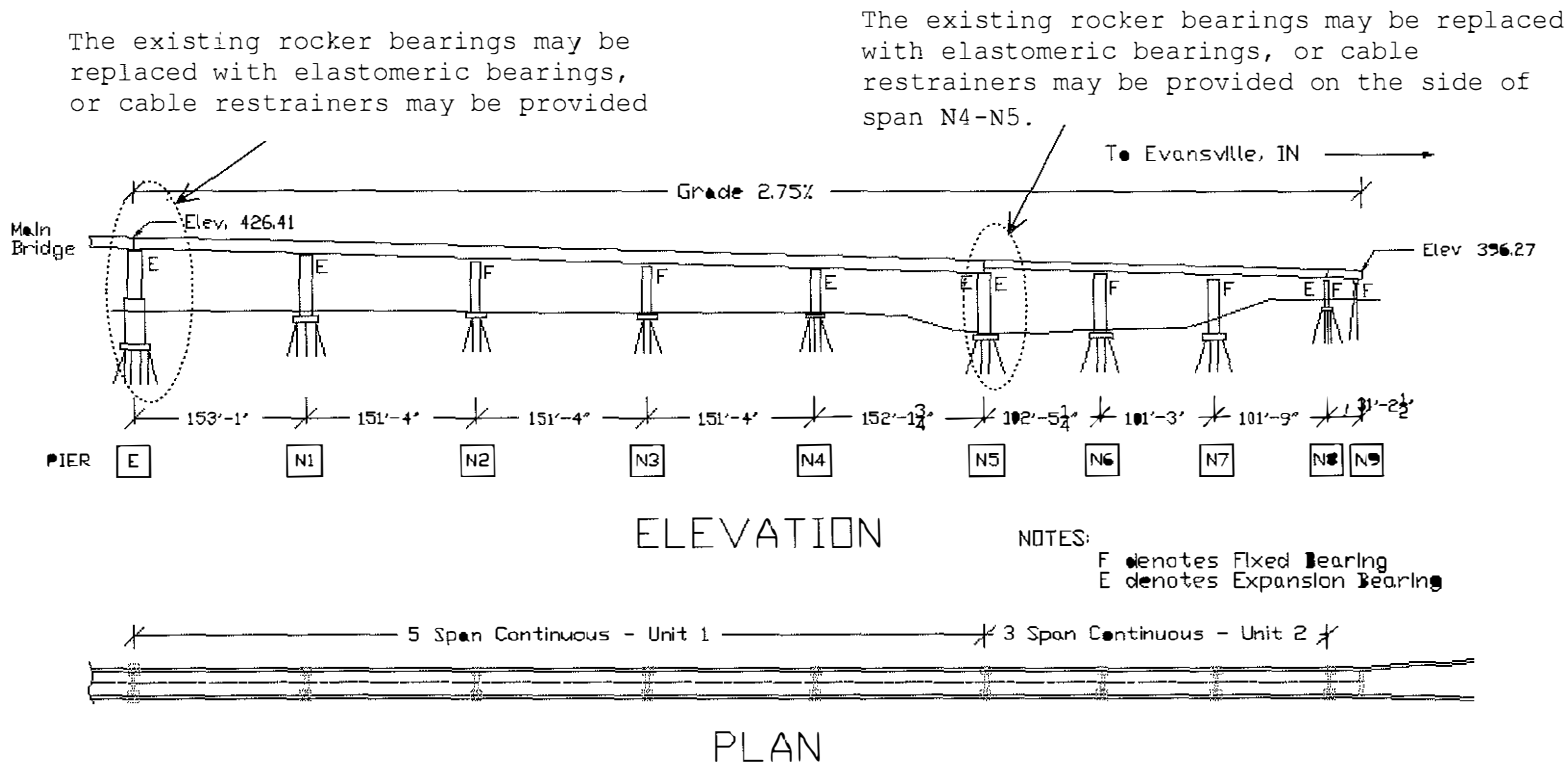

Figure E-8 Proposed Retrofit Measures for the Expansion Bearings on the Evansville, IN Approach, US41 Southbound Bridge

Note: Refer Figures 6.11 through 6.12 for more retrofit details

ACKNOWLEDGMENTS

The financial support for this project was provided by the Kentucky Transportation Cabinet and the Federal Highway Administration. The help of Dan Eaton, John Flekenstein, and Clark Graves in coordinating and conducting the bridge testing is especially noteworthy. The authors would like to acknowledge the cooperation, suggestions, and advise of the members of the study advisory committee: Donald Herd (committee chairperson), Glenn Givan, Ray Greer, David Moses, Ted Noe, N.B. Shah, and David Steele.

The authors would also like to acknowledge the partial support for equipment provided by the National Science Foundation under grant CMS-9601674-ARI.

Table of Contents

LIST OF TABLES

LIST OF FIGURES

1. INTRODUCTION

1.1 General

The need for evaluating the seismic adequacy of existing infrastructure has come into focus following the damage and collapse of numerous structures during recent earthquakes. In particular, the seismic rehabilitation of older bridges which were designed prior to the advent of modern seismic design codes is a matter of growing concern in regions of high seismicity. Bridge failures from earthquakes have so far only occurred in California and Alaska. The 1989 Loma Prieta earthquake [EERI 1990] and 1994 Northridge earthquake [EERI 1995] have brought the seismic risk to bridges and elevated freeway structures to the attention of the public. The partial collapse of the San Francisco - Oakland Bay Bridge and the Cypress Viaduct portion of Interstate 880 not only caused the loss of life, but created considerable problems to the transportation infrastructure. The Bay bridge was unusable for a month and transbay commuters were forced to travel on ferries or the crowded Bay Area Rapid Transit System. Following the Loma Prieta earthquake, the Federal Highway Administration commissioned the seismic evaluation of bridges located in the seismically active regions.

After the seismic evaluation, if the bridge is found to be deficient, not all bridges in highways system have to be retrofitted simultaneously; instead, only those bridges with the highest priority should be retrofitted first. It should always be remembered that seismic retrofitting is one of several possible courses of action. Other possible actions are closing the bridge, replacing the bridge, taking no action at all, and accepting the risk of seismic damage.

Seismic design of bridges throughout of the United States is governed by the AASHTO's Standard Specifications for Highway Bridges, Division I-A (1996). Use of the AASHTO specifications is intended: (1) to allow the structure to yield during a major earthquake, (2) to allow damage (yielding) only in areas that are accessible (visible) and repairable, and (3) to prevent collapse even during very large earthquakes (NHI 1996). There are many bridges in the Commonwealth of Kentucky which were designed before the seismic provisions were introduced into the AASHTO Code. Recently, the Brent-Spence bridge on Interstate 75 connecting Covington, Kentucky to Cincinnati, Ohio, a double-deck through-truss bridge, was evaluated for seismic excitation [Harik et al.(1997a,b)]. There are many long-span through-truss bridges in Kentucky which require seismic evaluation. The present work concentrates on the seismic evaluation of the US41 Southbound Bridge over the Ohio River. This bridge connects US41 across the Ohio River between Henderson, KY and Evansville, IN.

1.2 Field Testing

Nowadays, field testing of bridges has become an integral part of the seismic evaluation process in order to eliminate the uncertainties and assumptions involved in analytical modeling. Full-scale dynamic tests on structures can be performed in a number of ways. Hudson (1977) describes the different types of testing as: (1) free vibration tests, including (i) initial displacement as in the pullback, quick-release test, and (ii) initial velocity from impacts; (2) forced vibration tests, including (i) steady-state resonance testing, (ii) variable frequency excitation including sweep, rundown, random and pulse sequences, and (iii) transient excitations including earthquakes, wind, traffic, and explosions. Shelley et al. (1995) provides a very informative discussion of the advantages and disadvantages of the various test methods used on highway bridges.

An alternative technique used to dynamically test bridges measures the bridge's response under normal traffic and wind. In this method no equipment is required to excite the structure, instead equipment is required only to record the vibrations. This technique has been used by a number of researchers (Abdel-ghaffer and Scanlan, 1985a,b, Alampalli and Fu 1994, Buckland et al. 1979, Doll 1994, Farrar et al. 1995, Paultre et al. 1995, Saiidi et al. 1994, Shahawy 1995, Ventura et al. 1994, Wendichansky et al. 1995). Harik et. al. used this method with success to identify the vibration mode shapes and frequencies of the Brent-Spence Bridge at Covington, KY (Harik et al. 1997a,b) and US51 Bridge at Wickliffe, KY (Harik et al. 1998).

1.3 Earthquake Background

The test bridge is located in Henderson County, Kentucky, in the Wabash Valley Seismic Zone. The two largest earthquakes known to have occurred in this zone were in 1891 and 1968. Street et al. (1996) calculated an $m_{b,Lg}$ of 5.5 to 5.8 for the September 27, 1891, event. This earthquake was centered near Mt. Vernon, Illinois, where several chimneys were shaken down and a church was damaged. The November 9, 1968, earthquake was more damaging than the 1891 one since the area was much more denseley settled and more vulnerable to damage. Stover and Coffman (1993) estimated the $m_{b,Lg}$ of the two events as 5.2 and 5.5, respectively.

The most significant recent earthquake in the Wabash Valey Seismic Zone was on June 10, 1987. Taylor et al. (1989) estimated the $m_{b,Lg}$ of this event at 5.2 and described it as a predominantly strike-slip event with a focal depth of 10 km.

Nuttli and Herrmann (1978) estimated a maximum credible earthquake of 6.6 $m_{b,Lg}$ for the Wabash Valley Seismic Zone. More recently, Obermeier et al. (1992) found evidence of one or more strong earthquakes centered near Vincennes, IN. Based on the areal extent of liquefaction features (dikes), Obermeier et al. (1992) concluded that if all the dikes are from a single event, the level of shaking would have been on the order of 6.7 $m_{b,Lg}$, a magnitude that is in close agreement with Nuttli and Herrmann's (1978) maximum credible earthquake.

With increasing recognition of potential damage from a large Wabash Valley earthquake, or other less severe quake, the Kentucky Transportation Cabinet funded the research project *Evaluation and Analysis of Innovative Concepts for Bridge Seismic Retrofit*. Research was conducted by the Kentucky Transportation Center at the University of Kentucky. Fundamental to this research project was the characterization of the seismic potential affecting Kentucky from known seismic zones as well as unknown "local" events. Results from this seismological assessment of Kentucky were published in *Source Zones, Recurrence Rates, and Time Histories for Earthquakes Affecting Kentucky* (Street et al., 1996). In this report, three main tasks were covered: (1) definition and evaluation of earthquakes in seismic zones that have the potential to generate damaging ground motions in Kentucky, (2) specification of the source characteristics, accounting for the spreading and attenuation of the ground motions to top-of-bedrock at sites in Kentucky, and (3) determination of seismic zoning maps for the Commonwealth based on peak-particle accelerations, response spectra, and time-histories.

Time-histories generated in the aforementioned report were used in the seismic evaluation of the US41 Southbound bridge. Effects of these artificial earthquakes were calculated for bedrock elevation at the county seat of each Kentucky county. These acceleration time-histories were derived through the use of random vibration analysis and take into consideration the probability of earthquakes from nearby seismic zones, the attenuation of ground motions with distance in the Central United States, and the possibility of a random event occurring outside of the generally recognized seismic zones (Street et al., 1996).

1.4 Scope of the Work

The primary aim of this study is to assess the structural integrity of the US41 Southbound bridge when subjected to a 50-year earthquake event at Henderson Co., Kentucky. To achieve this, the scope of work was divided into four tasks: 1) Field testing of the main bridge, 2) finite element modeling, 3) time history seismic response analysis of the main bridge, and 4) seismic response of the approach bridge.

The ambient vibration properties of the main bridge are determined through field testing under traffic and wind induced excitation. The purpose of measuring the ambient vibration properties is to determine the mode shapes and the associated natural frequencies. Full scale ambient or forced vibration tests have been used extensively in the past to determine the dynamic characteristics of highway bridges (Abdel-ghaffer and Scanlan, 1985a,b).

A three dimensional finite element model of the main bridge is used for free vibration and seismic response analyzes. The model is first calibrated by comparing the free vibration analysis results with ambient vibration properties from field testing. After the calibration, the model is used for seismic response analysis to determine the maximum displacements, stresses in truss members, and forces on bearings.

The approach spans are modeled using simplified single-degree-of-freedom (SDOF) systems. The superstructure mass is lumped at the top of the piers. For the approach spans, the seismic analysis dealt only with the potential for loss-of-span due to longitudinal displacement and forces on the bearings. Seismic response is analyzed in the longitudinal direction only using the response spectrum method to determine the maximum displacements and forces.

2. The US41 Southbound Bridge over the Ohio River : Main Bridge

2.1 General

The Ohio River bridge on US41 Southbound shown in figures 2.1(a)-(e) is a cantilever through-truss bridge, a bridge type commonly employed for spans of 600' (183 m) to 1500' (457 m) through the mid 1970's. This bridge was originally designed by Hazelet and Erdal Consulting Engineers in 1963. Figures 2.1(a)-(e) show the different views of the main bridge. The total length of the bridge including approach spans is 5395'. The length of the four-span main bridge is 2293'. The plan and elevation views of the main bridge are shown in Figure 2.2. The superstructure truss members are made up of structural steel, and the substructure piers are made of reinforced concrete. The details of approach bridges and their seismic evaluation are discussed in separate Chapter 6.

2.2 Bridge Superstructure

The superstructure is described in terms of the vertical truss system, the lateral truss system and the floor system. The lateral truss is a combination of lateral bracing, sway and portal bracings. The bridge is a through-truss type with suspended spans, fixed spans, anchor arms and cantilever arms.

As seen from Figure 2.2, height of the vertical truss near each midspan is 55', and at each internal support is 100'.

The vertical truss system shown in Figure 2.2 consists of a semi-suspended span of 360' between piers A and B, which is supported over pier A and a cantilever arm 'B' of 180' as shown in Figure 2.3. A fixed arm 'B-C' (Figure 2.4), between piers B and C, spans 600'. In span C-D (Figure 2.5), there are two cantilever arms 'C' and 'D', spanning 180' each, supporting a suspended span of 360'. The span D-E (Figure 2.6) is an anchor arm, having a span of 432'. The lengths of spans AB, BC, CD and DE are 540' 4 3/4", 600', 720' and 432' respectively.

The vertical truss members are made up of ASTM A373 and A441. The upper chords of the main truss are made from A373 and HT steel. All shop and field connections are made of high-strength bolts (ASTM A325). The bolt size for main truss joints is 1" dia., while for bracings, sway frames and stringers bolt size is 7/8" dia. The

members are made of built-up sections using vertical plates, web plates and perforated cover plates.

The lateral truss system consists of lateral bracing members in the top and bottom chord planes combined with portals and sway bracing between the two vertical trusses as shown in Figures 2.1c-e. At the hinge locations, longitudinal sliding joints at both the top and bottom chords are designed for free thermal expansion.

The floor system consists of a 7" thick concrete slab supported by longitudinal 24WF stringers which are carried by transverse built-up floor beams as shown in Figure 2.7. The width of the roadway is 30'. The longitudinal stringers are spaced at 7' 6". The floor beams span 39' between the vertical trusses and are attached to the truss verticals.

2.3 Fixed and Expansion Bearings

The superstructure is supported by expansion bearings on piers C and E, and fixed bearings on piers A, B and D. The expansion rocker bearings on piers C and E permit longitudinal translation and longitudinal rotation.

The fixed bearings on pier A consist of a bottom shoe and a top shoe. The bottom shoe is fixed to the pier through anchor bolts. It has a plate at center with 4" wide. This plate has a rounded edge that is put into the socket of the top shoe at the bottom chord of the truss. The size of the bearing is 3' x 3', and there are a total of 2" dia. anchor bolts of length 4' and spaced at 2' 6". This fixed bearing allows only longitudinal rotation.

The fixed bearings on pier B and D have similar arrangements and construction but allow only a very limited longitudinal rotation because of the huge size of the bottom shoe. The size of the bearing plate is 6'x5', and it accommodates four anchor bolts of size 2" dia spaced at 5' 2" and 4' 2". The bottom and top shoes are connected through a 3.25" dia. pintle.

The expansion bearings on pier C have three rockers supported on a bearing plate of size 6' x 6'. The bottom shoe is placed on the rockers, and the top shoe is connected to the truss bottom chord. The two shoes are connected to each other through a pintle of 3.5" dia. There are a total of four 2" dia. anchor bolts connected to the bearing plate. This bearing allows longitudinal translation and a very limited longitudinal rotation.

The expansion rocker bearings on pier E consist of one rocker placed over the bearing plate which measures 2' 3" x 3'. The bearing plate is connected to the pier

through 4 anchor bolts of size 1.5" dia. The top rounded edge of the rocker is placed in the socket provided to the bottom chord of the truss. This bearing allows both longitudinal translation and rotation.

2.4 Bridge Substructure

The main bridge is supported on piers A, B, C, D and E shown in Figures 2.8 through 2.12. These piers are wall type piers made of reinforced concrete. Piers A, D and E are supported on pile foundations, and the piers B and C are supported on caisson foundations. The height of the pier A (Figure 2.8) above the top of pile is 106' 10" and is a stepped wall-type pier. The plan area of pile cap is 62' x 30'. All piles are of 14BP117 with allowable bearing capacity of 155 tons. The heights of caisson foundation for piers B (Figure. 2.9) and C (Figure 2.10) are 49' and 61'. The heights of piers B and C above caisson foundation are 118' 4" and 109' 2". The pier B is a stepped wall-type pier with the footing size of 63' x 24' (Figure 2.9) while pier C is 66' x 26' (Figure 2.10). The pier D (Figure 2.11) is 96' 3" in height above the pile footing of size 66' x 33'. Steel H piles and caisson piles are used. The pier E (Figure 2.12) is 70' 8" high above the top of pile footing of size 16' x 16'. Two circular columns are connected by web wall from 18' from the top of the pile footing. Steel H piles used belong to 14BP 89 and 73 categories.

3. Field Testing

3.1 General

Field testing a bridge provides an accurate and reliable description of its actual dynamic characteristics. Field testing was conducted on the US41 Southbound main bridge. Testing was conducted on right and left lanes. Since there is no symmetry in the longitudinal direction of the bridge, the full bridge was tested. All measurements were taken by placing the instruments on the pavement due to limited access to the actual floor beams and the time constraints involved. Each instrument was placed with its longitudinal axis aligned parallel to the longitudinal direction of the bridge. Ambient vibration measurements under traffic and wind induced excitations were recorded at 25 locations beginning from pier A to pier E.

3.2 Instrumentation

The equipment used to measure the acceleration-time histories consisted of a triaxial accelerometer (Figure 3.1a) in conjunction with its own data acquisition system. The system used consisted of Kinemetrics SSA-2 digital recording strong motion accelerograph. Two of the units contained internal accelerometers, and the remaining two were connected to Kinemetrics FBA-23 force balance accelerometers. Each of the accelerometers was capable of measuring accelerations of ±2g's with a frequency response of DC-50 Hz. All data were sampled using a 1002 Hz sampling rate and stored internally on the SSA-2, then downloaded to a personal computer. Each of these units was triggered simultaneously using laptop personal computers connected to each SSA-2. A nominal 30 sec record was obtained at each location. Accelerometers were mounted in order to measure vibrations in three orthogonal directions. To ensure the blocks were placed in level, adjustable feet and a carpenter's level were attached to each block. Accelerometers were connected to the data acquisition system by shielded cables.

Sets of three accelerometers were mounted to aluminum blocks in orthogonal directions. A block was positioned at each location with the accelerometers oriented in the vertical, transverse and longitudinal directions. To prevent any shifting of the accelerometers during testing, 25-pound bags of lead shot were laid on top of the accelerometer blocks once in position. During ambient vibration tests, traffic was allowed to cross at normal highway speed.

3.3 Testing Procedure

A reference location, hereinafter referred to as the base station, was selected based on the mode shapes from the preliminary finite element model at location 14 as shown in Figure 3.1b. Two of the accelerometers, one at each side of roadway width (Figure 3.1c), remained at the base station 14 throughout the testing sequence. Five triaxial accelerometers were used at moving station locations. From the preliminary finite element analysis, 25 locations were identified to be measured to represent the dynamic behavior of the bridge. In total, there were five sets of moving station data with each set having 5 moving station locations. Tables 3.1a and 3.1b describe the designations of moving and base station accelerometer on right lane. Tables 3.2a and 3.2b detail the designations of moving and base station accelerometers on left lane. First five stations 1, 2, 3, 4, 5 and 6 were placed in span A-B, stations 8-12 were placed in span B-C, stations 14-20 were placed in span C-D, and stations 22-25 were placed in span D-E. Data collection began from pier A to pier E on the right lane. The same procedure was repeated for the left lane without altering the base station. Stations 1, 7, 13, 21, and 25 were placed just above the piers A, B, C, D and E respectively.

One set of measurements consisted of recording acceleration-time history on two base stations and five moving stations simultaneously. Once the data was collected, the moveable stations were shifted to the next locations while the base stations remained stationary. This sequence was repeated five times to get measurements on all stations on the southbound lane.

3.4 Data Analysis

Once the data have been downloaded from the field test, a Fast Fourier Transform (FFT) was performed on each acceleration-time history using the DADiSP software. The program DADiSP (Data Analysis and Display Software) by DSP Development Corporation, Cambridge, Massachusetts, (DADiSP 1995) was used to view and analyze the large amount of data. The program has the ability to quickly access and display the large records of 30,000 data points. Also, the program has an extensive data handling and analysis library which was needed for this research. Fast Fourier transformation of the acceleration histories was possible in a few seconds. The speed of the program made analyzing and viewing such a huge amount of data manageable.

Acceleration records were transformed from the time domain to the frequency domain through the use of the Fourier transform. Equations 3.1 and 3.2 are the mathematical definitions of the Fourier transform pair. Equation 3.1 is referred to as

the Fourier transform of *f(t)* and the equation 3.2 as the inverse Fourier transform (Press et al. 1992, Chapra and Canale 1988).

$$\mathbf{F(\omega)} = \int_{-\infty}^{\infty} \mathbf{f(t)}\ \mathbf{e}^{\mathbf{i\omega t}}\ \mathbf{dt} \tag{3.1}$$

$$\mathbf{f(t)} = \frac{\mathbf{1}}{\mathbf{2\pi}} \int_{-\infty}^{\infty} \mathbf{F(\omega)}\ \mathbf{e}^{\mathbf{-i\omega t}}\ \mathbf{d\omega} \tag{3.2}$$

where **f(t)** = a function of time, **F(ω)** = amplitude as a function of frequency, and ω = circular frequency (radians per second).

From equations 3.1 and 3.2, a time function can be derived from a frequency function or vice versa. The problem with using equations 3.1 and 3.2 lies in the fact that a continuous function is required. For discretely sampled data, such as a dynamic bridge test, a different form of the Fourier transform is needed. A form of equation 3.1, known as the Discrete Fourier Transform (DFT), is used when points of data are known at evenly spaced intervals. Equations 3.3 and 3.4 are the discrete forms of the Fourier transform pair.

$$\mathbf{F_n} = \sum_{\mathbf{k=0}}^{\mathbf{N-1}} \mathbf{f_k e^{2\pi ikn/N}} \qquad \text{(for n=0 to N-1)} \tag{3.3}$$

$$\mathbf{f_k} = \frac{\mathbf{1}}{\mathbf{N}} \sum_{\mathbf{n=0}}^{\mathbf{N-1}} \mathbf{F_n e^{-2\pi ikn/N}} \qquad \text{(for k=0 to N-1)} \tag{3.4}$$

where N = number of sampled points and $\mathbf{f_k}$ = set of **N** sampled points.

The DFT as expressed in equation 3.3 is usually the most useful in civil engineering applications where frequency components are sought from discretely sampled (digitized) data. However, the direct application of equation 3.3 requires N^2 complex mathematical operations. This becomes prohibitively time-consuming even for modest length data records. Fortunately, there is a numerical operation that reduces computing time for the DFT substantially.

The method is called the Fast Fourier Transform (FFT) and owes its efficiency to exploitation of the periodicity and symmetry of trigonometric functions. An FFT can be computed in approximately $N\log_2 N$ operations. For a set of 1000 data points, the FFT is approximately 100 times faster than the DFT. The first FFT is attributed to

Gauss in 1805 but did not become widely known until the mid 1960's with the advent of the Cooley-Tukey algorithm. A more complete mathematical and numerical treatment of the FFT can be found in Press et al. (1992) and Chapra and Canale (1988). Using the Fast Fourier Transform (FFT), natural frequencies in three orthogonal directions were determined. Additional processing into a Power Spectral Density (PSD) plot, which squares the FFT amplitudes and divides out the record length, was sometimes helpful in identifying natural frequencies.

Mode shapes were determined by plotting the ratios of accelerometer FFT magnitude to base station FFT magnitude at their respective locations along the bridge. Comparing the phase angle of an FFT frequency to the base-station FFT phase angle determined the sign of the magnitude to be plotted (in-phase or out-of-phase with the base station).

A typical ambient vibration acceleration-time history obtained in the transverse direction at the moving station 6 is shown in Figure 3.2a. Similar time histories are shown for the vertical (figure 3.2c) and longitudinal (figure 3.2e) directions at moving station 6. For the transverse direction, the FFT of the acceleration time-history of moving station 6 is shown in Figure 3.2b. Similar FFTs for vertical and longitudinal direction time-histories are shown in figures 3.2d and 3.2f. By observing the peaks of all the stations, the natural frequencies were identified. These peaks do not always occur at exactly the same frequency at all locations. Therefore, the number of peaks of adjacent natural frequencies were calculated. Table 3.3 lists the distribution of frequencies from acceleration record obtained on longitudinal, transverse and vertical direction accelerometers. Then, the bridge natural frequency was identified as the one which has the maximum number of peaks. Also the natural frequency is based on the mode shape that follows closer to the preliminary finite element model results.

Table 3.3 also lists the comparison between the field tested natural frequency with that of the calibrated finite element model. They are discussed in the following section.

3.5 Finite Element Model Calibration

A logical next step to field testing in bridge evaluation is to create an analytical model which will correlate well to the measured dynamic properties. Many assumptions and modeling approximations must be made when creating a practical model of a bridge. For example, a finite element model requires input of the material properties which are inherently variable. This is one input where the analyst can only make a best estimate and later adjust to match the experimental results.

Using results from the eigenvalue analysis, generally the bridge model has to be calibrated to experimentally determined mode shapes and frequencies. A perfectly calibrated model would match all experimentally determined mode shapes and frequencies exactly. To hope for such a perfect calibration is not realistic. Therefore, only the most structurally significant modes and frequencies are used in the model calibration process. Namely, the first three transverse modes, first three vertical modes and the first longitudinal mode from field testing are selected as calibration targets.

Parameters which were used to correlate with the field test include the following: modulus of elasticity (E) of the frame elements, the bearing spring stiffness, and spring stiffnesses for the piers. Initial estimates of these parameters were obtained from the structural drawings. But the estimates do not account for (1) construction tolerances or errors that can make as-built dimensions different from design dimensions, or (2) actual strengths of materials such as actual compressive strength of concrete, which affects its modulus of elasticity. Calibration is performed by adjusting the stiffnesses and masses of the bridge members until an acceptable match is observed in the natural frequency and mode shape.

Since the bridge does not have a symmetry along the vertical direction, it is not possible to observe pure transverse modes. Instead, transverse flexural-torsional modes are obtained. But pure vertical modes are obtained, because the bridge is symmetric in the transverse direction. Longitudinal modes are accompanied by a little vertical bending mainly because of the unequal pier stiffnesses. For comparison purposes, only the transverse components from field testing are taken into consideration for the transverse flexural-torsional modes. All the transverse flexural-torsional modes are hereinafter referred to as transverse modes, because they have major mass participation in the transverse direction.

The finite element results for the mode shapes are generated at the end nodes in the floor beams. On the other hand, due to the limited access to the actual floor beams, all measurements were taken by placing the instruments on the pavement just above the floor stringers.

Figure 3.3a shows the comparison of the mode shape obtained from the test and finite element model. Although this mode is not a pure transverse mode, Figure 3.3a compares only the transverse components. This mode has four half-waves along the length of the bridge. The distribution of fundamental natural frequency is given in Figure 3.3b. It can be seen from this figure that the peak in the magnitude varied from 0.4008 Hz to 0.5344 Hz, with a maximum number of peaks occurring at 0.4676 Hz. Since the mode shape corresponding to 0.501 Hz matched well with the finite element model, 0.501 Hz is identified as the fundamental frequency from the field test. The natural frequency from the finite element model is 0.500 Hz, and the

difference is only about 0.11%.

Figure 3.4a shows the first vertical mode with a natural frequency of 0.7682 Hz from the test. The distribution of natural frequency is shown in Figure 3.4b. The maximum number of peaks appears to be at 0.7682 Hz, and hence this is identified as the natural frequency from field testing. The finite element model frequency is 0.7348 Hz, and the difference is only about 4.54%. This mode is a pure vertical mode with 4 half-waves along the length of the bridge.

The traffic induced excitation can produce clear acceleration records in the vertical direction, and the traffic combined with wind excitations can produce in the transverse direction. Since there was no excitation along the longitudinal direction, clear acceleration records in the longitudinal direction were not obtained. Therefore, matching the frequencies is difficult for this mode. The first longitudinal mode shape is shown in Figure 3.5a. The natural frequency from the field test according to Figure 3.5b is 1.0688 Hz.The mode shape corresponding to 1.0688 Hz matches well with the finite element model. The FE model frequency is 1.0758 Hz, and the difference is only about 3.76 %. Due to the difference in stiffness of the piers, pure longitudinal modes are not obtained. Therefore, longitudinal mode is accompanied with small vertical modal deformation; however, the mass participation in this mode is mainly due to the longitudinal deformation of the piers.

Figure 3.6a shows the mode shape of the second transverse mode. The distribution of natural frequency is shown in Figure 3.6b, and the natural frequency is identified as 0.6012 Hz. The natural frequency from the FE model is 0.6474 Hz, and the difference with the test is only 7.14%. This is not a pure transverse mode. It is a transverse flexural-torsional mode with four half-waves.

The mode shape of second vertical mode is shown in Figure 3.7a. The maximum number of peaks occurs at 1.035 Hz, and it matches closely in mode shapes. The natural frequency from the test is 1.0354 Hz, whereas the FE model is 0.9663 Hz and the difference with the test is 3.69%. Figure 3.7b shows the distribution of natural frequency of this mode. The mode shape consists of four half-waves along the length of the bridge.

Figure 3.8a shows the mode shape of the third transverse mode. This is a transverse flexural-torsional mode with the frequency of 0.8016 Hz from field testing and 0.8123 Hz from FE model. The difference of FE model natural frequency with test is only 1.32%. There are five half-waves in the mode shape along the length of the bridge. Figure 3.8b shows the distribution of the natural frequency and 0.8016 Hz is observed at 11 stations out of the total 25 stations.

Figure 3.9a shows the mode shape of the third vertical mode. The natural

frequency of 1.336 Hz is identified from the test and 1.297 Hz from the FE model. The Figure 3.9b shows that 1.336 Hz is observed at 19 stations. The difference of FE model frequency with the test is 0.43%. The mode shape consists of five half-waves along the length of the bridge. The frequency 1.336 Hz is identified as the natural frequency, since the mode shape corresponding to this frequency matches better with the finite element model.

4. Finite Element Modeling and Free Vibration Analysis

4.1 General

Based on the general dynamic characteristics of cantilever truss bridges and the proximity and activity of the seismic zones, the main bridge model was expected to remain elastic, and displacements were anticipated to be small enough to neglect the material and geometric nonlinear effects. Hence, the consideration of linear elastic small displacement analysis is considered to be appropriate.

Free vibration analysis is a key process in the dynamic analysis of a structure; the resulting natural frequency and mode shapes succinctly describe the dynamic characteristics of a complex structure. The analytical model is calibrated by comparing free vibration analysis results with ambient vibration measurements.

4.2 Finite Element Model

A three dimensional linear elastic finite element model (Figure 4.1) of the main bridge was developed in SAP90 finite element analysis software (Wilson and Habibullah, 1992). Developed for both free vibration analysis and earthquake response analysis, the model represents the structure in its current as-built configuration. All truss members of the superstructure are modeled using two noded frame elements which have three translational DOF and three rotational DOF at each node. Rotational degrees of freedom (DOF) of members are included in this bridge because the connections are of riveted type that could induce flexural stresses in addition to axial stresses. Based on the connection between the concrete deck and stringers, it is assumed that the deck and stringers will not contribute to the stiffness of the bridge. Wall type piers are idealized as frame elements with their gross cross-sectional properties.

The piers A, B and D are provided with fixed bearings while the piers C and E are provided with expansion bearings. All the fixed bearings are restrained against longitudinal translation. Fixed bearings at pier A allow longitudinal rotation. Fixed bearings at piers B and D allow very limited longitudinal rotation. Pier and bearings are represented by a set of spring elements that simulate the actual behavior.

The expansion bearings at the piers C and E were modeled by allowing longitudinal translation. Bearings at pier C allow limited rotation whereas the bearing at pier D allows substantial rotation.

While conducting free vibration analysis, it was found that the modeling of piers using frame elements resulted into less mass participation. This may be due to large differences in stiffness and masses of members in superstructure and piers of substructure. Therefore, the piers were replaced by springs at the bottom of bearings. The spring stiffnesses were obtained by applying unit displacement along the appropriate DOF.

4.3 Free vibration Analysis

An eigenvalue analysis is used to determine the undamped, free vibrations of the structure. The eigensolution results in the natural mode shapes and frequencies of the structure. Free vibration analysis is required first to calibrate the finite element model with the field ambient vibration test measurements. Secondly, to perform seismic response analysis using the modal time-history method, the natural frequencies and their associated mode shapes are required from free vibration. Free vibration analysis involves the solution of the following eigenvalue problem:

$$[M - \omega^2 K]u = 0 \qquad (4.1)$$

where **M** and **K** are system mass and stiffness matrices and $\boldsymbol{u}$ is modal displacement vector. The eigenvalue of a mode (ω^2) is the square of the circular frequency of that mode (ω) and relates to the cyclical frequency (f) by the relation $\mathbf{f = \omega/2\pi}$, and relates to the period of vibration (**T**) by the equation $\mathbf{T = 1/f}$.

SAP90 uses an "accelerated subspace iteration" algorithm to solve the eigenvalue problem. The subspace iteration method was developed by Bathe in 1971 and a detailed discussion of the method and its fundamentals can be found in Bathe (1982). Various techniques have been used to accelerate the basic subspace iteration method, and the particular algorithm used in the SAP90/SAP2000 programs can be found in Wilson and Tetsuji (1983).

Traditionally, mode-superposition analysis was performed using a structure's eigenvectors as the basis for the analysis. Research (Wilson, Yuan, and Dickens, 1982) indicates that this is not the best basis for a mode-superposition time-history analysis. Instead, a special set of load-dependent, orthogonal Ritz vectors yields more accurate results than the same number of natural mode shapes. Ritz vector analysis

significantly reduces computing time and automatically includes the proven numerical techniques of static condensation, Guyan reduction, and static correction due to higher mode truncation.

The reason that Ritz vector analysis yields better results than an equal number of eigenvectors is that the Ritz vectors take into account the spatial distribution of dynamic loading. In fact, the spatial distribution of loading serves as a starting load vector to begin the process of finding appropriate Ritz vectors. Subsequent Ritz vectors are formed based on the preceding Ritz vector and the neglected inertial effects. In contrast, the eigenvectors are computed from the stiffness and mass matrices only and, therefore, cannot account for the spatial distribution of loading. Eigenvectors that are orthogonal to loading do not participate in the structural response even if they are at or near the forcing frequency.

For model calibration, the natural frequencies and their mode shapes have to be accurate; therefore exact eigenvalues(natural frequencies) have been extracted. All the frequencies may not participate in calculating the response under seismic excitation kind of loading. In order to get full participation, many modes have to be extracted. In this work, around 450 modes were tried to improve the mass participation. But there was no increase in the mass participation. Therefore, Ritz-vector based (which are load dependent) extraction of eigenvalues has been carried out. This method gives more than 90% participation in all the three directions.

The natural frequencies and mass participation for the lowest 20 modes are presented in Table 4.1. Some of the frequencies and their mode shapes have been compared with the field testing in the earlier chapter. The natural frequency of the bridge ranges from 0.50 Hz to 2.65 Hz for the first 50 modes, and the period ranges from 1.998 sec to 0.3778 sec. The natural frequencies listed in Table 4.1 and their mode shapes are used only to calibrate the finite element model. They are not used for the seismic response analysis. It is seen from Table 4.1 that the mass participation of the first three modes are only in the transverse direction. Therefore, these three modes are treated as transverse modes based on the mass participation point of view, although there is some torsional and vertical displacement component as seen from Figure 4.2b.

Figures 4.2(a) and (b) show the first mode shape in isometric and plan views, respectively. The natural frequency of this mode is 0.50 Hz. The percentage of mass participation of this mode is about 3.35% (Table 4.1). This mode has a maximum modal displacement in the span C-D. Based on mass participation, this mode is identified as a transverse mode.

Figures 4.3(a) and (b) show the second mode shape with a frequency of 0.65 Hz in isometric and plan views, respectively. Contrary to the first mode, this mode has

two adjacent spans having modal deformations in the same direction. The mass participation for this mode is 0.02% . Based on mass participation, the second mode is also observed as a transverse mode.

Figures 4.4(a), (b) and (c) show the third mode shape with a frequency of 0.73 Hz in isometric and plan views, respectively. Based on mass participation, this mode is noted as the first vertical mode. The mass participation in the vertical direction is 1.1%. This mode has four half-waves along the length of the bridge.

The fourth mode shape in isometric view is shown in Figure 4.5. The natural frequency of this mode is 0.81 Hz. Based on mass participation and from Figures 4.5, it is seen that this mode is a transverse mode. The mass participation in the transverse direction is only 10.61%.

Figures 4.6(a) and (b) show the fifth mode shape with a frequency of 0.95 Hz, in the isometric and plan views, respectively. The mass participation for this mode is 7.18%. Based on mass participation, this mode is observed as a transverse mode.

The sixth mode shape in isometric, elevation and plan views is shown in Figures 4.7(a), (b) and (c), respectively. The natural frequency of this mode is 0.97 Hz, and the mass participation is 3.92% in the longitudinal direction and 0.14% in the vertical direction. Based on mass participation, this mode is treated as a vertical mode. Figures 4.8(a), (b) and (c) show the seventh mode shape with a frequency of 1.08 Hz. The mass participation is 90% in the longitudinal direction. Based on Figures 4.8(b) and (c), this mode is the first longitudinal mode.

Figures 4.9(a) and (b) show the eighth mode shape with a frequency of 1.11 Hz. The mass participation in the transverse direction 0.213%. Therefore, this mode is observed as a transverse mode. The ninth mode shape with a frequency of 1.21 Hz is shown in Figures 4.10(a), (b) and (c). The mass participation is only 0.326% in the transverse direction. This mode is identified as a transverse mode.

The tenth mode with a frequency of 1.30 Hz is shown in Figures 4.11(a), (b) and (c). The mass participation for this mode is 1.79% in vertical direction and 0.03% in the longitudinal direction. It is observed that this mode is a vertical mode.

Figures 4.12(a), (b) and (c) show the eleventh mode shape with a frequency of 1.36 Hz. The mass participation in transverse direction is 0.083%. This mode is identified as the transverse mode.

The twelveth mode shape with a frequency of 1.43 Hz is shown in Figure 4.13(a), (b) and (c). The mass participation for this mode is 2.46% in the vertical direction and 1.27% in the longitudinal direction. Based on the mode shape and mass

participation, this mode is identified as a transverse mode with many half-waves. Figures 4.14(a) and (b) show the thirteenth mode shape with a frequency of 1.47 Hz. The mass participation for this mode is 0.5% in the transverse direction. Therefore, this mode is identified as the transverse mode.

Figures 4.15(a) and (b) show the fourteenth mode shape with a frequency of 1.56 Hz. The mass participation for this mode is 0.347% in the transverse direction. Therefore, this mode is observed as a transverse mode. The fifteenth mode shape with a frequency of 1.57 Hz is shown in Figures 4.16(a) and (b). The mass participation for this mode is 0.462% in the transverse direction. Similar observations can be made for other modes from Table 4.1.

The mode shapes and natural frequencies discussed above consisted of all the system frequencies. For earthquake response analysis, all these frequencies and modes may not be excited and therefore all the frequencies are not required. The Ritz-vector based method yields frequencies and mode shapes that provide significant participation in all directions. These frequencies and their mass participation are presented in Table 4.2. By comparing Tables 4.1 and 4.2, it is seen that the modes with very less mass participation in all the three directions are omitted by Ritz vector based eigenvalue extraction method. From Table 4.2, it is seen that the mass participation in all the three directions are more than 90%, and this indicates that model will give reasonable response under earthquake type of loading.

5. Seismic Response Analysis

5.1 General

A number of different analytical methods have been developed for assessing the seismic vulnerability of existing bridges including elastic analysis, inelastic pushover analysis, capacity spectrum analysis and nonlinear dynamic analysis (Priestly et al. 1996). Each approach incorporates different assumptions and varies in complexity of application. The problem of an engineer assessing the seismic vulnerability of a bridge structure is to select the most appropriate and cost-effective method for performing the assessment. Under minor ground motions, a bridge will experience a little inelastic behavior and thus the linear elastic analysis is sufficient and reasonable for bridge design and assessment for minor earthquakes. A limitation of the elastic analysis method is that the linear analysis offers little information regarding the inelastic response of the structure. Disadvantages of nonlinear dynamic time-history analysis are that the structural elements of nonlinear models are considerably more complex than that of their linear elastic counterparts, the numerical algorithms do not always ensure convergence to a physically valid solution, processing and evaluation of the output often requires considerable effort, and the results can be extremely sensitive to input parameters and structural models.

In this work, modal time-history analysis is used because the bridge is assumed to behave elastically with small displacements under the expected earthquake loading. The modal time-history method was used instead of the response spectrum method for the main bridge due to the importance of the bridge and also due to the lack of seismic considerations in its initial design. Time-history analysis is the most sophisticated analysis technique available to the structural analyst. Using this level of analysis affords the engineer a complete description of the behavior of a structure at all times throughout an earthquake. Since no strong earthquake records are available for the Eastern U.S., time-history analyses for Kentucky bridges were performed using artificial earthquake records characteristic of the New Madrid and other nearby seismic zones.

The modal time-history method for the earthquake analysis involves the solution of the following equation of motion:

$$M\ddot{u} + C\dot{u} + Ku = -M\ddot{u}_g \qquad (5.1)$$

where **M, C** and **K** are the system mass, damping and stiffness matrices, respectively; $\ddot{u}$, $\dot{u}$ and u are the system nodal acceleration, velocity and displacement vectors. $\ddot{u}_g$ is the earthquake motion for which the bridge's response has to be calculated. The SAP90 software performs exact integration of the modal-response equations for a linear variation of the time-function between the input data time points. Therefore, the results are not dependent on the selection of a "time-integration interval" as in some other methods [Wislon and Habibullah, 1994]. Damping for all the modes is assumed to be 5%.

Time-histories representing the 50-year event and the 500-year event were generated for the vertical and two orthogonal horizontal directions in the report by Street et al. (1996). The 50-year event is defined as the peak horizontal particle acceleration, at the top of rock, that has a 90% probability of not being exceeded in 50 years (i.e. 10% probability of exceedance). Likewise, the 500-year event has a 90% probability of not being exceeded in 500 years. A recurrence rate (return period) can be calculated for the earthquakes which would produce the 50- and 500-year events.

The 50-year event that has a 10% probability of exceedance corresponds to AASHTO's (1996) design earthquake for highway bridges. For low probability of exceedance, the recurrence rate is approximately (National Highway Institute, 1996) the ratio of time and return period. Actual return period for the 50-year event is 475 years (Mayes et al. 1992). Some states require even longer return periods for their design earthquake. For example, California's Department of Transportation (Caltrans) uses a 2400-year return period, which has a 10% probability of exceedance every 250 years.

For the seismic zones affecting Kentucky, the 50-year and 500-year events defined in Street et al. (1996) correspond to the AASHTO design earthquake and near the maximum credible earthquake, respectively. For the bridge location in this study, Henderson, Kentucky, a time-history with peak horizontal acceleration of 15% gravity represents the AASHTO design earthquake. The time-history for the "near maximum credible earthquake" (500-year event) has a peak horizontal acceleration of 15% gravity in Henderson County.

5.2 Seismic Response

The seismic response of the US41 Southbound bridge is calculated for the 50-year earthquake. For the Henderson County bridge site, peak horizontal bedrock acceleration for this artificial earthquake is 15% gravity (Figure 5.1). For comparison, AASHTO's map (1996) of peak horizontal acceleration places the Henderson County bridge site in, approximately, the 25% gravity contour for the same probability event. Earthquake duration is 2.6 seconds with data points at 0.005 second intervals. The input motion along longitudinal, transverse and vertical directions is presented in Figures 5.2-5.4, respectively. The peak ground accelerations along horizontal, vertical and transverse directions are 56.3, 35.7 and 56 in/sec^2, respectively. Since the longitudinal direction of

the earthquake may not coincide with the longitudinal direction of bridge, it is necessary to analyze the bridge under different excitation cases as described in Table 5.1. Under LL11 excitation case, as mentioned in Table 5.1, the horizontal component of earthquake is applied along longitudinal direction of the bridge and vertical component of earthquake is applied along the vertical direction of the bridge. Similarly for other excitation cases, the vertical component of earthquake is considered to be acting in the vertical direction of the bridge. Only the horizontal and transverse components of earthquakes are reversed. On some excitation cases, all three components of earthquake are applied simultaneously.

Time-history analysis produces a very large quantity of output. It is difficult to monitor the maximum forces for all the members and maximum displacements at all the joints in a modal time-history analysis for the seismic excitation kind of loading. Therefore, members and joints are selected based on their proximity to critical locations. From SAP90 software, forces and moments are obtained for selected members. Stresses are calculated externally using simple computer programs/spreadsheets. Table 5.2 presents the cross-sectional properties of members that are selected for stress calculation.

As an example, for the L1T2V3 (Table 5.1) earthquake, the time history plots of transverse, vertical and longitudinal displacements at joint 44 (Fig. 2.5) are presented in Figures 5.5 through 5.7, respectively. It is observed that the maximum transverse displacement of 0.428" occurs at 0.845 secs, maximum vertical displacement of 0.36" occurs at 1.53 secs, and the maximum in longitudinal direction is 0.23" at 2.2 secs. The axial force time history for member 1 (Fig. 2.6) is presented in Figure 5.8. The maximum axial force of 299 kips occurs at 1.06 secs.

For stress calculations, the axial stresses are calculated from P/A and bending stresses are calculated from M_{12}/Z_{13} and M_{13}/Z_{12}. M_{12} and M_{13} are the bending moments in the local 1-2 and 1-3 planes respectively. Z_{12} and Z_{13} are the section modulus about the 1-2 and 1-3 planes, respectively. Combined stresses are calculated as the sum of P/A, M_{12}/Z_{13}, M_{13}/Z_{12} with appropriate signs to get the maximum stresses.

Axial stress = σ_a = Axial force/A
Bending stress in 1-2 plane at I^{th} joint = σ_{b12i} = Absolute(M_{12} at Node I / Z_{13})
Bending stress in 1-2 plane at J^{th} joint = σ_{b12j} = Absolute(M_{12} at Node J / Z_{13})
Bending stress in 1-3 plane at I^{th} joint = σ_{b13i} = Absolute(M_{13} at Node I / Z_{12})
Bending stress in 1-3 plane at J^{th} joint = σ_{b13j} = Absolute(M_{13} at Node J / Z_{12})

Combined axial and bending stress:

Stress at node I = $\sigma_a + \sigma_{b12i} + \sigma_{b13i}$
Stress at node J = $\sigma_a + \sigma_{b12j} + \sigma_{b13j}$

Shear stress is calculated from the shear forces in 1-2 and 1-3 plane, i.e.,

$$\text{Shear stress} = \tau = \sqrt{(SF_{12}^2 + SF_{13}^2)} / A$$

The absolute maximum of stresses obtained from the maximum and minimum responses from time-history analysis are presented in tabular form and are discussed in the following. Table 5.3 lists the stresses at selected members (Figs. 2.3-2.7) due to seismic excitation case L1T2V3 (Table 5.1). Due to earthquake motion alone, the axial stresses are with a maximum of 1.11 ksi in member 98. Bending stresses are calculated and presented at nodes I and J of the member. Table 5.3 also presents the maximum of the combined stresses from the Dead load ± Earthquake load (EQ) ± Thermal load (90° F). Shear stress is found to be much less with a maximum of 1.54 ksi in member 166. The maximum of combined axial and bending stress is found to be 39.2 ksi in member 66.

Table 5.4 lists the stresses at selected members (Figs. 2.3-2.7) when two of the excitation directions are reversed, i.e. under L2T1V3 (Table 5.1) case. Axial stresses due to seismic forces alone are found to have a maximum of 1.39 ksi in member 16. This Table 5.4 also presents the maximum of the combined stresses from the Dead load ± Earthquake load (EQ) ± Thermal load (90° F). Shear stresses are much less with a maximum of 1.56 ksi in member 166. Maximum of the combined stresses is found to be 40 ksi in member 66.

Under the seismic excitation case LL11, the stresses calculated for selected members (Figs. 2.3-2.7) are presented in Table 5.5. The maximum axial stress is found to be 2.34 ksi in member 205. Maximum of the combined axial and bending stress is found to be 3.304 ksi in member 295, which is less than the yield strength. Shear stress is found to have a maximum of 0.065 ksi in member 268.

Table 5.6 lists the stresses at selected members (Figs. 2.3-2.7) when the seismic excitation LL22 is applied. The maximum axial stress is found to be 2.45 ksi in member 205. The maximum of the combined axial and bending stress is 3.39 ksi in member 295, which is far less than the yield stress of steel. Shear stress is found to have a maximum of 0.077 ksi in member 268.

For the seismic excitation case TT11, the stresses at selected members (Figs. 2.3-2.7) are presented in Table 5.7. The maximum axial stress is found to be 2.45 ksi in member 205. Maximum of the combined axial and bending stress is 6.13 ksi in member 295, which is less than the yield strength of steel. Shear stress is found to have a maximum of 0.28 ksi in member 268.

Table 5.8 lists the stresses at selected members (Figs. 2.3-2.7) when the seismic excitation TT22 is applied. The maximum axial stress is found to be 2.48 ksi in member 205. Maximum of the combined axial and bending stresses is 5.22 ksi in member 295 which is less than the yield stress of steel. The shear stress is found to have a maximum of 0.19 ksi in member 268.

The stresses at selected members (Figs. 2.3-2.7) due to a differential temperature of 90°F are presented in Table 5.9. The coefficient of thermal expansion for steel is taken as 6.5×10^{-6}/°F. Maximum axial stress is found to be 11.57 ksi in member 1. Maximum shear stress is obtained as 0.066 ksi in member 268. Combined stress due to axial stress and bending stress is 21.45 ksi in member 1.

Table 5.10 lists the stresses at selected members (Figs. 2.3-2.7) due to the self-weight of the bridge. Maximum axial stress is found to be 20.07 ksi in member 98. Maximum shear stress is obtained as 1.41 ksi in member 166. Combined stresses from axial and bending stresses have a maximum of 24.6 ksi in member 98.

In previous calculations, the stresses produced were checked purely from the material yield point of view. Under earthquake loading, truss members may experience tensile force at one time interval and compressive force at some other time interval. Therefore, it is necessary to check for the buckling of truss members. Since the bridge truss members are subjected to axial forces and bending moments, the equations (10-42) to (10-44) from AASHTO is used to check whether they satisfy the inequality condition.

AASHTO Eq. (10.42):

$$\frac{C_{mx} f_{bx}}{\left(1 - \frac{f_a}{F_{ex}}\right) F_{bx}} + \frac{C_{my} f_{by}}{\left(1 - \frac{f_a}{F_{ey}}\right) F_{by}} \leq 1.0 \qquad (5.2)$$

AASHTO Eq. (10-43): At points of support

$$F_{ex} = \frac{\pi^2 E}{(0.75\ L/r)^2} \qquad (5.4)$$

$$\frac{f_a}{F_y} + \frac{f_{bx}}{F_{bx}} + \frac{f_{by}}{F_{by}} \leq 1.0 \qquad (5.3)$$

AASHTO Eq. (10-44): Euler Buckling Stress:

$$F_{ey} = \frac{\pi^2 E}{(0.75\ L/r_y)^2} \qquad (5.5)$$

In Table 5.11 and 5.12, the stresses are checked by also considering the buckling of the member for the earthquake excitation cases L1T2V3 and L2T1V3, respectively. It is seen that the inequalities given in equations 10-42 and 10-43 are satisfied and hence there will not be any member failure due to combined axial and bending stresses.

The displacements at selected nodes (Figs. 2.3-2.7) are presented in Table 5.13 for different excitation cases (Table 5.1). Maximum displacement in the longitudinal direction is 0.4" at joint 10 under LL22 case. Maximum displacement in the transverse direction is 0.61" at joint 127 under L1T2V3 case. Maximum displacement in the vertical direction is 0.46" at joint 8 under LL22 case.

Under static dead load and temperature, the displacements at selected joints (Figs. 2.3-2.7) are listed in Table 5.14. Due to a temperature difference of 90°F, maximum displacement in the longitudinal direction is 2.6" at joint 1. The transverse displacement is maximum at joint 101 is 0.298". Maximum vertical displacement is 1.304" at joint 62. Due to dead load, maximum longitudinal displacement is 1.69" at 140. Transverse displacement is with a maximum of 0.28" at joint 101. The maximum vertical displacement is 11.4" at joint 44.

Maximum and minimum base shears obtained for the bridge are listed in Table 5.15. These values are presented for different excitation cases listed in Table 5.1. Then, based on the translational stiffnesses of the piers, longitudinal and transverse seismic forces on top of the pier are calculated and presented in Table 5.16.

5.3 Capacity/Demand Ratios

Since the superstructure of the bridge is connected to the substructure through bearings, it is necessary to check these bearings against the anchor bolt shear failure. Table 5.16 lists the available anchor bolt shear capacity (V_c) and seismic forces on each pier. The anchor bolt capacity V_c is calculated by assuming the shear strength of the bolt as 18 ksi. The resultant of seismic force is calculated as the square root of the sum of squares (SRSS) of the longitudinal and transverse seismic forces. Then the seismic demand (V_b) is calculated by multiplying by 1.25 as per *FHWA Retrofitting manual.* All the piers have C/D ratio less than 1.0. Therefore, additional anchor bolts are required.

The expansion bearings at piers A, B and E are roller bearings. Hence complete loss-of-span may not occur. Therefore, the bearing displacement capacity/demand ratio is not calculated.

5.4 Retrofit for the Main Bridge

From the previous sections it is clear that all the bearings are to be strengthened to resist the 0.15g earthquake corresponding to 50-year event. It is suggested that additional anchor bolts may be provided to retrofit the bearings at piers A, B, C, D and E (Table 5.16). Alternatively, the existing bearings may be replaced with seismic isolation bearings. The recommendations are listed in Tables 5.16 and in Figures 5.9 through 5.13.

6. Approach Bridges

6.1 General

The US41 Southbound bridge over the Ohio river consists of straight approach spans towards Kentucky and Indiana. The approach bridges towards the Henderson, KY side and Evansville, IN side are shown in Figures 6.1a-b. The plan and elevation views of the Evansville, IN and Henderson, KY approaches are shown in Figures 6.2 and 6.3, respectively. The Evansville, IN approach, consists of a 5-span continuous unit, a 3-span continuous unit and a single span unit with a total length of 1096′. The Henderson, KY approach consists of 20 spans made of five continuous span units of a 3-span, three 4-spans and a 5-span covering a total length of 2038′. The bridge provides a clear 30′ wide roadway and 2′ wide side walk on either sides. The spans in both the approaches are supported on piers through fixed bearing and expansion bearing as indicated in Figures 6.2 and 6.3. All the piers and abutments are founded on friction piles which extend from 50′ to 120′ depending on the soil resistance.

The Evansville, IN approach has continuous 5 girder spans of approximately 151' each, continuous 3 girder spans of approximately 101' each and a single span of 31'. The 151' spans are made of two deck- type plate girders spaced at 28' c/c. The 7″ thick concrete deck is supported on steel stringer and floor beam system. The superstructure in the 100′-spans are made of 5 plate girders and diaphragm system supporting the concrete deck. The 31′ span is made of concrete girders supporting the deck and is monolithically constructed with the piers. The Henderson, KY approach has continuous 3-150′ spans made of 2 plate girders with floor beams and stringers supporting concrete deck, three numbers of 4-span continuous units and a 5-span continuous unit made of five girders and cross frame system supporting concrete deck of 7″ thick. The reinforced concrete bridge piers have two types of configurations. In type-I, a rectangular section which has a taper with batter of $\frac{1}{2}$″ per foot length is provided with a pier cap at the top extending to the width of the bridge. In pier type-II, 2-circular columns are connected by a web wall and are prismatic along the depth. The plan views in Figures 2 and 3 indicate the type of pier at any location. The sub-structure in the approach spans is made with class D concrete.

6.2 Structural Modeling

The approach spans in the Evansville, IN side and Henderson, KY side are idealized as simple structural units depending on the type of bearing (attachment of superstructure mass) to the pier top and the continuity of a unit. These idealized units are assumed to act independently when subjected to motion in the longitudinal direction of the bridge. These simplified systems are treated as single degree of freedom systems (SDOF) for mathematical modeling of the bridge in the longitudinal direction. The

models are designated as EV1 and EV2 for the Evansville, IN approach and HE1-HE5 for the Henderson, KY approach. The details of the components of these models are given in Figures 6.4 and 6.5 respectively. The mass of the SDOF systems is assumed to be contributed by the mass of the superstructure and one-third mass of the pier. The stiffness is the longitudinal translation stiffness of the piers that are calculated using $\frac{3EI}{L^3}$. If more than one pier is supporting a continuous deck by fixed bearing, their individual stiffness is added up. For type-I piers, the average moment of inertia of the pier is used for the stiffness calculation. Modulus of elasticity of concrete E is taken as 3600 ksi.

An important point to be noted is that there exists a lot of uncertainty in quantifying the soil-structure (pile foundation) interaction effect in the stiffness calculation. Due to the unavailability of detailed site soil investigations, representative models with maximum and minimum stiffness are adopted in the forces and displacements calculation, respectively. The maximum stiffness is obtained by assuming the pier is fixed at the bottom of pile cap. The minimum stiffness is obtained by assuming the pier is extended up to an imaginary depth equal to half-pile-length and fixed at this level. The extended length is assumed to have the same flexural properties as that of the pier. This simplified procedure for stiffness estimation has been validated to represent the most stiff and most flexible model and hence adopted for the conservative estimate of seismic forces and displacements in this study.

The weight calculation for the superstructure for different continuous units is given in Tables 6.1a-g. The dimensions and section properties of the pier and the calculation of stiffness (maximum and minimum) in the longitudinal direction for all the models in the approach spans are listed in Table 6.2. The mass includes one-third mass of the pier and full mass of the superstructure attached to the pier by fixed bearing.

6.3 Seismic Response Analysis

Since the bridge is located in Henderson county, KY, it is analyzed under seismic motion corresponding to 0.15g earthquake of the 50-year event. The response spectra of this earthquake is available in Street et al. (1996). The results of the seismic analysis are utilized to determine the possibility of any loss-of-span due to excessive longitudinal displacements at expansion bearings or shear failure of anchor bolts in fixed bearings. Seismic analysis is carried out using the response spectrum method.

The natural frequencies of the SDOF models are presented in Table 6.3 with corresponding masses and stiffness. The calculated natural frequencies range from 0.65 Hz to 0.85 Hz for the model with maximum stiffness, and 0.23 Hz to 0.38 Hz for the model with minimum stiffness.

The response spectra for the 50 year event for the Henderson county, KY shown in Figure 6.6 is reported in Street et al. (1996). The response spectra corresponds to a

damping of 5%. The site soil coefficient S is assumed as 1.5 for the calculation of factor C_s based on AASHTO formula (Div. IA, Section 3), as $\mathbf{C_s}=\frac{1.2(PSA)(S)}{g}$. The C_s is limited to 2.5A, i.e 0.375 as per AASHTO. Seismic forces and displacements are calculated and presented in Table 6.3. The calculated SDOF displacements range from 5.0 inch to 6.50 inches. The seismic forces range from 417 kips to 1041 kips.

6.4 Capacity/Demand Ratios

For both the approach spans, the bearing force capacity $V_b(c)$ / demand $V_b(d)$ ratios (r_{bf}), have been calculated as per section A.4.3 of FHWA Seismic Retrofitting Manual for Highway Bridges. The seismic force demand $V_b(d)$ is considered as the maximum of 1.25 × seismic force and 0.2 × weight of super structure. The anchor bolt ultimate shear capacity $V_b(c)$ is calculated by assuming the shear strength of bolt material as 19.0 ksi (for 33 ksi steel). The Capacity / Demand ratios are less than 1.0 for ten out of twelve supports having fixed bearings. Therefore, at those ten supports of both the approach spans, the fixed bearings are to be retrofitted so as to withstand the forces due to an earthquake.

For both the approach spans, the expansion bearing displacement Capacity/Demand ratios (r_{bd}) are calculated as per Section A.4.2, FHWA Seismic Retrofitting Manual for Highway Bridges, May 1995. The relative displacements occurring at the expansion bearings situated at the ends of continuous units are considered. All the expansion bearings are of roller type, and the method-2 is used for C/D calculations. The r_{bd} ratio is less than 1.0 for three out of twenty five supports having expansion bearings (rocker bearings). Therefore, replacement of those bearings by elastomeric bearings or providing cable restrainers is recommended in those cases to avoid any loss-of-span due to the relative displacements occurring due to an earthquake.

For the Evansville, IN approach, the bearing force capacity $V_b(c)$ /demand $V_b(d)$ ratios (r_{bf}) and displacement Capacity/Demand ratios are presented in Tables 6.4 and 6.5 respectively. Similarly for the Henderson, KY approach spans, the bearing force capacity $V_b(c)$ /demand $V_b(d)$ ratios (r_{bf}) and displacement Capacity/Demand ratios are presented in Tables 6.6 and 6.7 respectively.

6.5 Retrofit for the Approach Spans

From the previous sections it is clear that ten out twelve supports having fixed bearings are to be strengthened to resist the 0.15g earthquake corresponding to a 50-year event in the Henderson county. For both the approach spans, it is suggested that additional anchor bolts may be provided to retrofit these bearings. Alternatively, the existing fixed bearings may be replaced with seismic isolation bearings. For the expansion bearings where the Capacity/Demand ratio is less than one, it is suggested to replace the existing rocker bearings with elastomeric bearings or provide cable restrainers.

For the Evansville, IN approach spans, the retrofit recommendations for the fixed bearings are listed in Table 6.4 and in Figures 6.7 through 6.10, and for the expansion bearings in Tables 6.5 and in Figures 6.11 through 6.12. Similarly, for the Henderson, KY approach spans, the recommendations for the fixed bearings are presented in Table 6.6 and in Figures 6.13 through 6.18, and for the expansion bearings, the recommendations are in Table 6.7 and in Figure 6.19.

7. Conclusions and Recommendations

7.1 General

The US41 Southbound bridge over the Ohio river may be subjected to future earthquakes. Therefore, it is important to evaluate the bridge under the projected seismic motion. In this evaluation, since the bridge is located in Henderson Co. of Kentucky, 0.15g earthquake for the 50-year event is applied. Depending upon the importance of the bridge, it has been decided to use more rigorous methods for the evaluation of the main bridge and simplified methods for the approach spans.

7.2 Main Bridge

The seismic evaluation of the main bridge consisted of field ambient vibration testing, finite element modeling and seismic response analysis using the modal time-history method. Field testing was mainly carried out to identify the natural frequencies and their mode shapes. These frequencies and mode shapes have been compared with the results from the finite element model. Comparisons have been performed for three transverse modes, three vertical modes and one longitudinal mode.

Three dimensional finite element model was developed with frame elements and spring elements. This model has been calibrated with the field test for natural frequencies and mode shapes. Frequencies from the field test for the first modes in the transverse, vertical and longitudinal directions are 0.501, 0.7682 and 1.0688 Hz, respectively. Frequencies from the finite element model for the first modes in the transverse, vertical and longitudinal directions are 0.500, 0.7348 and 1.0758 Hz, respectively. Reasonable agreement between the field test and finite element model has been obtained.

Seismic response analyses have been carried out using the modal time-history method. Displacements of selected joints and stresses for selected members have been calculated. The results are presented also for different seismic excitation cases by reversing the seismic excitation directions. Stresses for selected members are also presented for combined earthquake, dead load and thermal loads. For the selected joints, under earthquake excitation, the maximum displacement in the transverse, vertical and longitudinal direction was found to be 0.61", 0.46" and 0.40", respectively. Maximum of combined axial and bending stress in the member is found to be 40 ksi. Bending stresses have been combined with axial stresses by considering the buckling of members. It was found that for the selected members buckling failure will not occur.

Bearing force Capacity/Demand ratios have been calculated for the bearings at all the piers. All the piers have C/D ratios less than 1.0, and hence retrofit is required in the form of additional anchor bolts. Alternatively, the existing bearings may be replaced with seismic isolation bearings. Recommendations for retrofit are listed in Table 5.16 and in Figures 5.9 through 5.13.

7.3 Approach Spans

The US41 Southbound bridge has approach spans on Kentucky and Indiana sides. Single-degree-of-freedom models were used along with response spectrum method for the seismic response analysis. Response analysis has been carried out only in the longitudinal direction of the bridge, and maximum displacement and force responses have been calculated. Displacement and force Capacity/Demand ratios have been calculated for all the supports of both the approach spans.

At ten out of twelve supports having fixed bearings of both the approach spans, force Capacity /Demand ratios were less than 1.0; therefore, retrofit in the form of additional anchor bolts or replacing existing fixed bearings with seismic isolation bearings is recommended. Displacement C/D ratios are less than 1.0 at three out of twenty-five supports having expansion bearings (rocker bearings), hence loss-of-span may occur from the displacement considerations. It is recommended to replace all those expansion bearings by elastomeric bearings or provide cable restrainers.

The retrofit recommendations, for the Evansville, IN approach, are presented in Table 6.4 and in Figures 6.7 through 6.10 for the fixed bearings, and in Table 6.5 and in Figures 6.11 through 6.12 for the expansion bearings. Similarly, for the Henderson, KY approach spans, the recommendations for the fixed bearings and expansion bearings are given in Table 6.6 and in Figures 6.13 through 6.18, and in Table 6.7 and in Figure 6.19, respectively.

REFERENCES

AASHTO, (1996), *Standard Specifications for Highway Bridges*, 16th Edition, American Association of State Highway and Transportation Officials, Washington D.C.

Abdel-ghaffer, A.M. and R. H. Scanlan (1985a), Ambient Vibration Studies of Golden Gate Bridge: I. Suspended Structure, ASCE J. of Engrg. Mech., 111(4), 463-482.

Abdel-ghaffer, A.M. and R. H. Scanlan (1985b), Ambient Vibration Studies of Golden Gate Bridge: II. ASCE J. of Engrg. Mech., 111(4).

Alampalli, S., and Fu, G., (1994), "Instrumentation for Remote and Continuous Monitoring of Structural Condition," Paper No. 940261 Presented at the Transportation Research Board's 73rd Annual Meeting, Washington D.C., January, 1994.

Bathe, K.J., (1982), *Finite Element Procedures in Engineering Analysis*, Prentice-Hall, Inc., Englewood Cliffs, New Jersey, chapter 12.

Buckland, P.G., et al., (1979), "Suspension Bridge Vibrations: Computed and Measured," *Journal of the Structural Division*, Vol. 105, No. ST5, pp. 859-874.

Buckle, I.G. and I. M. Friedland (editors), Seismic Retrofitting Manual for Highway Bridges, Report No. FHWA-RD-94-052, Federal Highway Administration, May 1995.

Chapra, S.C., and Canale, R.P., (1988), *Numerical Methods for Engineers*, 2nd Edition, McGraw-Hill, Inc., New York, New York, Chapter 13.

DADiSP 4.0 User Manual, (1995), DSP Development Corporation, Cambridge, Massachusetts.

Doll, H., (1994), "Eigenfrequencies and Normal Modes of the Norderelb Bridge Near Hamburg: Numerical and Measuring Investigations," Proceedings of *the 12th International Modal Analysis Conference*, Honolulu, Hawaii, pp. 449-455.

EERI, Loma Prieta earthquake renaissance report, Earthqukae spectra, Special supplement to Vol.6, 448pp, May 1990.

EERI, Northridge earthquake renaissance report, Earthquake spectra, Special supplement to Vol.11, 116pp, Feb.95.

Farrar, C., White, K., and Mayes, R., (1995), "Vibration Testing of the I-40 Bridge Before and After the Introduction of Damage," Presented at the North-American

Workshop on Instrumentation and Vibration Analysis of Highway Bridges, Cincinnati, Ohio, July, 1995.

Harik, I.E., D. Dietz, C. Hill and M.W. Guo, Seismic Evaluation and Retrofit of Bridges, Research Report KTC-96-5, Kentucky Transportation Center, University of Kentucky, 1997.

Harik, I.E., D. L. Allen, R. L. Street, M.W. Guo, R.C. Graves, J. Harrison and M. J. Gawry (1997a), Free and Ambient Vibration of Brent-Spence Bridge, ASCE J. of Struct. Engrg., 123(9), 1262-1268.

Harik, I.E., D. L. Allen, R. L. Street, M. W. Guo, R.C. Graves, J. Harrison, and M. J. Gawry(1997b), Seismic Evaluation of Brent-Spence Bridge, ASCE J. of Struct. Engrg., 123(9), 1269-1275.

Harik, I.E., C.M. Madasamy, D. Chen, L. Zhou, K. Sutterer, R. Street, and D.L. Allen , Seismic Evaluation of the Ohio River Bridge on US51 at Wickliffe, KY, Research Report KTC-98-20, Kentucky Transportation Center, University of Kentucky, 1998.

Hudson, D.E., (1977), "Dynamic Tests of Full-Scale Structures," Journal of the Engineering Mechanics Division, Vol. 103, No. EM6, pp. 1141-1157.

Mayes, R.L., et al., (1992), "AASHTO Seismic Isolation Design Requirements for Highway Bridges," *Journal of Structural Engineering*, Vol. 118, No. 1, pp. 284-304.

National Highway Institute (NHI) Course No. 13063, (1996), "Seismic Bridge Design Applications," Notes from Sessions 1 & 2.

Nuttli, O.W., and R.B. Herrman (1978), State-of-the-art for assessing earthquake hazards in the United States: Report 12, Credible earthquakes for the central United States, U.S. Army Corps of Engineers Miscellaneous Paper S-73-1, 99pp.

Obermeier, S.F., P.J. Munson, C.A. Munson, J.R. Martin, A.D.Frankel, T.L.Youd, and E.C.Pond (1992), Liquefaction evidence for strong Holocene earthquakes in the Wabash Valley of Indiana-Illinois, Seismological Research Letters,63, 321-335.

Paultre, P., Proulx, J., and Talbot, M., (1995), "Dynamic Testing Procedures for Highway Bridges Using Traffic Loads," *Journal of Structural Engineering*, Vol. 121, No. 2, pp. 362-376.

Press, W.H., et al., (1992), *Numerical Recipes in FORTRAN: The Art of Scientific Computing*, 2nd Edition, Cambridge University Press, New York, New York, chapter 12.

Priestly, M.J.N., F. Seible and G. M. Calvi, Seismic Design and Retrofit of Bridges, John-Wiley & Sons, Inc., 1996.

Saiidi, M., Douglas, B., and Feng, S., (1994), "Prestress Force Effect on vibration Grequency of Concrete Bridges," *Journal of Structural Engineering*, Vol. 120, No. 7, pp. 2233-2241.

Shahawy, M.A., (1995), "Non Destructive Strength Evaluation of Florida Bridges," Proceedings of SPIE Nondestructive Evaluation of Aging Infrastructure Conference, Oakland, California, June, 1995.

Shelley, S.J., et al., (1995), "Dynamic Testing (Vibration Analysis) of Highway Bridges," Notes Presented at the *North-American Workshop on Instrumentation and Vibration Analysis of Highway Bridges*, Cincinnati, Ohio, July, 1995.

Stover, C.W. and Hoffman, J.L. (1993), Seismicity of the United States, 1568-1989 (Revised), U.S. Geological Survey Professional Paper 1527, 418 p.

Taylor, K.B., R.B. Herrmann, M.W. Hamburger, G.L. Pavlis, A. Johnston, C. Langer, and C. Lam (1989), The Southern Illinois Earthquake of 10 June 1987, Seismological Research Letters, 60, 101-110.

Street, R., Z. Wang, I. E. Harik, D. L. Allen and J. J. Griffin, Source Zones, Recurrence Rates, and Time Histories for Earthquakes Affecting Kentucky, Report No. KTC-96-4, Kentucky Transportation Center, University of Kentucky, 1996.

Ventura, C.E., Felber, A.J., and Prion, G.L., (1994), "Seismic Evaluation of a Long Span Bridge by Modal Testing," Proceedings of the *12th International Modal Analysis Conference*, Honolulu, Hawaii, pp. 1309-1315.

Wendichansky, D.A., Chen, S.S., and Mander, J.B., (1995), "In-Situ Performance of Rubber Bearing Retrofits," Presented at National Seismic Conference on Bridges and Highways, San Diego, California, December, 1995.

Wilson, E.L. and A. Habibullah, SAP90 - Structural Analysis Users Manual, Computers and Structures, Inc, May 1992.

Wilson, E.L., M.W. Yuvan, and J.M. Dickens (1982), Dynamic Analysis by Direct Superposition of Ritz Vectors, Earthquake Engineering and Structural Dynamics, 10, 813-823.

Wilson, E.L., and Tetsuji, I.J., (1983), "An Eigensolution Strategy for Large Systems," *Computers and Structures*, Vol. 16, pp. 259-265.

Zimmerman, R. M. and Brittain, R. D. (1979), Seismic response of multi-simple span highway bridges, In: proceedings of the 3rd Canadian Conference on Earthquake Engg., Montreal, pp1091-1120.

Table 3.1a US41 Southbound Bridge Testing Details - Moving Stations on Right Lane

Station	Filename	Accelerometer Block	Channel Number (xx)	Orientation
25	A1chXX.dat	Yellow	20 21 22	Horizontal Transverse Vertical
24		White	17 18 19	Horizontal Transverse Vertical
23		Red	14 15 16	Horizontal Transverse Vertical
22		Orange	11 12 13	Horizontal Transverse Vertical
21		Green	8 9 10	Horizontal Transverse Vertical
20	A2chXX.dat	Yellow	20 21 22	Horizontal Transverse Vertical
19		White	17 18 19	Horizontal Transverse Vertical
18		Red	14 15 16	Horizontal Transverse Vertical
17		Orange	11 12 13	Horizontal Transverse Vertical
16		Green	8 9 10	Horizontal Transverse Vertical
15	A3chXX.dat	Yellow	20 21 22	Horizontal Transverse Vertical
14		White	17 18 19	Horizontal Transverse Vertical
13		Red	14 15 16	Horizontal Transverse Vertical
12		Orange	11 12 13	Horizontal Transverse Vertical
11		Green	8 9 10	Horizontal Transverse Vertical
10	A4chXX.dat	Yellow	20 21 22	Horizontal Transverse Vertical
9		White	17 18 19	Horizontal Transverse Vertical
8		Red	14 15 16	Horizontal Transverse Vertical
7		Orange	11 12 13	Horizontal Transverse Vertical
6		Green	8 9 10	Horizontal Transverse Vertical
5	A5chXX.dat	Yellow	20 21 22	Horizontal Transverse Vertical
4		White	17 18 19	Horizontal Transverse Vertical
3		Red	14 15 16	Horizontal Transverse Vertical
2		Orange	11 12 13	Horizontal Transverse Vertical
1		Green	8 9 10	Horizontal Transverse Vertical

Table 3.1b US41 Southbound Bridge Testing Details - Base Station on Right Lane

Moveable Station Locations	Filename	Accelerometer Block	Channel Number (XX)	Orientation
25 24 23 22 21	B1chXX.dat	Black	0 1 2	Horizontal Transverse Vertical
		Blue	3 4 5	Horizontal Transverse Vertical
20 19 18 17 16	B2chXX.dat	Black	0 1 2	Horizontal Transverse Vertical
		Blue	3 4 5	Horizontal Transverse Vertical
15 14 13 12 11	B3chXX.dat	Black	0 1 2	Horizontal Transverse Vertical
		Blue	3 4 5	Horizontal Transverse Vertical
10 9 8 7 6	B4chXX.dat	Black	0 1 2	Horizontal Transverse Vertical
		Blue	3 4 5	Horizontal Transverse Vertical
5 4 3 2 1	B5chXX.dat	Black	0 1 2	Horizontal Transverse Vertical
		Blue	3 4 5	Horizontal Transverse Vertical

Black Accelerometer: West side of Bridge (Left lane)
Blue Accelerometer: East side of Bridge (Right lane)
All data saved in g's

Table 3.2a US41 Soutbound Bridge Testing Details- Moving Station on Left Lane

Station	Filename	Accelerometer Block	Channel Number (xx)	Orientation
25	C1chXX.dat	Yellow	20 21 22	Horizontal Transverse Vertical
24		White	17 18 19	Horizontal Transverse Vertical
23		Red	14 15 16	Horizontal Transverse Vertical
22		Orange	11 12 13	Horizontal Transverse Vertical
21		Green	8 9 10	Horizontal Transverse Vertical
20	C2chXX.dat	Yellow	20 21 22	Horizontal Transverse Vertical
19		White	17 18 19	Horizontal Transverse Vertical
18		Red	14 15 16	Horizontal Transverse Vertical
17		Orange	11 12 13	Horizontal Transverse Vertical
16		Green	8 9 10	Horizontal Transverse Vertical
15	C3chXX.dat	Yellow	20 21 22	Horizontal Transverse Vertical
14		White	17 18 19	Horizontal Transverse Vertical
13		Red	14 15 16	Horizontal Transverse Vertical
12		Orange	11 12 13	Horizontal Transverse Vertical
11		Green	8 9 10	Horizontal Transverse Vertical
10	C4chXX.dat	Yellow	20 21 22	Horizontal Transverse Vertical
9		White	17 18 19	Horizontal Transverse Vertical
8		Red	14 15 16	Horizontal Transverse Vertical
7		Orange	11 12 13	Horizontal Transverse Vertical
6		Green	8 9 10	Horizontal Transverse Vertical
5	C5chXX.dat	Yellow	20 21 22	Horizontal Transverse Vertical
4		White	17 18 19	Horizontal Transverse Vertical
3		Red	14 15 16	Horizontal Transverse Vertical
2		Orange	11 12 13	Horizontal Transverse Vertical
1		Green	8 9 10	Horizontal Transverse Vertical

Table 3.2b US41 Southbound Bridge Testing Details - Base Station on Left Lane

Moveable Station Locations	Filename	Accelerometer Block	Channel Number (XX)	Orientation
25 24 23 22 21	D1chXX.dat	Black	0 1 2	Horizontal Transverse Vertical
		Blue	3 4 5	Horizontal Transverse Vertical
20 19 18 17 16	D2chXX.dat	Black	0 1 2	Horizontal Transverse Vertical
		Blue	3 4 5	Horizontal Transverse Vertical
15 14 13 12 11	D3chXX.dat	Black	0 1 2	Horizontal Transverse Vertical
		Blue	3 4 5	Horizontal Transverse Vertical
10 9 8 7 6	D4chXX.dat	Black	0 1 2	Horizontal Transverse Vertical
		Blue	3 4 5	Horizontal Transverse Vertical
5 4 3 2 1	D5chXX.dat	Black	0 1 2	Horizontal Transverse Vertical
		Blue	3 4 5	Horizontal Transverse Vertical

Black Accelerometer: East Side of Bridge (Left lane)
Blue Accelerometer: West Side of Bridge (Right lane)
All data saved in g's
Sampling rate is 1002 Hz

Table 3.3 Frequency Identification from the Field Test Data

Field Tested Frequencies, f_1 (Hz)	Number of Peaks			Mode Type	Finite Element Frequencies, f_2 (Hz)	Relative Error 100*(f1-f2)/f1
	Transverse	Vertical Direction	Longitudinal			
0.1336	15	14	14			
0.167	6	8	9			
0.2004	7	8	6			
0.2338	10	10	8			
0.2672	8	8	6			
0.3006	6	5	8			
0.334	11	8	8			
0.3674	8	9	9			
0.4008	4	10	6			
0.4342	7	6	7			
0.4676	11	4	7			
0.501	**8**	6	10	**First Transverse**	0.500454	0.109101
0.5344	5	11	5			
0.5678	6	9	10			
0.6012	**11**	9	**8**	**Second Transverse**	0.647442	7.142261
0.6346	7	4	6			
0.668	6	6	10			
0.7014	5	5	8			
0.7348	9	7	9			
0.7682	7	**15**	9	**First Vertical**	0.734827	4.541613
0.8016	11	5	9	**Third Transverse**	0.812302	1.31749
0.835	5	6	7			
0.8684	16	7	10			
0.9352	4	9	3			
0.9686	2	9	12			
1.002	15	9	3			
1.0354	6	**12**	4	**Second Vertical**	0.966303	3.694183
1.0688	11	8	**19**	**First Longitudinal**	1.075847	3.759549
1.1022	5	5	6			
1.1356	14	11	7			
1.169	6	8	13			
1.2024	10	7	5			
1.2358	2	4	6			
1.2692	10	3	5			
1.3026	10	5	4			
1.336	7	**19**	18	**Third Vertical**	1.297047	0.428126
1.3694	4	3	3			
1.4028	5	9	5			
1.4362	9	2	12			
1.4696	5	2	1			
1.503	14	15	11			
1.5364	8	3	9			
1.5698	3	16	10			
1.6032	11	3	4			
1.6366	5	16	10			

Table 3.3 (Cont'd) Frequency Identification from the Field Test Data

Field Tested Frequencies (Hz)	Number of Peaks			Mode Type	Finite Element Frequencies (Hz)	Relative Error 100*(f1-f2)/f1
	Transverse	Vertical	Longitudinal			
1.67	14	8	3			
1.7034	6	9	11			
1.7368	4	7	1			
1.7702	5	3	11			
1.8036	14	10	9			
1.837	6	9	10			
1.8704	6	2	10			
1.9038	4	16	2			
1.9372	13	7	10			
1.9706	7	10	5			
2.004	12	5	10			

Table 4.1 Natural Frequencies and Mass Participation of the Main Bridge (Exact Eigen System)

Mode Number	Angular Frequency (rad/sec)	Circular Frequency (Hz)	Period (sec)	Mass Participation			Cumulative Mass Participation		
				X-DIR	Y-DIR	Z-DIR	X-SUM	Y-SUM	Z-SUM
1	3.14	0.50	1.9982	0	3.353	0	0	3.353	0
2	4.07	0.65	1.5445	0	0.024	0	0	3.377	0
3	4.62	0.73	1.3609	0	0	1.104	0	3.377	1.104
4	5.10	0.81	1.2311	0	10.608	0	0	13.985	1.104
5	5.99	0.95	1.0486	0.001	7.184	0	0.001	21.169	1.104
6	6.07	0.97	1.0349	3.917	0.003	0.138	3.918	21.172	1.242
7	6.76	1.08	0.9295	90.012	0	0.004	93.93	21.172	1.246
8	6.99	1.11	0.8985	0.001	0.213	0	93.931	21.385	1.246
9	7.59	1.21	0.8278	0	0.326	0	93.931	21.711	1.246
10	8.15	1.30	0.7710	0.025	0	1.791	93.956	21.711	3.037
11	8.52	1.36	0.7379	0.03	0.083	0	93.986	21.793	3.037
12	8.96	1.43	0.7015	1.266	0.019	2.457	95.252	21.812	5.494
13	9.23	1.47	0.6810	0.021	0.501	0.03	95.273	22.313	5.524
14	9.81	1.56	0.6406	0	0.347	0.004	95.273	22.66	5.529
15	9.85	1.57	0.6382	0	0.462	0.011	95.273	23.121	5.54
16	9.91	1.58	0.6342	0.158	0.001	8.746	95.432	23.123	14.286
17	10.70	1.71	0.5847	0.284	0.027	0.214	95.716	23.149	14.5
18	10.80	1.72	0.5815	2.181	0.002	2.358	97.898	23.151	16.857
19	11.50	1.83	0.5459	0	0.616	0	97.898	23.767	16.857
20	12.30	1.96	0.5110	0	0.04	0.004	97.898	23.807	16.862
21	12.30	1.96	0.5096	0.011	0	0.689	97.909	23.807	17.551
22	12.70	2.02	0.4959	0	0.134	0.004	97.91	23.941	17.555
23	13.10	2.08	0.4808	0.696	0	0.079	98.605	23.941	17.633
24	13.50	2.15	0.4647	0	0.186	0	98.605	24.127	17.633
25	14.30	2.27	0.4397	0	0	0.003	98.605	24.127	17.637
26	14.50	2.30	0.4346	0	0	0.001	98.605	24.127	17.638
27	14.50	2.31	0.4336	0.003	0	0.001	98.608	24.127	17.639
28	14.90	2.38	0.4209	0	0.03	0	98.608	24.157	17.639
29	15.00	2.39	0.4185	0.001	0	0.002	98.609	24.157	17.64
30	15.00	2.39	0.4183	0	0	0.004	98.609	24.157	17.645
31	15.10	2.41	0.4157	0	0	0.003	98.609	24.157	17.648
32	15.10	2.41	0.4148	0.001	0.004	0.001	98.61	24.161	17.649
33	15.20	2.42	0.4140	0	0	0.001	98.61	24.162	17.65
34	15.20	2.42	0.4139	0	0.066	0.002	98.61	24.228	17.652
35	15.20	2.42	0.4137	0	0.192	0.001	98.61	24.42	17.653
36	15.20	2.42	0.4133	0	0	0.003	98.61	24.42	17.655
37	15.20	2.42	0.4130	0.001	0	0	98.611	24.42	17.656
38	15.30	2.44	0.4103	0	0	0.001	98.612	24.42	17.657
39	15.40	2.45	0.4079	0	0	0	98.612	24.42	17.657
40	15.40	2.45	0.4077	0	0	0	98.612	24.42	17.657
41	15.40	2.46	0.4072	0	0.001	0	98.612	24.421	17.657
42	16.10	2.57	0.3891	0.011	0.004	0.008	98.623	24.425	17.665
43	16.20	2.58	0.3880	0	0	0	98.623	24.425	17.665
44	16.20	2.58	0.3877	0	0	0.028	98.623	24.425	17.693
45	16.30	2.60	0.3853	0	0	0.006	98.623	24.425	17.699
46	16.30	2.60	0.3852	0	0.001	0.017	98.623	24.426	17.715
47	16.40	2.61	0.3839	0.001	0.001	0.007	98.624	24.427	17.722
48	16.50	2.63	0.3801	0.003	0.005	0.007	98.627	24.432	17.73
49	16.60	2.63	0.3796	0	0	0	98.627	24.432	17.73
50	16.60	2.65	0.3778	0	0.004	0.001	98.627	24.435	17.731

Table 4.2 Natural Frequencies and Mass Participation of the Main Bridge (Ritz-vector based)

Mode Number	Angular Frequency (rad/sec)	Circular Frequency (Hz)	Period (sec)	Mass Participation			Cumulative Mass Participation		
				X-DIR	Y-DIR	Z-DIR	X-SUM	Y-SUM	Z-SUM
1	3.14	0.50	1.9982	0	3.353	0	0	3.353	0
2	4.07	0.65	1.5445	0	0.024	0	0	3.377	0
3	4.62	0.73	1.3609	0	0	1.105	0	3.377	1.105
4	5.10	0.81	1.2311	0	10.607	0	0	13.984	1.105
5	5.99	0.95	1.0486	0.001	7.186	0	0.001	21.171	1.105
6	6.07	0.97	1.0349	3.917	0.003	0.138	3.917	21.174	1.243
7	6.76	1.08	0.9295	90.013	0	0.004	93.93	21.174	1.247
8	6.99	1.11	0.8985	0.001	0.212	0	93.932	21.386	1.247
9	7.59	1.21	0.8278	0	0.325	0	93.932	21.711	1.248
10	8.15	1.30	0.7710	0.024	0	1.789	93.956	21.712	3.037
11	8.52	1.36	0.7379	0.03	0.083	0	93.986	21.794	3.037
12	8.96	1.43	0.7015	1.266	0.019	2.454	95.252	21.813	5.491
13	9.23	1.47	0.6810	0.021	0.502	0.031	95.273	22.315	5.522
14	9.81	1.56	0.6406	0	0.348	0.005	95.274	22.663	5.527
15	9.85	1.57	0.6382	0	0.459	0.011	95.274	23.122	5.538
16	9.91	1.58	0.6342	0.158	0.001	8.747	95.431	23.124	14.285
17	10.70	1.71	0.5847	0.286	0.027	0.215	95.717	23.151	14.5
18	10.80	1.72	0.5815	2.18	0.001	2.357	97.897	23.152	16.856
19	11.50	1.83	0.5459	0	0.61	0	97.897	23.762	16.856
20	12.30	1.96	0.5110	0	0.037	0.005	97.897	23.799	16.861
21	12.30	1.96	0.5096	0.011	0	0.688	97.908	23.799	17.549
22	12.70	2.02	0.4959	0.001	0.132	0.004	97.909	23.932	17.553
23	13.10	2.08	0.4809	0.695	0	0.079	98.604	23.932	17.632
24	13.50	2.15	0.4647	0	0.18	0	98.604	24.112	17.632
25	14.30	2.28	0.4389	0	0	0.004	98.604	24.112	17.636
26	14.60	2.32	0.4318	0.005	0	0.001	98.609	24.112	17.637
27	15.10	2.41	0.4149	0	0.131	0.009	98.609	24.243	17.646
28	15.20	2.41	0.4144	0	0.164	0.008	98.609	24.406	17.653
29	15.60	2.48	0.4031	0.007	0	0.001	98.616	24.407	17.654
30	16.30	2.60	0.3844	0.003	0.013	0.082	98.619	24.42	17.736
31	16.70	2.65	0.3771	0.024	0.024	0.001	98.643	24.444	17.737
32	16.90	2.69	0.3712	0.001	0.761	0	98.644	25.205	17.737
33	18.60	2.95	0.3386	0.044	1.582	0.035	98.688	26.787	17.772
34	18.60	2.96	0.3380	0.005	10.816	0	98.693	37.603	17.772
35	19.00	3.03	0.3303	0.001	0.281	0.499	98.695	37.884	18.271
36	20.80	3.31	0.3017	0.007	0.338	1.012	98.701	38.222	19.284
37	21.40	3.41	0.2931	0	25.093	0.018	98.701	63315	19.302
38	22.90	3.64	0.2748	0.001	13.436	0.005	98.702	76.751	19.307
39	22.90	3.64	0.2744	0.477	0.032	0.022	99.179	76.783	19.329
40	26.20	4.17	0.2399	0.73	0.002	0.017	99.91	76.785	19.346
41	27.80	4.42	0.2263	0.01	0.289	0.8	99.92	77.074	20.146
42	28.70	4.57	0.2188	0	0.981	0.307	99.92	78.055	20.452
43	31.50	5.02	0.1992	0.03	0.006	0.324	99.951	78.061	20.777
44	34.80	5.54	0.1807	0.004	0.009	5.195	99.954	78.069	25.971
45	40.30	6.41	0.1559	0.017	0.011	0.105	99.972	78.08	26.076
46	44.50	7.08	0.1412	0	9.907	0.105	99.972	87.987	26.181
47	49.20	7.83	0.1278	0	0.503	7.842	99.972	88.49	34.023
48	54.50	8.68	0.1152	0.028	0.021	0.162	99999	88.512	34.186
49	57.70	9.18	0.1089	0	10.072	0.399	99.999	98.584	34.585
50	68.00	10.82	0.0924	0	0.023	54.751	99.999	98.607	89.336

Table 5.1 Description of Seismic Excitation Cases

Seismic Excitation Cases	Description
LL11	Horizontal Component of 50-year Earthquake Applied Along Longitudinal Direction of the Bridge.
LL22	Transverse Component of 50-year Earthquake Applied Along Longitudinal Direction ofthe Bridge.
TT11	Horizontal Component of 50-year Earthquake Applied Along Transverse Direction of the Bridge.
TT22	Transverse Component of 50-year Earthquake Applied Along Transverse Direction of the Bridge.
L1T2V3	Horizontal, Vertical and Transverse Component of 50-year Earthquake are Applied Along Longitudinal, Vertical, and Transverse Directions respectively.
L2T1V3	Horizontal, Vertical and Transverse Component of 50-year Earthquake are Applied Along Transverse, Vertical, and Longitudinal Directions respectively.

Table 5.2 Cross Sectional Properties of Members for Stress Calculation

Member Number	Area A (in^2)	Moment of Inertia, I_{13} (in^4)	Section Modulus, Z_{13} (in^3)	Distance from centroid to extrem fiber, y (in)	Moment of Inertia, I_{12} (in^4)	Section Modulus, Z_{12}, (in^3)	Distance from centroid to extreme fiber, x (in)
1	60.438	3070	252.2	12.1875	2110	237.4	8.875
16	85.781	4280	349.4	12.25	3300	371.8	8.875
17	104.344	5140	419.9	12.25	4460	492.5	9.0625
32	104.344	5140	419.9	12.25	4460	492.5	9.0625
33	85.781	4280	349.4	12.25	3300	371.8	8.875
54	85.781	4280	349.4	12.25	3300	371.8	8.875
55	96.586	4710	384.6	12.25	3930	438.0	8.96875
66	60.906	2790	228.6	12.1875	1880	201.8	9.3125
81	55.563	2300	192.0	12	3270	405.3	8.0625
82	55.625	2300	192.0	12	3320	408.7	8.125
97	55.625	2300	192.0	12	3320	408.7	8.125
98	55.563	2300	192.0	12	3270	405.3	8.0625
119	55.563	2300	192.0	12	3270	405.3	8.0625
120	55.563	2300	192.0	12	3270	405.3	8.0625
131	68	5000	406.0	12.3125	4100	453.9	9.03125
163	78.25	5960	483.9	12.3125	4640	509.9	9.09375
166	23.438	840	116.9	7.1875	1100	125.1	8.8125
167	74.875	5100	417.5	12.21875	4700	515.2	9.125
168	72.75	4770	391.7	12.1875	4650	509.6	9.125
169	86	5860	478.6	12.25	5410	586.5	9.21875
171	23.438	840	116.9	7.1875	1100	125.1	8.8125
205	23.438	840	116.9	7.1875	1100	125.1	8.8125
209	86	5860	478.6	12.25	5410	586.5	9.21875
210	74.875	5100	417.5	12.21875	4700	515.2	9.125
211	72.75	4770	391.7	12.1875	4650	509.6	9.125
212	78.25	5960	483.9	12.3125	4640	509.9	9.09375
217	23.438	840	116.9	7.1875	1100	125.1	8.8125
262	78.25	5960	483.9	12.3125	4640	509.9	9.09375
265	23.438	840	116.9	7.1875	1100	125.1	8.8125
266	77	5430	443.4	12.25	4750	520.8	9.125
267	74.875	5100	417.5	12.21875	4700	515.2	9.125
268	23.438	840	116.9	7.1875	1100	125.1	8.8125
269	86	5860	478.6	12.25	5410	586.5	9.21875
295	50.875	3950	323.2	12.21875	2960	333.6	8.875

Table 5.3 Stresses (ksi) in Members due to Seismic Excitation Case L1T2V3[a], Dead Load and Temperature

Member Number	Stresses due to L1T2V3 Earthquake								Maximum stresses from (DL ± EQ ± Temperature)		
	Axial Stress	Bending stress in 1-2 plane		Bending stress in 1-3 plane		Combined stress		Shear stress			
		Node I	Node J	Node I	Node J	Node I	Node J		Combined stress at Node I	Combined stress at Node J	Shear
1	0.494	0.46	0.24	0.386	0.182	1.294	0.901	0.008	36.675	23.287	0.641
16	0.88	0.265	0.386	0.077	0.254	1.213	1.45	0.003	11.126	11.059	0.357
17	0.808	0.474	0.255	0.366	0.113	1.604	1.175	0.007	14.724	13.541	0.36
32	0.818	0.329	0.553	0.118	0.343	1.219	1.714	0.009	14.029	15.736	0.338
33	0.828	0.541	0.332	0.193	0.081	1.561	1.227	0.003	13.258	15.65	0.056
54	0.867	0.246	0.55	0.129	0.268	1.216	1.685	0.003	16.33	16.433	0.065
55	0.799	0.569	0.26	0.365	0.168	1.678	1.227	0.002	14.511	11.615	0.058
66	0.787	0.289	0.674	0.176	0.359	1.213	1.82	0.003	30.822	39.187	0.058
81	1.049	0.267	0.303	0.022	0.074	1.338	1.314	0.004	24.955	26.426	0.651
82	1.095	0.217	0.22	0.064	0.03	1.349	1.344	0.013	23.322	25.276	0.724
97	1.097	0.233	0.29	0.028	0.049	1.356	1.436	0.01	29.973	27.005	0.647
98	1.105	0.341	0.309	0.052	0.038	1.495	1.452	0.003	27.74	31.457	0.13
119	0.739	0.202	0.329	0.028	0.053	0.961	1.092	0.002	28.425	27.433	0.11
120	0.759	0.227	0.239	0.042	0.035	1.003	1.016	0.015	26.349	29.435	0.035
131	0.377	0.424	0.242	2.247	1.868	3.048	2.324	0.002	9.8	7.951	0.433
163	0.454	0.271	0.068	1.041	0.331	1.731	0.854	0.007	7.239	9.366	0.509
166	1.019	0.584	0.302	0.523	0.263	2.116	1.584	0.034	20.086	19.654	1.537
167	0.559	0.202	0.081	1.444	0.862	2.188	1.443	0.003	10.135	12.543	0.481
168	0.396	0.105	0.104	0.445	0.275	0.905	0.774	0.013	7.912	8.819	0.498
169	0.744	0.37	0.364	1.349	0.832	2.463	1.907	0.002	10.96	9.237	0.36
171	1.003	0.184	0.239	0.282	0.533	1.451	1.76	0.007	19.121	18.341	1.32
205	1.07	0.278	0.16	0.453	0.22	1.707	1.418	0.007	18.927	18.79	1.307
209	0.654	0.474	0.395	1.304	0.812	2.433	1.857	0.002	11.426	9.452	0.366
210	0.538	0.22	0.058	1.413	0.844	2.171	1.4	0.002	12.311	14.238	0.068
211	0.385	0.105	0.122	0.418	0.239	0.897	0.746	0.005	10.629	10.791	0.098
212	0.799	0.845	0.897	1.21	0.759	2.803	2.233	0.003	6.956	9.163	0.063
217	1.071	0.24	0.448	0.262	0.569	1.566	1.987	0.007	18.11	22.619	0.302
262	0.707	0.804	1.252	1.139	0.694	2.276	2.653	0.003	7.576	11.811	0.078
265	0.904	0.371	0.134	0.34	0.182	1.604	1.22	0.006	21.652	16.807	0.263
266	0.403	0.345	0.08	1.231	0.734	1.915	1.217	0.003	10.499	13.064	0.065
267	0.305	0.172	0.167	0.351	0.206	0.784	0.652	0.002	10.097	10.006	0.075
268	0.89	0.241	0.378	0.228	0.447	1.261	1.644	0.204	17.159	17.834	0.703
269	0.683	0.796	0.848	1.032	0.636	2.329	2.067	0.001	8.6	4.668	0.049
295	0.773	1.491	1.501	2.038	1.759	4.243	3.877	0.002	9.778	9.445	0.003

[a] Seismic excitation cases described in Table 5.1

Table 5.4 Stresses (ksi) in Members due to Seismic Excitation Case L2T1V3[a], Dead Load and Temperature

Member Number	Stresses due to L2T1V3 Earthquake								Maximum stresses from (DL± E● ± Temperature)		
	Axial Stress	Bending stress in 1-2 plane		Bending stress in 1-3 plane		Combined stress		Shear stress			
		Node I	Node J	Node I	Node J	Node I	Node J		Combined stress at Node I	Combined stress at Node J	Shear
1	0.748	0.587	0.316	1.129	0.855	2.369	1.738	0.019	37.75	24.124	0.652
16	1.386	0.355	0.515	0.207	0.476	1.916	2.312	0.004	11.829	11.921	0.358
17	0.972	0.529	0.3	0.668	0.231	2.168	1.388	0.009	15.288	13.754	0.362
32	0.888	0.329	0.61	0.264	0.668	1.481	2.087	0.016	14.291	16.109	0.345
33	1.369	0.676	0.449	0.36	0.178	2.262	1.988	0.003	13.959	16.411	0.056
54	1.107	0.252	0.515	0.409	0.683	1.734	2.306	0.003	16.848	17.054	0.065
55	0.634	0.468	0.243	0.964	0.546	2.027	1.295	0.002	14.86	11.683	0.058
66	1.3	0.345	0.661	0.525	0.748	2.103	2.533	0.006	31.712	39.9	0.061
81	0.986	0.26	0.351	0.029	0.071	1.275	1.4	0.006	24.892	26.512	0.653
82	0.998	0.273	0.23	0.079	0.047	1.313	1.262	0.02	23.286	25.194	0.731
97	1.001	0.223	0.278	0.052	0.066	1.261	1.279	0.014	29.878	26.848	0.651
98	0.91	0.356	0.316	0.063	0.048	1.329	1.251	0.004	27.574	31.256	0.131
119	0.952	0.228	0.312	0.041	0.058	1.176	1.314	0.002	28.64	27.655	0.11
120	0.952	0.267	0.217	0.047	0.028	1.25	1.197	0.029	26.596	29.616	0.049
131	0.636	0.672	0.369	3.018	2.512	4.125	3.451	0.004	10.877	9.078	0.435
163	0.634	0.349	0.106	1.173	0.337	2.035	1.077	0.011	7.543	9.589	0.513
166	0.875	0.76	0.473	0.524	0.365	2.149	1.618	0.053	20.119	19.688	1.556
167	0.57	0.223	0.114	1.999	1.17	2.629	1.839	0.004	10.576	12.939	0.482
168	0.431	0.191	0.152	0.675	0.385	1.297	0.867	0.018	8.304	8.912	0.503
169	0.743	0.489	0.387	1.824	1.079	2.881	2.129	0.002	11.378	9.459	0.36
171	0.879	0.245	0.299	0.298	0.704	1.353	1.882	0.014	19.023	18.463	1.327
205	0.969	0.287	0.214	0.768	0.305	2.025	1.484	0.008	19.245	18.856	1.308
209	0.635	0.556	0.43	1.944	1.137	3.135	2.174	0.003	12.128	9.769	0.367
210	0.565	0.204	0.115	2.387	1.388	2.987	2.013	0.003	13.127	14.851	0.069
211	0.425	0.145	0.142	0.814	0.459	1.385	0.871	0.007	11.117	10.916	0.1
212	0.707	0.802	0.771	1.844	1.134	3.352	2.515	0.003	7.505	9.445	0.063
217	0.982	0.285	0.482	0.26	0.68	1.491	2.143	0.009	18.035	22.775	0.304
262	0.475	0.806	0.965	1.128	0.677	2.346	2.058	0.004	7.646	11.216	0.079
265	0.867	0.342	0.157	0.606	0.251	1.805	1.271	0.005	21.853	16.858	0.262
266	0.429	0.334	0.097	1.246	0.732	1.892	1.258	0.003	10.476	13.105	0.065
267	0.332	0.209	0.18	0.379	0.221	0.898	0.733	0.003	10.211	10.087	0.076
268	0.914	0.203	0.366	0.445	0.84	1.345	2.036	0.273	17.243	18.226	0.772
269	0.609	0.783	0.798	1.021	0.634	2.351	1.975	0.001	8.622	4.576	0.049
295	0.784	1.247	1.074	2.524	2.17	4.555	3.734	0.003	10.09	9.302	0.004

[a] Seismic excitation cases described in Table 5.1

Table 5.5 Stresses in Members due to Seismic Excitation Case: LL11[a]

Member Number	Stresses due to LL11 Earthquake							
	Axial Stress	Bending stress in 1-2 plane		Bending stress in 1-3 plane		Combined stress		Shear stress
		Node I	Node J	Node I	Node J	Node I	Node J	
1	0.81	0.619	0.338	0.106	0.095	1.474	1.243	0.009
16	0.704	0.338	0.558	0.027	0.054	1.069	1.256	0.004
17	0.764	0.755	0.424	0.034	0.016	1.553	1.112	0.011
32	0.548	0.448	0.736	0.009	0.021	0.933	1.302	0.007
33	0.589	0.85	0.535	0.045	0.024	1.484	1.148	0.003
54	0.807	0.449	0.801	0.059	0.102	1.264	1.626	0.004
55	0.546	0.572	0.296	0.082	0.051	1.126	0.886	0.002
66	1.057	0.406	0.997	0.034	0.038	1.48	2.075	0.002
81	1.2	0.217	0.305	0.028	0.035	1.408	1.54	0.005
82	1.167	0.516	0.366	0.035	0.039	1.541	1.564	0.018
97	1.055	0.322	0.397	0.04	0.025	1.412	1.449	0.013
98	1.079	0.552	0.389	0.034	0.06	1.536	1.529	0.003
119	0.934	0.437	0.588	0.043	0.034	1.415	1.461	0.003
120	0.926	0.318	0.293	0.046	0.045	1.29	1.259	0.007
131	0.453	0.606	0.569	0.485	0.408	1.519	1.308	0.003
163	0.612	0.727	0.179	0.263	0.082	1.574	0.871	0.009
166	1.689	1.104	0.503	0.407	0.321	3.163	2.472	0.046
167	0.718	0.357	0.223	0.196	0.114	1.271	0.93	0.004
168	0.48	0.083	0.129	0.105	0.052	0.668	0.657	0.015
169	1.122	0.654	0.537	0.218	0.13	1.994	1.769	0.002
171	1.622	0.292	0.379	0.267	0.392	2.181	2.389	0.012
205	2.339	0.338	0.214	0.221	0.128	2.897	2.68	0.013
209	1.136	0.662	0.575	0.069	0.042	1.867	1.741	0.003
210	0.718	0.335	0.107	0.069	0.041	1.106	0.866	0.002
211	0.418	0.107	0.223	0.047	0.026	0.564	0.627	0.003
212	1.252	1.327	1.593	0.049	0.036	2.5	2.882	0.005
217	2.336	0.365	0.654	0.201	0.397	2.867	3.269	0.008
262	0.766	1.428	1.926	0.052	0.048	2.233	2.61	0.004
265	1.286	0.768	0.264	0.173	0.134	2.044	1.656	0.006
266	0.558	0.383	0.158	0.047	0.029	0.976	0.745	0.006
267	0.362	0.275	0.218	0.045	0.023	0.609	0.591	0.003
268	1.321	0.286	0.519	0.087	0.186	1.656	2.006	0.065
269	0.791	0.909	0.959	0.045	0.034	1.599	1.784	0.001
295	1.025	2.308	2.042	0.051	0.054	3.304	3.105	0.001

[a] Seismic excitation cases described in Table 5.1

Table 5.6 Stresses in Members due to Seismic Excitation Case: LL22[a]

Member Number	Stresses due to LL22 Earthquake							
	Axial Stress	Bending stress in 1-2 plane		Bending stress in 1-3 plane		Combined stress		Shear stress
		Node I	Node J	Node I	Node J	Node I	Node J	
1	1.215	0.591	0.341	0.11	0.087	1.872	1.63	0.009
16	1.033	0.372	0.624	0.029	0.058	1.428	1.715	0.004
17	0.443	0.788	0.431	0.037	0.014	1.26	0.886	0.01
32	0.376	0.436	0.719	0.008	0.019	0.82	1.077	0.008
33	0.928	0.87	0.538	0.048	0.025	1.841	1.491	0.003
54	0.878	0.472	0.933	0.054	0.103	1.403	1.741	0.004
55	0.526	0.593	0.307	0.081	0.051	1.186	0.884	0.002
66	1.148	0.377	0.626	0.044	0.038	1.557	1.812	0.002
81	1.177	0.251	0.346	0.028	0.028	1.45	1.55	0.006
82	1.133	0.445	0.315	0.046	0.037	1.511	1.481	0.021
97	0.997	0.319	0.46	0.04	0.032	1.349	1.307	0.009
98	1.01	0.547	0.421	0.038	0.062	1.493	1.469	0.003
119	0.783	0.405	0.552	0.039	0.033	1.101	1.367	0.004
120	0.803	0.366	0.27	0.045	0.04	1.214	1.06	0.008
131	0.505	0.633	0.49	0.679	0.564	1.817	1.492	0.003
163	0.618	0.729	0.191	0.273	0.086	1.62	0.891	0.01
166	1.616	1.121	0.542	0.411	0.331	3.109	2.489	0.048
167	0.722	0.405	0.263	0.258	0.15	1.377	1.031	0.004
168	0.475	0.178	0.19	0.105	0.055	0.722	0.719	0.015
169	1.089	0.694	0.541	0.225	0.135	2.008	1.758	0.002
171	1.574	0.295	0.392	0.271	0.405	2.132	2.372	0.008
205	2.447	0.354	0.208	0.211	0.13	3.002	2.785	0.011
209	1.06	0.679	0.575	0.084	0.05	1.822	1.672	0.002
210	0.691	0.28	0.117	0.078	0.046	1.049	0.848	0.003
211	0.392	0.152	0.196	0.044	0.03	0.585	0.618	0.004
212	1.289	1.42	1.659	0.065	0.037	2.666	2.986	0.004
217	2.394	0.369	0.678	0.186	0.388	2.922	3.358	0.008
262	0.787	1.459	1.862	0.055	0.046	2.279	2.595	0.005
265	1.033	0.78	0.236	0.194	0.137	2.007	1.404	0.008
266	0.401	0.483	0.126	0.048	0.031	0.871	0.551	0.005
267	0.301	0.172	0.273	0.044	0.02	0.506	0.591	0.003
268	1.057	0.3	0.473	0.093	0.178	1.442	1.708	0.077
269	0.615	0.783	0.877	0.041	0.031	1.439	1.523	0.001
295	0.91	2.429	2.256	0.047	0.051	3.387	3.203	0.001

[a] Seismic excitation cases described in Table 5.1

Table 5.7 Stresses in Members due to Seismic Excitation Case: TT11[a]

Member Number	Stresses due to TT11 Earthquake							
	Axial Stress	Bending stress in 1-2 plane		Bending stress in 1-3 plane		Combined stress		Shear stress
		Node I	Node J	Node I	Node J	Node I	Node J	
1	1.108	0.801	0.456	1.142	0.88	2.722	2.112	0.019
16	1.594	0.507	0.787	0.207	0.484	2.275	2.541	0.006
17	0.969	0.8	0.46	0.688	0.238	2.457	1.606	0.011
32	0.618	0.467	0.788	0.264	0.668	1.349	2.054	0.017
33	1.207	0.89	0.57	0.358	0.188	2.455	1.965	0.004
54	0.775	0.478	0.856	0.452	0.764	1.665	2.25	0.004
55	0.665	0.64	0.307	0.995	0.571	2.181	1.448	0.003
66	0.595	0.435	0.958	0.555	0.783	1.585	2.312	0.006
81	1.187	0.367	0.504	0.031	0.073	1.485	1.759	0.008
82	1.223	0.48	0.375	0.064	0.037	1.636	1.635	0.027
97	1.17	0.317	0.403	0.042	0.059	1.526	1.554	0.017
98	1.14	0.651	0.415	0.057	0.06	1.721	1.613	0.005
119	0.602	0.427	0.594	0.046	0.061	1.038	1.257	0.003
120	0.587	0.339	0.228	0.059	0.046	0.962	0.828	0.03
131	0.618	0.749	0.63	3.041	2.534	4.408	3.753	0.004
163	0.713	0.75	0.185	1.306	0.382	2.738	1.281	0.015
166	1.832	1.181	0.626	0.649	0.357	3.488	2.777	0.065
167	0.704	0.414	0.244	1.815	1.054	2.819	1.883	0.006
168	0.475	0.192	0.172	0.659	0.365	1.271	0.987	0.021
169	1.294	0.696	0.564	1.773	1.052	3.763	2.847	0.003
171	1.801	0.303	0.348	0.507	0.856	2.611	2.947	0.016
205	2.447	0.341	0.226	0.647	0.247	3.38	2.92	0.013
209	1.212	0.65	0.568	1.961	1.13	3.742	2.911	0.004
210	0.831	0.316	0.107	2.368	1.366	3.501	2.161	0.003
211	0.418	0.167	0.212	0.82	0.479	1.357	1.108	0.008
212	1.38	1.401	1.62	1.826	1.104	4.452	4.104	0.005
217	2.42	0.392	0.559	0.333	0.662	3.031	3.5	0.011
262	0.802	1.684	1.932	1.124	0.669	3.554	3.339	0.005
265	1.251	0.85	0.269	0.735	0.328	2.605	1.848	0.008
266	0.522	0.471	0.121	1.237	0.724	2.015	1.366	0.006
267	0.31	0.197	0.256	0.396	0.229	0.864	0.732	0.003
268	1.283	0.256	0.551	0.381	0.79	1.808	2.624	0.28
269	0.827	1.032	1.111	1.015	0.626	2.74	2.534	0.001
295	1.131	2.485	2.147	2.515	2.164	6.13	5.281	0.003

[a] Seismic excitation cases described in Table 5.1

Table 5.8 Stresses in Members due to Seismic Excitation Case: TT22[a]

Member Number	Stresses due to TT22 Earthquake							
	Axial Stress	Bending stress in 1-2 plane		Bending stress in 1-3 plane		Combined stress		Shear stress
		Node I	Node J	Node I	Node J	Node I	Node J	
1	0.994	0.547	0.318	0.506	0.269	1.96	1.476	0.01
16	0.948	0.366	0.624	0.087	0.255	1.402	1.737	0.004
17	0.724	0.741	0.419	0.363	0.112	1.792	1.249	0.01
32	0.846	0.431	0.707	0.115	0.349	1.328	1.903	0.009
33	0.912	0.824	0.489	0.211	0.079	1.948	1.478	0.003
54	0.635	0.495	0.85	0.145	0.293	1.263	1.773	0.004
55	0.781	0.538	0.258	0.418	0.191	1.737	1.176	0.003
66	0.799	0.35	0.809	0.181	0.376	1.307	1.844	0.003
81	1.319	0.259	0.358	0.031	0.072	1.601	1.731	0.005
82	1.243	0.526	0.378	0.085	0.041	1.601	1.661	0.02
97	0.992	0.335	0.453	0.045	0.066	1.372	1.392	0.012
98	1.055	0.52	0.419	0.063	0.068	1.501	1.542	0.004
119	0.62	0.44	0.62	0.052	0.057	1.112	1.189	0.003
120	0.598	0.301	0.274	0.06	0.049	0.952	0.921	0.014
131	0.383	0.539	0.497	2.051	1.708	2.955	2.524	0.003
163	0.702	0.705	0.172	1.045	0.373	2.452	1.169	0.011
166	1.864	1.095	0.549	0.677	0.38	3.512	2.782	0.05
167	0.722	0.366	0.215	1.464	0.881	2.461	1.735	0.004
168	0.466	0.103	0.156	0.434	0.251	1.002	0.869	0.016
169	1.152	0.646	0.516	1.368	0.864	3.159	2.402	0.003
171	1.832	0.287	0.34	0.393	0.705	2.475	2.744	0.01
205	2.479	0.323	0.232	0.541	0.238	3.291	2.893	0.01
209	1.128	0.637	0.52	1.258	0.784	3.024	2.37	0.003
210	0.682	0.319	0.09	1.425	0.866	2.425	1.567	0.003
211	0.363	0.118	0.2	0.426	0.255	0.901	0.81	0.006
212	1.292	1.37	1.614	1.204	0.755	3.687	3.647	0.005
217	2.471	0.353	0.679	0.262	0.603	3.049	3.581	0.009
262	0.809	1.583	2.149	1.13	0.694	3.181	3.476	0.004
265	1.315	0.851	0.255	0.364	0.205	2.303	1.774	0.008
266	0.437	0.433	0.117	1.219	0.73	1.945	1.28	0.006
267	0.245	0.196	0.228	0.349	0.219	0.739	0.677	0.003
268	1.339	0.276	0.487	0.299	0.46	1.753	2.286	0.189
269	0.631	0.85	0.9	1.037	0.656	2.34	2.188	0.001
295	0.935	2.401	2.157	2.038	1.753	5.223	4.609	0.002

[a] Seismic excitation cases described in Table 5.1

Table 5.9 Stresses Due to a Temperature of 90° F

Member Number	Axial Stress	Bending stress in 1-2 plane		Bending stress in 1-3 plane		Combined stress		Shear stress
		Node I	Node J	Node I	Node J	Node I	Node J	
1	11.566	2.736	-1.721	0.128	-0.199	14.431	13.486	0.043
16	4.214	0.181	-0.954	0.027	0.005	4.422	5.163	0.006
17	11.015	1.459	-0.967	0.073	-0.047	12.547	12.029	0.003
32	10.723	-0.848	1.255	-0.047	0.073	11.618	12.051	0.019
33	8.856	-0.541	-0.214	0.063	-0.041	9.335	9.111	0.01
54	9.195	-0.077	-0.97	-0.038	0.063	9.31	10.101	0.003
55	7.15	1.526	-0.705	0.014	0.035	8.69	7.82	0.008
66	16.773	-2.407	4.467	-0.334	0.21	19.514	21.449	0.001
81	5.012	0.848	-1.24	0.019	0.043	5.879	6.208	0.026
82	4.978	-0.159	-0.004	0.038	-0.005	5.099	4.987	0.013
97	5.278	0.189	-0.356	-0.006	0.038	5.461	5.595	0.066
98	5.315	-0.813	0.062	0.034	0.027	6.094	5.404	0.023
119	5.049	0.604	-0.825	0.025	0.037	5.678	5.837	0.028
120	5.051	-0.623	0.26	0.04	-0.016	5.635	5.296	0.001
131	1.098	1.756	0.261	0.091	-0.089	2.944	1.27	0.006
163	0.589	0.365	0.069	-0.037	0.026	0.917	0.684	0.012
166	3.436	0.37	-0.409	-0.069	0.03	3.738	3.816	0.097
167	-2.519	0.978	-0.058	0.081	-0.078	-1.46	-2.383	0.019
168	-1.972	-0.652	-0.241	0.002	0.101	-1.323	-1.833	0.027
169	1.61	1.066	-0.028	0.068	-0.044	2.744	1.682	0.014
171	3.511	-0.26	0.351	-0.006	-0.014	3.777	3.848	0.05
205	4.285	0.443	-0.32	-0.064	0.084	4.664	4.521	0.049
209	1.602	-0.899	-0.008	0.036	-0.025	2.466	1.635	0.011
210	-2.789	-0.71	0.04	-0.004	-0.026	-2.075	-2.775	0.006
211	-2.105	0.296	0.12	0.015	0.099	-1.793	-1.886	0.004
212	1.807	-0.431	0.23	0.066	-0.055	2.172	1.982	0.001
217	4.252	0.15	-0.777	0.129	-0.17	4.531	5.198	0.055
262	1.721	-1.433	2.51	0.053	-0.046	3.1	4.185	0.005
265	3.841	0.082	-0.138	-0.056	0.064	3.867	3.916	0.067
266	-2.588	0.773	0.138	0.021	-0.049	-1.795	-2.499	0.008
267	-1.987	-0.165	-0.077	0.015	0.103	-1.836	-1.96	0.005
268	3.88	-0.223	-0.034	0.05	-0.063	4.053	3.976	0.066
269	0.448	1.165	-0.025	0.021	-0.018	1.634	0.49	0.012
295	1.867	-2.875	-0.5	0.048	-0.068	4.694	2.435	0

Table 5.10 Self-Weight Induced Stresses

Member Number	Axial Stress	Bending stress in 1-2 plane		Bending stress in 1-3 plane		Combined stress		Shear stress
		Node I	Node J	Node I	Node J	Node I	Node J	
1	2.623	18.201	6.323	0.126	-0.045	20.95	8.9	0.59
16	-9.143	3.67	13.631	-0.018	-0.042	-5.491	4.446	0.348
17	-5.375	5.954	5.694	-0.006	0.018	0.573	0.337	0.35
32	-7.17	5.946	5.255	0.033	-0.055	-1.192	-1.971	0.31
33	-10.054	12.49	4.691	-0.074	0.05	2.362	-5.312	0.043
54	-9.546	3.693	14.263	0.049	-0.071	-5.804	4.647	0.059
55	-8.621	4.496	6.094	-0.018	-0.041	-4.143	-2.568	0.048
66	2.877	7.268	13.008	-0.05	0.033	10.095	15.918	0.054
81	16.146	1.861	2.47	-0.269	0.255	17.738	18.904	0.621
82	16.121	0.487	2.998	0.266	-0.141	16.874	18.945	0.698
97	19.916	3.383	-0.319	-0.143	0.294	23.156	19.974	0.571
98	20.069	-0.21	4.669	0.292	-0.103	20.151	24.601	0.104
119	19.346	2.602	0.815	-0.162	0.309	21.786	20.504	0.08
120	19.378	0.026	3.92	0.307	-0.141	19.711	23.123	0.019
131	-7.632	6.615	0.72	-2.791	2.461	-3.808	-4.357	0.425
163	-8.317	-4.257	-0.047	0.53	-0.352	-4.591	-7.828	0.49
166	12.235	2.568	1.301	-0.571	0.684	14.232	14.254	1.406
167	-9.047	-2.051	-0.064	-0.509	0.281	-6.487	-8.717	0.459
168	-6.855	1.053	0.341	0.118	0.245	-5.684	-6.212	0.458
169	-6.229	0.413	-0.404	0.064	-0.086	-5.753	-5.648	0.344
171	12.083	1.081	1.575	0.729	-0.892	13.893	12.733	1.263
205	11.448	1.52	1.204	-0.412	0.166	12.556	12.851	1.251
209	-6.551	0.064	0.49	-0.088	0.01	-6.527	-5.96	0.353
210	-10.337	2.354	0.202	-0.082	-0.038	-8.065	-10.063	0.06
211	-8.299	-0.417	-0.257	0.057	0.341	-7.939	-8.159	0.089
212	-9.184	7.41	-4.252	-0.207	0.106	-1.981	-4.948	0.059
217	11.613	-0.495	4.15	0.095	-0.296	12.013	15.434	0.24
262	-9.015	6.879	-13.896	-0.064	-0.006	-2.2	4.973	0.07
265	10.761	5.778	-0.994	-0.358	0.119	16.181	11.671	0.19
266	-9.862	-3.006	-0.336	-0.067	-0.064	-6.789	-9.348	0.054
267	-8.01	0.482	0.197	0.051	0.363	-7.477	-7.394	0.068
268	10.655	1.05	2.02	0.139	-0.427	11.845	12.214	0.433
269	-6.717	2.169	-4.467	-0.089	-0.048	-4.637	-2.111	0.036
295	-4.456	-3.417	0.925	-0.199	0.305	-0.841	-3.133	0.001

Table 5.11 Stress Requirement Based on AASHTO Equations for L1T2V3 Earthquake

Member Number	Axial stress f_a (ksi)	Bending stress (ksi)		Euler buckling stress AASHTO Eq. (10-44) (ksi)		Stress requirement ≤ 1.0	
		f_{bx}	f_{by}	F_{ex}	F_{ey}	AASHTO Eq.10-42	AASHTO Eq.10-43
1	0.494	1.294	0.901	3491316	1692662	0.093288	0.138823
16	0.88	1.213	1.45	966786.9	1381482	0.113178	0.184939
17	0.808	1.604	1.175	2005213	1076038	0.118108	0.186502
32	0.818	1.219	1.714	1129992	2234033	0.124653	0.19479
33	0.828	1.561	1.227	1808505	1117385	0.11849	0.188129
54	0.867	1.216	1.685	1000929	1921924	0.123293	0.196074
55	0.799	1.678	1.227	2244217	1199969	0.123463	0.192272
66	0.787	1.213	1.82	1208778	2721246	0.128903	0.197966
81	1.049	1.338	1.314	827819.7	798388.4	0.11271	0.194335
82	1.095	1.349	1.344	772271.7	766557.6	0.114453	0.199092
97	1.097	1.356	1.436	777464.6	871906.9	0.11866	0.20416
98	1.105	1.495	1.452	931391.6	878583.7	0.125248	0.212381
119	0.739	0.961	1.092	860463.4	1111043	0.087253	0.146141
120	0.759	1.003	1.016	888572.4	911755.4	0.085808	0.145618
131	0.377	3.048	2.324	33259959	19335884	0.22831	0.290787
163	0.454	1.731	0.854	7397022	1800439	0.109863	0.155968
166	1.019	2.116	1.584	2194105	1229.522	0.15725	0.244969
167	0.559	2.188	1.443	7795527	3390654	0.154318	0.214448
168	0.396	0.905	0.774	2657549	1943865	0.071358	0.107255
169	0.744	2.463	1.907	5576445	3342951	0.185725	0.262285
171	1.003	1.451	1.76	1064897	1566744	0.136468	0.219578
205	1.07	1.707	1.418	1295013	893633.4	0.132813	0.219221
209	0.654	2.433	1.857	7042116	4102445	0.182325	0.252989
210	0.538	2.171	1.4	8285707	3445609	0.151768	0.210212
211	0.385	0.897	0.746	2762091	1910428	0.069828	0.104808
212	0.799	2.803	2.233	6262203	3974279	0.21403	0.298822
217	1.071	1.566	1.987	1087875	1751424	0.151003	0.24068
262	0.707	2.276	2.653	5273272	7164900	0.209483	0.288058
265	0.904	1.604	1.22	1601940	926738.7	0.12002	0.194402
266	0.403	1.915	1.217	11489522	4640295	0.13311	0.180317
267	0.305	0.784	0.652	3362071	2325252	0.06103	0.08975
268	0.89	1.261	1.644	1021468	1736193	0.123463	0.197628
269	0.683	2.329	2.067	5916598	4660302	0.18683	0.259995
295	0.773	4.243	3.877	15330685	12799915	0.3451	0.451492

Table 5.12 Stress Requirement Based on AASHTO Equations for L2T1V3 Earthquake

Member Number	Axial stress f_a (ksi)	Bending stress (ksi)		Euler buckling stress AASHTO Eq. (10-44) (ksi)		Stress requirement ≤ 1.0	
		f_{bx}	f_{by}	F_{ex}	F_{ey}	AASHTO Eq.10-42	AASHTO Eq.10-43
1	0.748	2.369	1.738	138.4954	95.18738	0.175679	0.249371
16	1.386	1.916	2.312	200.4786	164.3925	0.181092	0.292968
17	0.972	2.168	1.388	125.3725	96.66568	0.152449	0.235003
32	0.888	1.481	2.087	191.3865	148.9989	0.152465	0.23066
33	1.369	2.262	1.988	97.71601	127.9614	0.182905	0.293067
54	1.107	1.734	2.306	112.8624	160.4608	0.173111	0.267148
55	0.634	2.027	1.295	185.7122	171.1465	0.141685	0.203412
66	1.3	2.103	2.533	178.7691	174.2717	0.198494	0.308307
81	0.986	1.275	1.4	124.9832	108.4484	0.114664	0.191777
82	0.998	1.313	1.262	160.2021	147.8999	0.110152	0.187484
97	1.001	1.261	1.279	84.26121	110.3421	0.109092	0.18591
98	0.91	1.329	1.251	104.9092	151.4342	0.110466	0.182555
119	0.952	1.176	1.314	124.9832	108.4484	0.106703	0.180526
120	0.952	1.25	1.197	172.8841	159.608	0.104597	0.178376
131	0.636	4.125	3.451	117.232	153.5181	0.323546	0.416229
163	0.634	2.035	1.077	113.1238	163.2917	0.132926	0.192912
166	0.875	2.149	1.618	172.7625	159.2125	0.160942	0.239845
167	0.57	2.629	1.839	208.5162	203.2705	0.190416	0.256945
168	0.431	1.297	0.867	634.698	489.37	0.09204	0.133565
169	0.743	2.881	2.129	200.7647	156.3001	0.213812	0.294226
171	0.879	1.353	1.882	84.23404	110.3065	0.138736	0.21348
205	0.969	2.025	1.484	97.30988	138.3493	0.150443	0.232477
209	0.635	3.135	2.174	131.5159	101.4024	0.226861	0.302821
210	0.565	2.987	2.013	242.2236	188.5767	0.213054	0.283251
211	0.425	1.385	0.871	455.9038	597.0169	0.095961	0.137812
212	0.707	3.352	2.515	109.1108	155.1271	0.250766	0.334958
217	0.982	1.491	2.143	178.8802	156.479	0.15537	0.239492
262	0.475	2.346	2.058	200.6427	184.906	0.187632	0.248154
265	0.867	1.805	1.271	123.6867	103.2035	0.131729	0.204824
266	0.429	1.892	1.258	216.6974	200.0568	0.134149	0.182747
267	0.332	0.898	0.733	455.9038	597.0169	0.069363	0.101089
268	0.914	1.345	2.036	104.9925	149.272	0.144728	0.22284
269	0.609	2.351	1.975	120.7451	81.36232	0.184995	0.25214
295	0.784	4.555	3.734	253.9687	190.3158	0.353538	0.460589

Table 5.13 Displacements (in) due to Seismic Excitation of the 50-year Earthquake

Joint Number	L1T2V3[a]			L2T1V3[a]			LL11[a]			LL22[a]			TT11[a]			TT22[a]		
	Ux	Uy	Uz	Ux	Uy	Uz	Ux	Uy	Uz	Ux	Uy	Uz	Ux	Uy	Uz	Ux	Uy	Uz
1	0.207	0.023	0.01	0.321	0.076	0.01	0.226	0.006	0.016	0.344	0.006	0.016	0.053	0.081	0.017	0.057	0.021	0.017
8	0.198	0.399	0.27	0.358	0.28	0.335	0.213	0.019	0.313	0.394	0.032	0.457	0.056	0.27	0.316	0.067	0.4	0.273
9	0.193	0.386	0.246	0.361	0.232	0.332	0.209	0.026	0.283	0.398	0.034	0.445	0.065	0.235	0.284	0.072	0.393	0.248
10	0.189	0.348	0.219	0.362	0.239	0.322	0.206	0.025	0.256	0.399	0.031	0.407	0.071	0.238	0.249	0.073	0.359	0.234
11	0.186	0.3	0.191	0.361	0.274	0.281	0.204	0.022	0.195	0.398	0.025	0.347	0.072	0.283	0.194	0.073	0.305	0.212
13	0.176	0.239	0.149	0.335	0.245	0.221	0.188	0.022	0.145	0.363	0.026	0.266	0.061	0.244	0.16	0.048	0.238	0.173
17	0.184	0.047	0.013	0.324	0.147	0.014	0.183	0.002	0.025	0.328	0.002	0.024	0.026	0.147	0.025	0.028	0.047	0.025
24	0.208	0.507	0.409	0.338	0.344	0.377	0.201	0.007	0.395	0.351	0.011	0.397	0.04	0.342	0.416	0.031	0.51	0.388
25	0.201	0.549	0.406	0.353	0.443	0.372	0.201	0.012	0.391	0.356	0.013	0.397	0.036	0.45	0.41	0.033	0.55	0.387
26	0.194	0.546	0.399	0.369	0.39	0.37	0.201	0.014	0.384	0.36	0.014	0.392	0.034	0.4	0.416	0.037	0.543	0.381
33	0.185	0.053	0.017	0.352	0.15	0.016	0.185	0.002	0.029	0.354	0.002	0.028	0.03	0.15	0.027	0.052	0.053	0.028
37	0.178	0.339	0.291	0.326	0.204	0.191	0.185	0.003	0.212	0.331	0.004	0.2	0.044	0.204	0.237	0.057	0.338	0.265
39	0.201	0.423	0.358	0.332	0.27	0.23	0.188	0.01	0.25	0.3	0.01	0.245	0.069	0.271	0.278	0.051	0.425	0.337
43	0.222	0.421	0.395	0.312	0.325	0.342	0.19	0.012	0.264	0.286	0.011	0.308	0.06	0.322	0.269	0.062	0.421	0.325
44	0.227	0.428	0.36	0.299	0.33	0.349	0.191	0.006	0.312	0.281	0.006	0.347	0.065	0.329	0.306	0.067	0.429	0.307
45	0.228	0.405	0.287	0.291	0.313	0.335	0.191	0.008	0.288	0.275	0.008	0.332	0.066	0.308	0.279	0.073	0.403	0.287
49	0.2	0.4	0.226	0.278	0.194	0.2	0.174	0.019	0.208	0.245	0.017	0.244	0.084	0.191	0.243	0.082	0.402	0.237
51	0.138	0.346	0.214	0.229	0.178	0.186	0.141	0.009	0.17	0.216	0.009	0.199	0.083	0.175	0.192	0.07	0.347	0.207
55	0.129	0.017	0.007	0.22	0.055	0.007	0.137	0.006	0.012	0.2	0.006	0.012	0.071	0.06	0.012	0.05	0.019	0.012
60	0.116	0.429	0.351	0.196	0.231	0.251	0.146	0.009	0.302	0.188	0.009	0.254	0.074	0.229	0.334	0.042	0.422	0.283
61	0.116	0.473	0.388	0.19	0.255	0.273	0.143	0.005	0.356	0.182	0.005	0.247	0.071	0.252	0.355	0.049	0.475	0.306
62	0.117	0.488	0.413	0.176	0.268	0.297	0.126	0.008	0.397	0.167	0.007	0.248	0.06	0.266	0.375	0.062	0.494	0.316
67	0.096	0.011	0.002	0.103	0.043	0.002	0.08	0.004	0.003	0.097	0.004	0.003	0.039	0.048	0.003	0.061	0.016	0.003
101	0.2	0.251	0.108	0.36	0.171	0.133	0.215	0.036	0.109	0.37	0.048	0.183	0.07	0.165	0.111	0.045	0.261	0.109
102	0.207	0.212	0.077	0.359	0.138	0.092	0.216	0.032	0.077	0.373	0.046	0.127	0.066	0.124	0.078	0.05	0.237	0.072
127	0.187	0.613	0.381	0.296	0.323	0.254	0.175	0.008	0.235	0.283	0.014	0.235	0.073	0.326	0.28	0.059	0.608	0.346
129	0.184	0.565	0.418	0.282	0.314	0.326	0.171	0.008	0.244	0.266	0.012	0.251	0.064	0.317	0.255	0.058	0.56	0.342
139	0.181	0.234	0.164	0.259	0.173	0.15	0.153	0.006	0.166	0.266	0.007	0.208	0.08	0.167	0.182	0.091	0.233	0.188
140	0.185	0.181	0.105	0.245	0.16	0.099	0.162	0.004	0.11	0.257	0.004	0.146	0.102	0.158	0.127	0.11	0.182	0.122

[a] Seismic excitation cases described in Table 5.1

Ux = Longitudinal displacement; Uy = Transverse displacement; Uz=Vertical displacement

Table 5.14 Displacements (in) due to Self-weight and Temperature

Joint Number	Temperature			Self-weight		
	Ux	Uy	Uz	Ux	Uy	Uz
1	2.631	0.137	0.000	-0.373	0.000	-0.009
8	1.902	0.142	-0.160	0.420	0.190	-7.918
9	1.769	0.140	0.067	0.567	0.196	-7.772
10	1.621	0.148	0.230	0.646	0.189	-7.315
11	1.458	0.124	0.464	0.719	0.155	-6.309
13	1.746	0.144	0.654	0.842	0.105	-4.734
17	1.008	0.137	-0.002	0.351	0.000	-0.027
24	0.396	0.152	0.041	0.092	-0.043	-1.819
25	0.283	0.152	0.123	0.121	-0.038	-1.724
26	0.170	0.150	0.056	0.143	-0.033	-1.712
33	-0.463	0.137	-0.001	-0.274	0.000	-0.029
37	-0.915	0.142	1.015	-0.834	0.003	-5.506
39	0.155	0.140	0.863	-0.734	0.011	-7.228
43	-0.199	0.141	1.084	-0.270	0.012	-11.098
44	-0.296	0.141	1.022	-0.092	0.012	-11.401
45	-0.394	0.141	1.153	0.085	0.011	-11.182
49	-0.737	0.175	1.236	0.576	0.010	-7.570
51	-0.007	0.172	1.292	0.703	0.002	-5.834
55	-0.441	0.137	-0.002	0.177	0.000	-0.025
60	-1.106	0.146	-0.877	-0.336	-0.005	-0.642
61	-1.210	0.151	-1.045	-0.370	-0.002	-0.936
62	-1.151	0.155	-1.304	-0.323	0.000	-1.222
67	-1.143	0.137	0.000	-0.063	0.000	-0.004
101	1.657	0.208	-0.076	-0.560	-0.281	-3.019
102	1.642	0.193	-0.286	-0.690	-0.202	-2.087
127	0.000	0.142	0.422	0.713	-0.010	-8.308
129	-0.161	0.161	0.569	0.337	-0.023	-10.436
139	0.182	0.180	0.170	-1.540	-0.008	-3.669
140	0.286	0.168	-0.207	-1.687	-0.002	-2.329

Ux = Longitudinal displacement;
Uy = Transverse displacement;
Uz=Vertical displacement

Table 5.15 Maximum and Minimum Base Shears (kips) from Modal Time-History for the 50-Year Earthquake

Seismic Excitation Case	Longitudinal Direction				Transverse Direction				Vertical Direction			
	Maximum		Minimum		Maximum		Minimum		Maximum		Minimum	
	Force (kips)	Time (sec)	Force (kips)	Time (sec)	Force (kips)	Time (sec)	Force (kips)	Time (sec)	Force (kips)	Time (sec)	Force (kips)	Time (sec)
L1L1	770.3	1.22	-831.9	2.63	324.1	1.625	-336.4	2.095	6973	1.36	-7807	1.59
T1T1	84.33	1.365	-58.12	1.66	4766	0.965	-6225	1.13	7051	0.92	-7530	1.59
L2L2	1355	0.745	-1468	1.175	317.8	1.625	-333.7	2.095	6996	1.36	-7760	1.59
T2T2	78.1	1.36	-58.22	1.65	2447	0.545	-1519	1.44	6896	1.36	-7678	1.59
L1T2V3	745.3	2.25	-807.7	2.615	2435	0.545	-1395	1.01	4373	1.05	-4233	0.765
L2T1V3	1362	0.745	-1518	1.21	4855	0.965	-6189	1.13	4336	1.045	-4243	0.765

Table 5-16 Bearing Force Capacity/Demand Ratios of the US 41 Southbound Main bridge without site soil coefficients for the 50-Year Earthquake

Pier (Each pier has two bearings)	Anchor Bolt Capacity, V_c			Seismic Force per Pier (kips)			Seismic Demand per pier V_b=1.25x H_R (kips)	C/D ratio $r_{bf}=V_c/V_b$	Additional capacity of bolts required[b] per pier to make $r_{bf} \geq 1$ (kips)
	Number of bolts per bearing available at present	Available shear area of bolts per bearing (in^2)	Available force capacity of two bearings on each pier[a] (kips)	Longitudinal H_L	Transverse H_T	Resultant H_R			
A	4#, 2" dia.	12.566	452.4	128.74	1253.71	1260.303	1575.378	0.287169	1125
B	4#, 2" dia.	12.566	452.4	387.25	709.9	808.6536	1010.817	0.447559	560
C	4#, 2" dia.	12.566	452.4	351.87	794.6	869.0234	1086.279	0.416468	635
D	4#, 2" dia.	12.566	452.4	170.43	1787.7	1795.806	2244.757	0.201536	1795
E	4#, 1.5" dia.	7.0686	254.5	429.54	1689.5	1743.248	2179.06	0.116793	1925

[a]Shear strength of existing anchor bolts is assumed as 18 ksi

[b]Alternate retrofit would be to replace the existing fixed bearings with a seismic isolation bearings

Table 6.1a Calculation of Superstructure Weights:
Five Span Continuous- Unit I (Evansville, IN)(151′3″)

Component		Particulars		Weight (kips)
Plate Girder	Web	2x8x151.25x3/(8x12)x0.49 =37.07	2x1.1x (37.07+31.83x2)*	241.75
	Flange	2x2x20/144 x(7/8x13.54+ 9/8x13.17+ 3/2x12.08+ 31/16x46+ 3/2x11.67 + 9/8x12.42+7/8x16.17+ 9/8x4.80+ 9/8x3.1+2x7.75+ 2.813x10.63) x 0.49=31.83		
Floor beams	Type A	1.1/144x(48x3/8+2x9x3/8)x30x0 .49 =2.70	2.7+ 2.71x4+3.92 +2.744	20.28
	Type B&D	1.1x(48x3/8x30)+2x9x7/16x11+ 2x9x5/16x19)x1/144x0.49 =2.744		
	Type C	1.1x(48x3/8+2x9x15/16)x1/144x 30x0.49 = 3.92		
Stringers		62x3x151.25/1000		28.13
Deck (concrete)		32x7/12+((8+11)/(2x12) x3.125x2 + 10.5/12 x 1.5x2)x151.25x0.145		575

* For 2 Girders and 10% extra for joints, splices etc. **Total Weight of One Span≈ 865 kips**

Table 6.1b Calculation of Superstructure Weights:
Three Span Continuous - Unit II (Evansville, IN) (101′)

Component		Particulars		Weight (kips)
Plate Girder	Web	5.5x3/(8x12)x101x0.49=8.51	5x1.1x (8.51+ 6.47)*	82.4
	Flange	2x14x(5/8x14+11/16x56+5/8x21+3/4x10)x1/144x0.49=6.47		
Diaphragm		(7.2x2x(7+6.1x2)+60x7.5+8.5x(2x7+2x9)x2+ 3/8x1/12x 5x 7.5x0.49x1000+6x3/8x1/144x7.5x0.49x1000)x1/1000=1.9	6x1.1x1.9	12.54
Deck (concrete)		32x7/12+((8+11)/(2x12) x3.125x2 + 10.5/12 x 1.5x2)x101x0.145		384

* For 5 Girders and 10% extra for joints, splices etc. **Total Weight of One Span≈ 479 kips**

Table 6.1c Calculation of Superstructure Weights:
Three Span Continuous- Unit 1 (Henderson, KY) (453′11″)

Components		Particulars		Weight (kips)
Plate Girder	Web	3/8x1/12x8x (151.33+151.24+151.33)x0.490=55.6	2x1.1x (55.6+ 96.88)*	336
	Flange	20/144x(7/8x13+9/8x12+3/2x10.5+2x52.75+3/2x11.5+9/8x13+7/8x14.25+9/8x8+2x8.4+21/8x8)x3x2x0.49=96.88		
Floor Beams	TypeA	(3/8x48x30+3/8x9x2x10.25x2+9x7/16x2x4.75x2)x1/144x0.49=2.56	1.1x (2.56x 4+3.37x12 +3.56x3 + 3.37 x12)	112
	Type B&D	(3/8x48x30+9x7/16x2x5.5x2+9x17/16x2x9.5x2)x1/144x0.49=3.37		
	TypeC	(3/8x48x30+9x15/16x2x30)x1/144x0.49=3.56		
Stringers		62x3x454x1/1000		84.4
Deck(concrete)		(7/12x32+2x(8+11)/2x1/12x3+2x10.5/12x1.5)x0.145x454		1714

* For 2 Girders and 10% extra for joints, splices etc. **Total Weight of Unit I ≈2246 Kips**

Table 6.1d Calculation of Superstructure Weights:
Four Span Continuous- Unit 2 (Henderson, KY) (386′3″)

Components		Particulars		Weight (kips)
Internal Girders	Web	52x3/8x1/144x(92+92+100.625+100.44)x0.49=25.55	1.1x (57x3+ 59x2)*	318
	Flange	2x14/144x(5/8x15+3/4x50+3/4x14+9/8x20+5/8x14+5/8x92+5/8x 48.5+5/8x12+12/8x26+3/4x18+12/8x57.5+5/8x15.5)x0.49 =57		
External Girders	Web	52x3/8x1/144x(92+92+100.625+100.44)x0.49=25.55		
	Flange	2x14/144x(5/8x15+1x50+3/4x14+1.25x20+5/8x14+5/8x62+3/4x 12+5/8x18+5/8x48.5+5/8x12+1.5x26+3/4x18+12/8x57.5+ 5/8x15.5)x0.49=59		
Cross Frame	CF1	8.5/1000x(7.5x2+8.3x2) =0.269	0.269x 14x4+ 0.412x 3x4+0. 687x2 x4)	25.5
	CF2	3/8x43x7.5x1/144x0.49=0.412		
	CF3& CF4	2x7.2/1000x(7.5+2x5)+58/1000x7.5=0.687		
Deck (concrete)		(7/12x32+2x((8+11)/2x3/12+10.5/12x1.5))x0.145x385		1454

*10% extra for joints, splices etc. **Total Weight of Unit II ≈1798 Kips**

Table 6.1e Calculation of Superstructure Weights:
Four Span Continuous- Unit 3 (Henderson, KY) (368′)

Components		Particulars		Weig-ht (kips)
Internal Girder	Web	52x3/8x1/144x(92x4)x0.49=24.4	1.1x (51.8x3+ 54x2)*	263.4
	Flange	2x14/144x(5/8x16.4+3/4x51+3/4x10+9/8x28+3/4x10+3/4x42+5/8x19+5/8x14+5/8x17+3/4x54+9/8x28+3/4x51+5/8x19)x0.49=27.7		
External Girder	Web	52x3/8x1/144x(92x4)x0.49=24.4		
	Flange	2x14/144x(5/8x16.4+1x51+9/8x28+3/4x10+3/4x42+5/8x19+5/8x 14+5/8x17+3/4x54+9/8x28+3/4x10+1x51+5/8x19)x0.49 =29.1		
Cross Frame	CF1	8.5/1000x(7.5x2+8.3x2) =0.269	0.269x12 x4+0.412 x4x4+ 0.687x2 x4)	25
	CF2	3/8x43x7.5x1/144x0.49=0.412		
	CF3& CF4	2x7.2/1000x(7.5+2x5)+58/1000x7.5=0.687		
Deck (concrete)		(7/12x32+2x((8+11)/2x3/12+10.5/12x1.5))x0.145x368		1390

*10% extra for joints, splices etc. **Total Weight of Unit III = 1678 Kips**

Table 6.1f Calculation of Superstructure Weights:
Four Span Continuous- Unit 4 (Henderson, KY) (368′)

Components		Particulars		Weight (kips)
Internal Girders	Web	52x3/8x1/144x(92x4)x0.49=24.4	1.1x (53.23 x 2+50.8 x2)*	285
	Flange	2x14/144x(5/8x14.5+3/4x51+3/4x10+9/8x28+3/4x10+3/4x42+5/8x 19+5/8x14+5/8x17+3/4x54+9/8x28+3/4x51+5/8x16.5)x0.49=26.4		
External Girders	Web	52x3/8x1/144x(92x4)x0.49=24.4		
	Flange	2x14/144x(5/8x14.5+1x51+9/8x28+3/4x10+3/4x42+5/8x19 +5/8x14+5/8x17+3/4x54+9/8x28+3/4x10+1x51+5/8x16.5) x0.49=28.83		
Cross Frame		Same as in Previous table.		25
Deck (concrete)		(7/12x32+2x((8+11)/2x3/12+10.5/12x1.5))x0.145x368		1390

*10% extra for joints, splices etc. **Total Weight of Unit IV ≈1700 Kips**

Table 6.1g Five Span Continuous- Unit 5 (Henderson, KY) (460′)

(Based on Calculations from the previous Table)

Total weight of Unit V : 1700/4x5 = 2125 Kips

Table 6.2 Calculation of Pier Stiffness and Pier Mass of SDOF Systems

Model[4]	Pier (Type-II)	Pier Height	L^{1}_{max}	Rectangular		Dia. of Circular Portion	Area	Moment of Inertia	Stiffness		Weight (1/3xtotal)	Mass
				Width	Depth				Min[2]	Max[3]		
EV1	N2	46.75	96.75	24.5	1.5	5.5	84.27	96.73	166	1474	189	12.13
	N3	49.25	94.25	24.5	1.5	5.5	84.27	96.73	180	1261	199	
EV2	N6	51	83	25.5	1.5	4.5	70.06	47.43	129	557	171	10.47
	N7	49	74	25.5	1.5	4.5	70.06	47.43	182	628	164	
HE1	S1	63	96	24.5	1.5	5.5	84.27	96.73	170	602	254	14.88
	S2	55	90	24.5	1.5	5.5	84.27	96.73	207	905	222	

Model	Pier Type-I	Height	L^{1}_{max}	Top		Bottom		Area			Volume of Pier Head	Total Vol.	Weight (1/3x total)	Moment of Inertia (Average)	Stiffness	
				Width	Depth	Width	Depth	Top	Bottom	Average					Min[2]	Max[3]
HE2	S5	40.33	80.33	17	2	18.6	3.55	34	66.0	50.0	446.25	1629	90	42	126	994
HE3	S9	33.35	68.35	17	2	18.1	3.25	34	58.8	46.4	446.25	1188	71	31	152	1305
HE4	S13	29.75	64.75	17	2	18.0	3	34	54.0	44.0	446.25	968	62	26	151	1553
HE5	S17	27.75	60.25	17	2	17.9	2.875	34	51.4	42.7	446.25	854	57	24	168	1724

All quantities are in Ft and Kip units, Modulus of Elasticity E=520000 ksf.

[1]The height of Pier + Depth of pile cap + Half depth of pile

[2]Assumed the pier is fixed at bottom of pile cap (for force calculation)

[3]Assumed the pier extends up to half depth of pile where it is fixed (for displacement calculation)

[4]Models are shown in Figure 6.4 and 6.5

Table 6.3 Calculation of Seismic Response

Model	Mass			Seismic Force							Seismic Displacement						
	Pier	Super Structure	Total	Stiffness (max)	Frequency (Hz)	Period	PSA[1]	C_s[2]	C_s[3]	Force P	Stiffness (min)	Frequency (Hz)	Period	PSA[1]	C_s[2]	C_s[3]	Displacement (in)
EV1	12.13	135.2	147.3	2735	0.68	1.46	120	0.221	0.221	1041	346	0.24	4.10	20	0.037	0.037	6.00
EV2	10.47	44.9	55.4	1185	0.74	1.36	110	0.203	0.203	476	312	0.38	2.65	32	0.059	0.059	5.30
HE1	14.88	70.2	85.1	1508	0.67	1.49	120	0.221	0.221	601	377	0.34	2.98	32	0.059	0.059	5.10
HE2	2.82	56.2	59.0	994	0.65	1.53	120	0.221	0.221	417	126	0.23	4.30	15	0.028	0.028	5.00
HE3	2.22	52.5	54.7	1305	0.78	1.29	130	0.24	0.24	420	152	0.27	3.77	25	0.046	0.046	6.40
HE4	1.94	52.5	55.1	1553	0.85	1.18	150	0.277	0.277	488	151	0.26	3.80	25	0.046	0.046	6.50
HE5	1.78	66.4	68.2	1724	0.80	1.25	130	0.24	0.24	523	169	0.25	4.00	20	0.037	0.037	5.70

All units are in kips and ft. unless stated otherwise

[1]Acceleration determined from Figure. A 4, Ref. Harik et al. (1997)

[2]As per AASHTO formula, $C_S = \frac{1.2 \times PSA \times S}{g}$, with S = 1.5

[3]C_S limited to 2.5A, i.e 2.5x0.15 = 0.375

Table 6-4 Bearing Force Capacity/Demand Ratios for Fixed Bearings on the Evansville, IN Approach on the US 41 Southbound Bridge for the 50 -Year Earthquake

Pier (Number of Fixed Bearings)	Seismic Force (kips)	Minimum Bearing Force Demand[1] (kips)	Force Demand[2] (1.25 x Seismic Force), V_d (kips)	Available Number of Bolts for Pier/Bolt diameter	Available Shear Capacity[3] of the Bolts V_c (kips)	$r_{bf} = \frac{V_c}{V_d}$	Minimum Additional Capacity of Bolts Required[4] per Pier to make $r_{bf} \geq 1$ (kips)
N2 (Two Bearings)	521	471	651	8/1.5″	269	0.41	385
N3 (Two Bearings)	521	471	651	8/1.5″	269	0.41	385
N 6 (Five Bearings)	238	235	298	20/(7/8)"	229	0.77	70
N 7 (Five Bearings)	238	235	298	20/(7/8)"	229	0.77	70

[1, 2] As per FHWA Seismic Retrofitting Manual for Highway Bridges
[3] Assumed capacity of Bolt in Shear = 19.0 ksi (33ksi steel)
[4] Alternate retrofit would be to replace the existing fixed bearings with seismic isolation bearings

Table 6-5 Displacement Capacity/Demand ratio (r_{bd}) for Expansion Bearings of the Evansville, IN Approach on the US41 Southbound Bridge

Pier (Number of Bearings)	Span	Method-2 [1]				Retrofit required?	Retrofit Suggested
		Displacement Demand [2] $\Delta_{eq}(d)$ (in.)	Available seat width[3] $\Delta_s(c)$ (in.)	Contraction due to Temperature[4] $\Delta_i(d)$ (in)	$r_{bd} = \frac{\Delta_s(c) - \Delta_i(d)}{\Delta_{eq}(d)}$		
E (Two Bearings)	E-N2	6	5.1	2.13	0.50	Yes	Existing expansion bearings (rocker bearings) may be replaced with elastomeric bearings, or cable restrainers may be provided
N5 (Two Bearings)	N3-N5	6	5.1	2.13	0.50	Yes	Existing expansion bearings (rocker bearings) may be replaced with elastomeric bearings, or cable restrainers may be provided
N5 (Five Bearings)	N5-N6	5.3	6.86	0.72	1.15	No	None
N8 (Five Bearings)	N7-N8	5.3	6.86	0.72	1.15	No	None

[1] As per FHWA Seismic Retrofitting Manual for Highway Bridges

[2] Derived from analysis of the projected 50-year seismic event

[3] The existing rocker bearings are assumed to be in good condition.

[4] A temperature difference of $\Delta T = 90°F$ is assumed conservatively, and the thermal expansion coefficient is taken to be $\alpha = 6.5 \times 10^{-6}/°F$.

Table 6-6 Bearing Force Capacity/Demand Ratios for Fixed Bearings on the Henderson, KY Approach on the US 41 Southbound Bridge for the 50-Year Earthquake

Fixed Bearing at Pier	Seismic Force (kips)	Minimum Bearing Force Demand[1] (kips)	Force Demand[2] (1.25xSeismic Force) V_d (kips)	Available Number of Bolts for Pier/Bolt Diameter	Available Shear Capacity of the Bolts[3] V_c (kips)	$r_{bf} = \frac{V_c}{V_d}$	Minimum Additional Capacity of Bolts Required[4] for Pier to make $r_{bf} \geq 1$ (kips)
S1	301	272	376	8/1.5″	269	0.71	110
S2	301	272	376	8/1.5″	269	0.71	110
S5	417	378	522	10/1.25″ diadia	233	0.45	290
S9	420	350	525	10/1.25″	233	0.44	295
S13	488	352	610	10/1.25″	233	0.38	380
S17	523	436	654	10/1.25″	233	0.36	425

[1, 2] As per FHWA Seismic Retrofitting Manual for Highway Bridges
[3] Assumed capacity of Bolt in Shear = 19.0 ksi (33ksi steel)
[4] Alternate retrofit would be to replace the existing fixed bearings with seismic isolation bearings

Table 6-7 Displacement Capacity/Demand ratio (r_{bd}) for Expansion Bearings of the Henderson, KY Approach Spans on the US 41 Southbound Bridge

Pier (Number of Expansion Bearings)	Span	Method-2[1]				Retrofit Required?	Retrofit Proposed?
		Displacement Demand [2] $\Delta_{eq}(d)$ (in.)	Available Seat Width [3] $\Delta_s(c)$ (in.)	Contraction due to Temperature [4] $\Delta_i(d)$ (in.)	$r_{bd} = \frac{\Delta_s(c) - \Delta_i(d)}{\Delta_{eq}(d)}$		
S3 (Two Bearings)	S3-S2	5.1	5.00	1.07	0.77	Yes	Existing expansion bearings (rocker bearings) may be replaced with elastomeric bearings, or provide cable restriners
S3 (Five Bearings)	S3-S5	5.0	8.50	1.41	1.42	No	None
S7 (Five Bearings)	S7-S5	5.0	8.50	1.29	1.13	No	None
	S7-S9	6.4		1.29			
S11 (Five Bearings)	S11-S9	6.4	8.50	1.29	1.13	No	None
S11 (Five Bearings)	S11-S13	6.5		1.29		No	None
S15 (Five Bearings)	S15-S13	6.5	8.50	1.29	1.26	No	None
	S15-S17	5.7		1.29			
S20 (Five bearings)	S20-S17	5.7	8.50	1.94	1.15	No	None

[1] As per FHWA Seismic Retrofitting Manual for Highway Bridges.
[2] Derived from analysis of 50-Year seismic event
[3] Existing rocker bearings are assumed to be in good condition
[4] A temperature difference of $\Delta T = 90°F$ is assumed conservatively, and the thermal expansion coefficient is taken to be $\alpha = 6.5 \times 10^{-6}/°F$

Figure 2.1a US41 Northbound and Southbound Bridges over the Ohio River at Henderson, KY - Entrance View

Figure 2.1b Side Views of the US41 Bridges over the Ohio river

Figure 2.1c End portal of the US41 Bridges

Figure 2.1d Typical Hinge Location on US41 Bridges

Figure 2.1e Inside View Showing Portals, Cross Bracings, etc

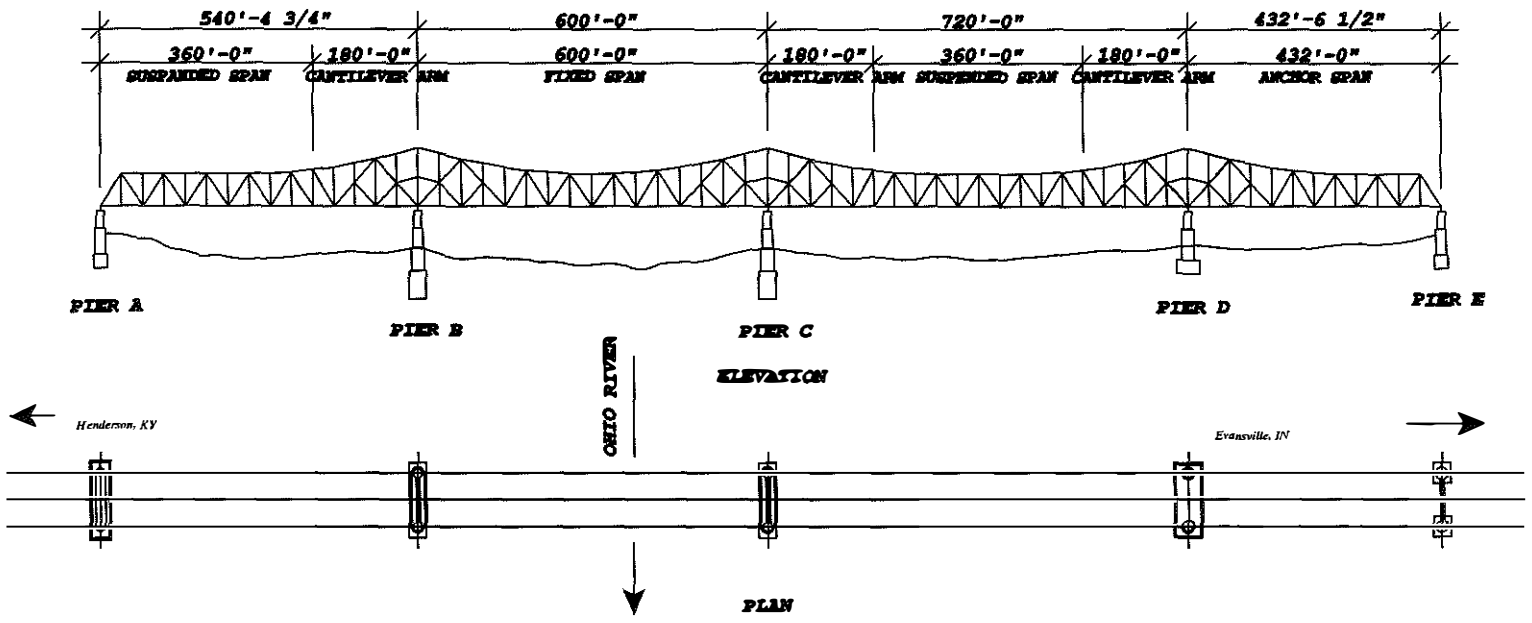

Figure 2.2 Plan and Elevation Views of the US41 Southbound Main Bridge over the Ohio River

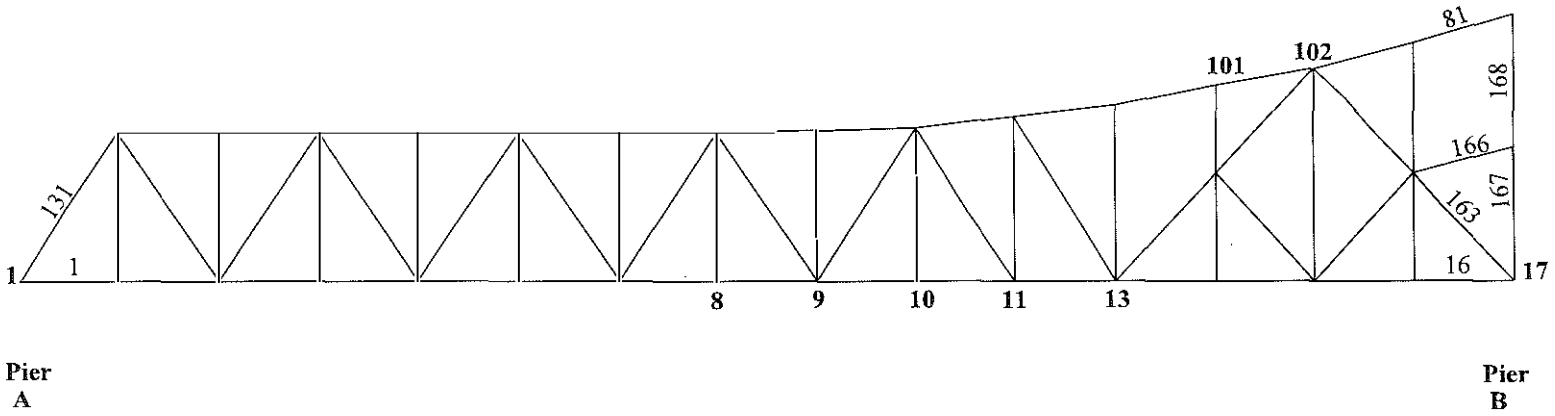

Figure 2.3 Elevation of the first span A-B

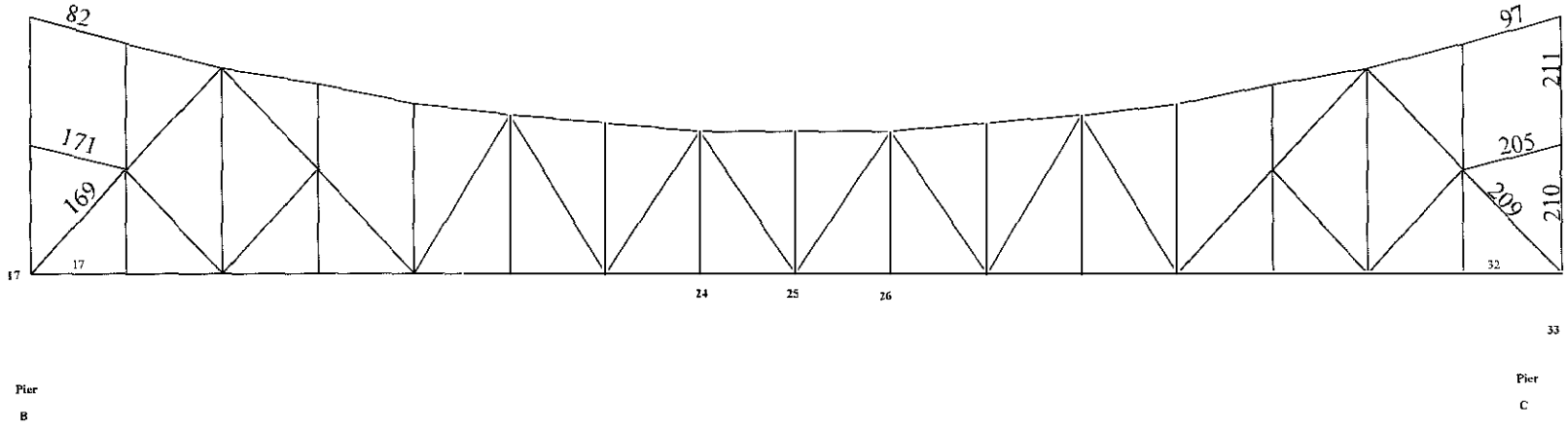

Figure 2.4 Elevation of the second span B-C

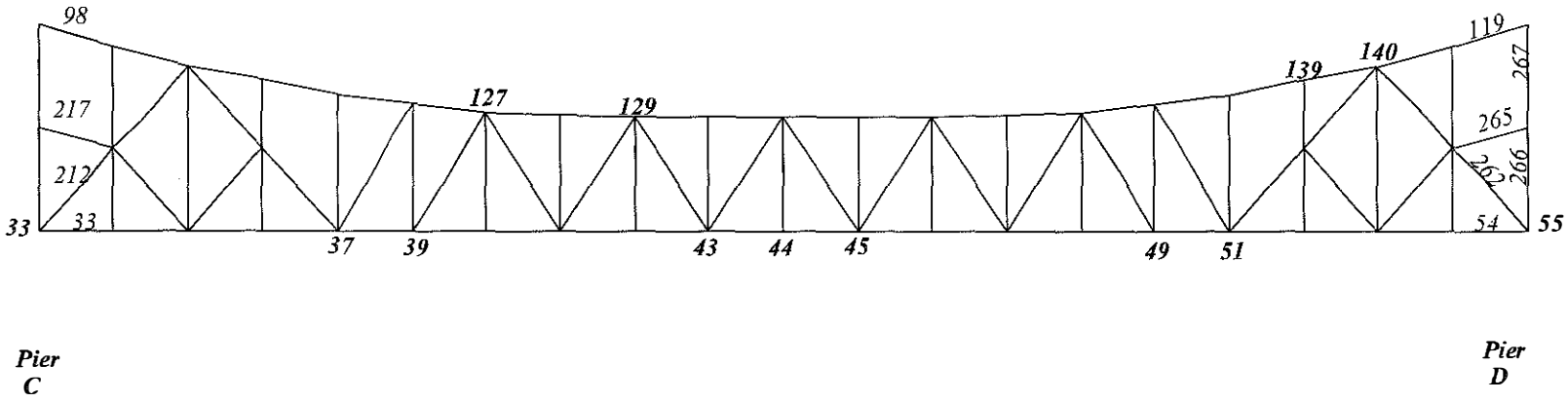

Figure 2.5 Elevation of the third span C-D

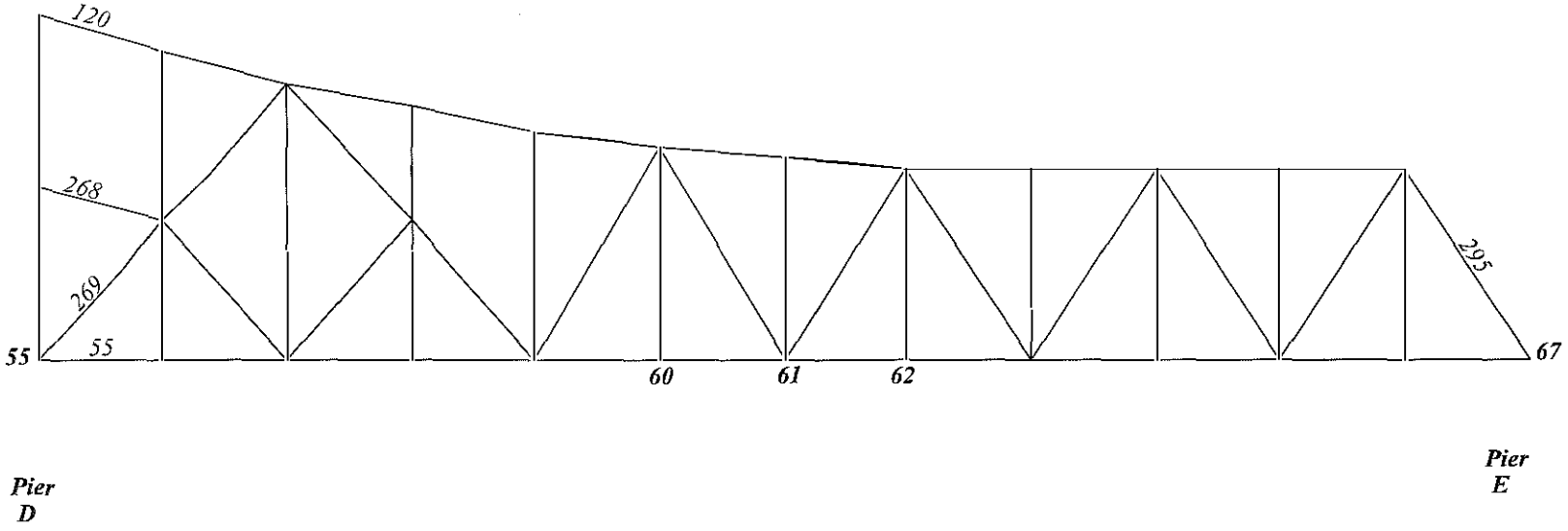

Figure 2.6 Elevation of the fourth span D-E

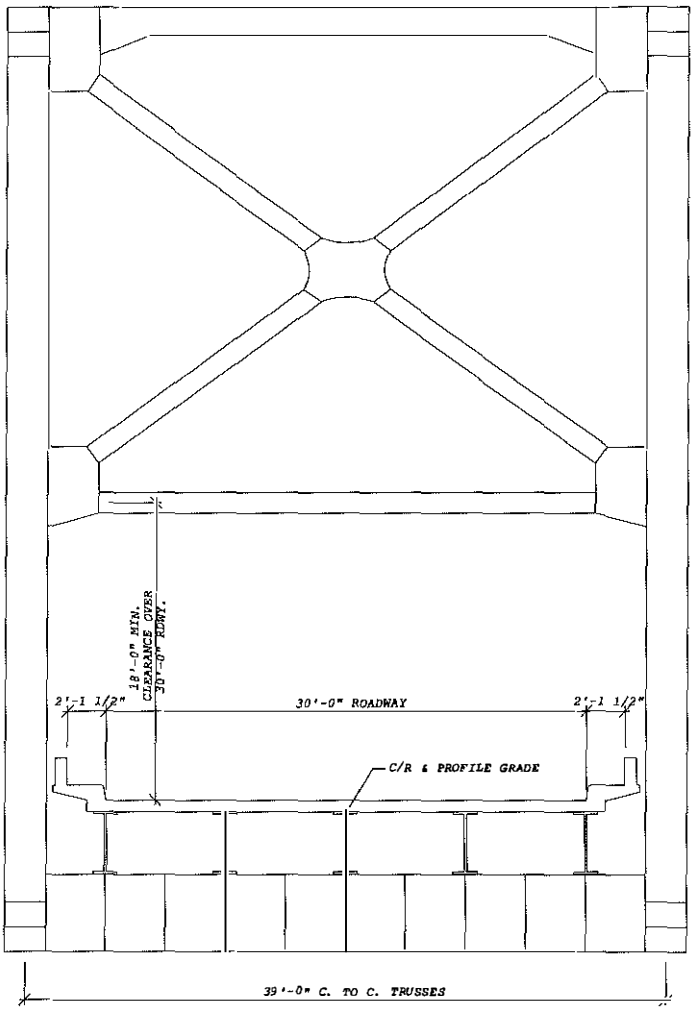

TYPICAL SECTION THRU TRUSS

Figure 2.7 Cross section of the main bridge deck

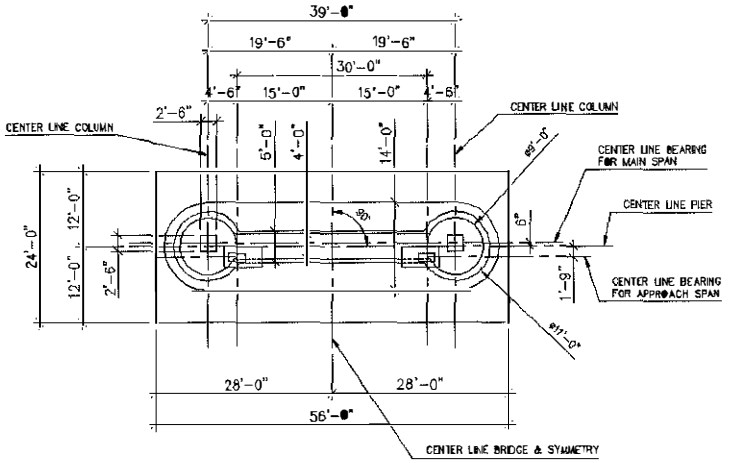

Plan

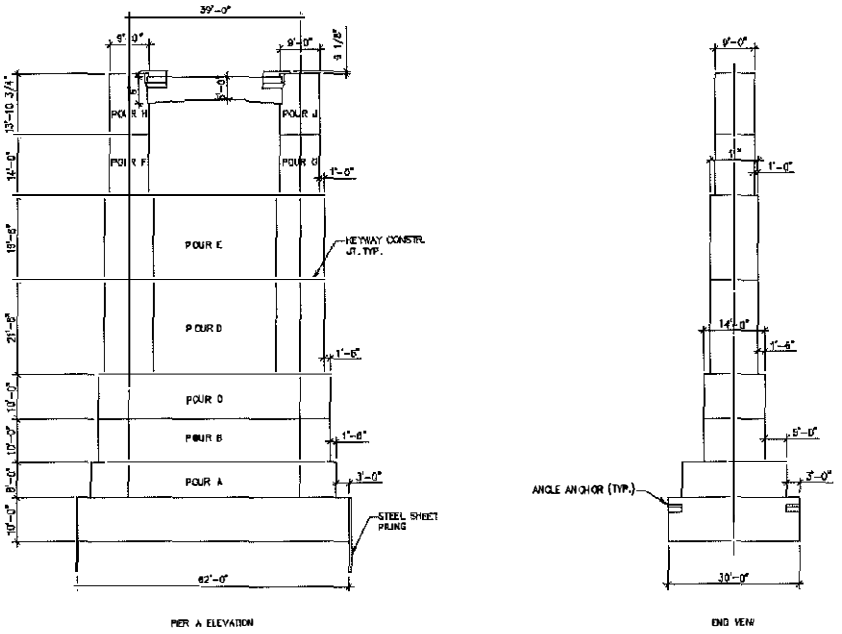

Elevation

Figure 2.8 Details of Pier A of the Main Bridge on the US41 Southbound

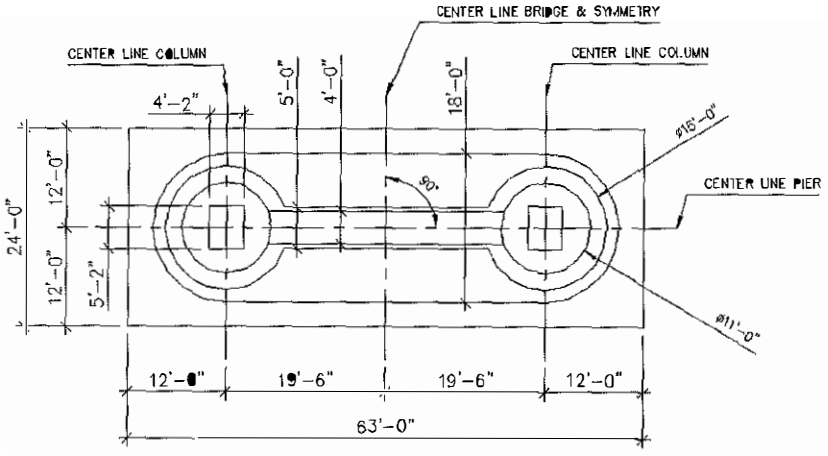

Plan

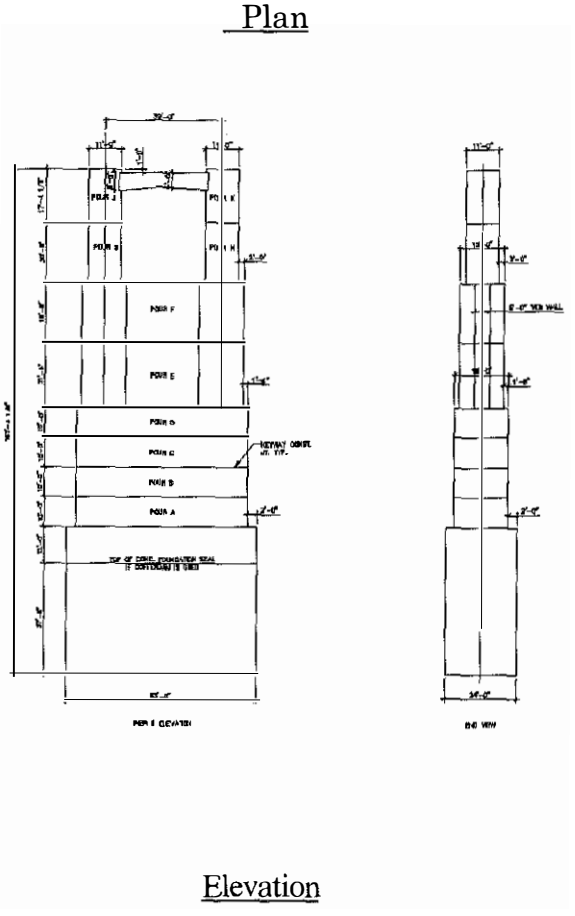

Elevation

Figure 2.9 Details of Pier B of Main Bridge on the US41 Southbound

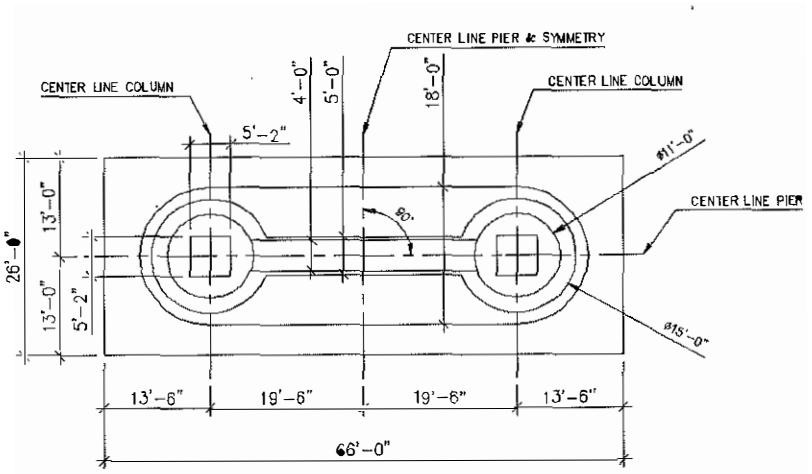

Plan

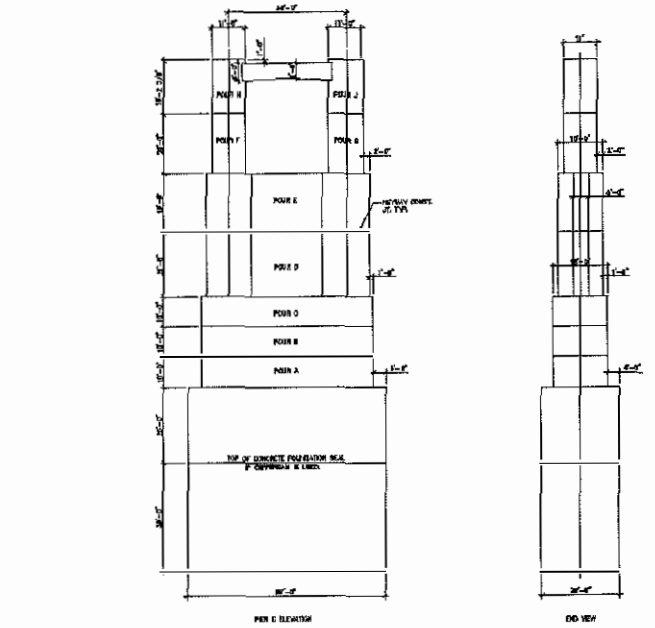

Elevation

Figure 2.10 Details of Pier C of the Main bridge on the US 41 Southbound

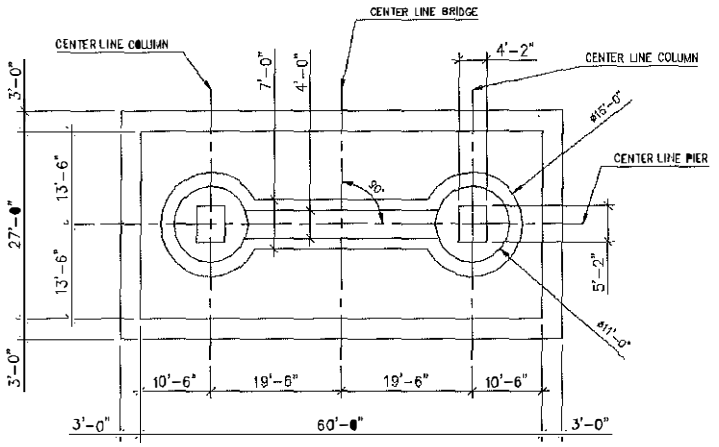

Plan

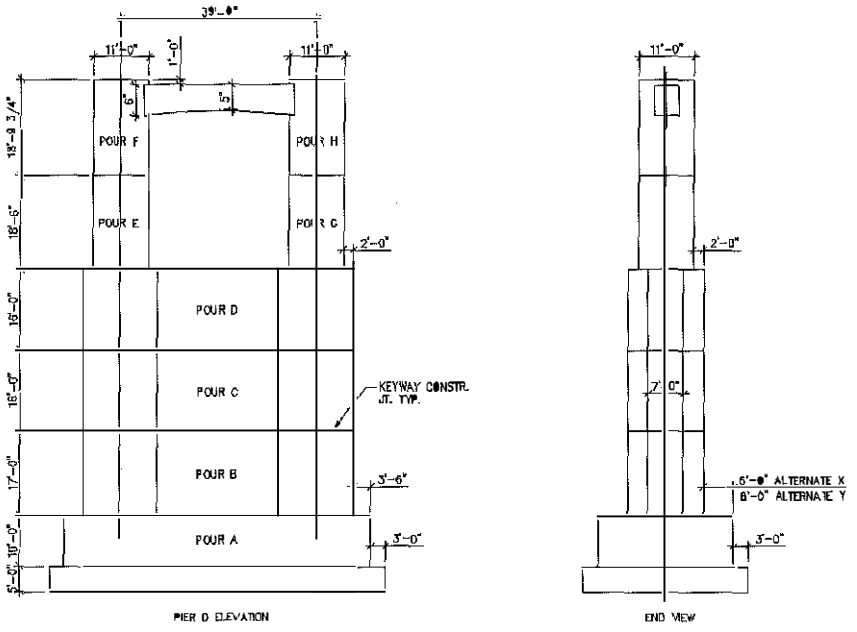

Elevation

Figure 2.11 Details of Pier D of the Main Bridge on the US41 Southbound

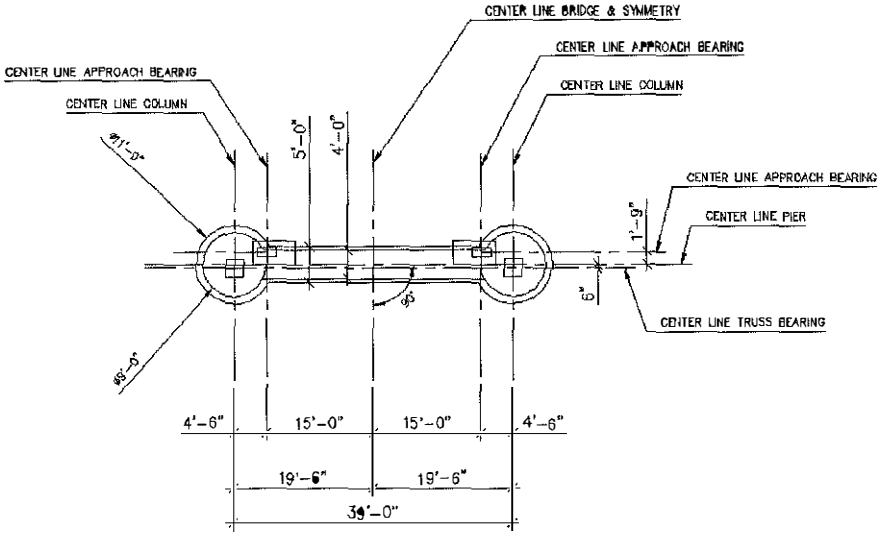

Plan

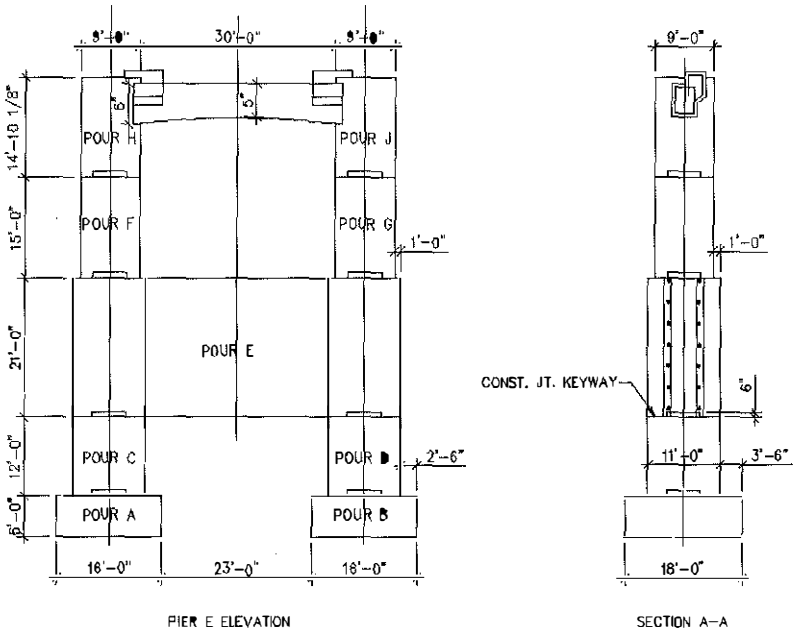

Elevation

Figure 2.12 Details of Pier E of the Main Bridge on the US41 Southbound

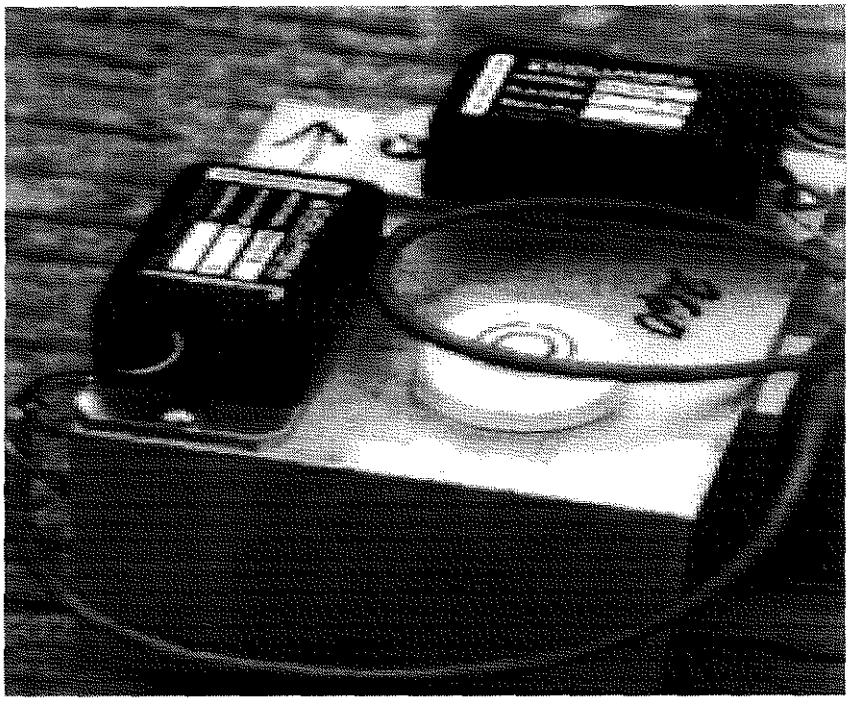

Figure 3.1a Triaxial Accelerometer Block

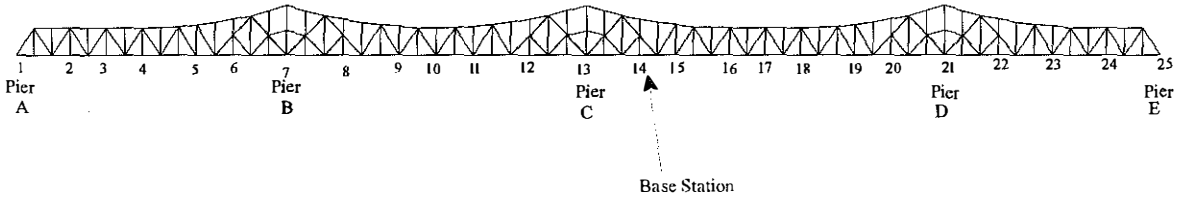

Figure 3.1b Accelerometer positions on the main bridge

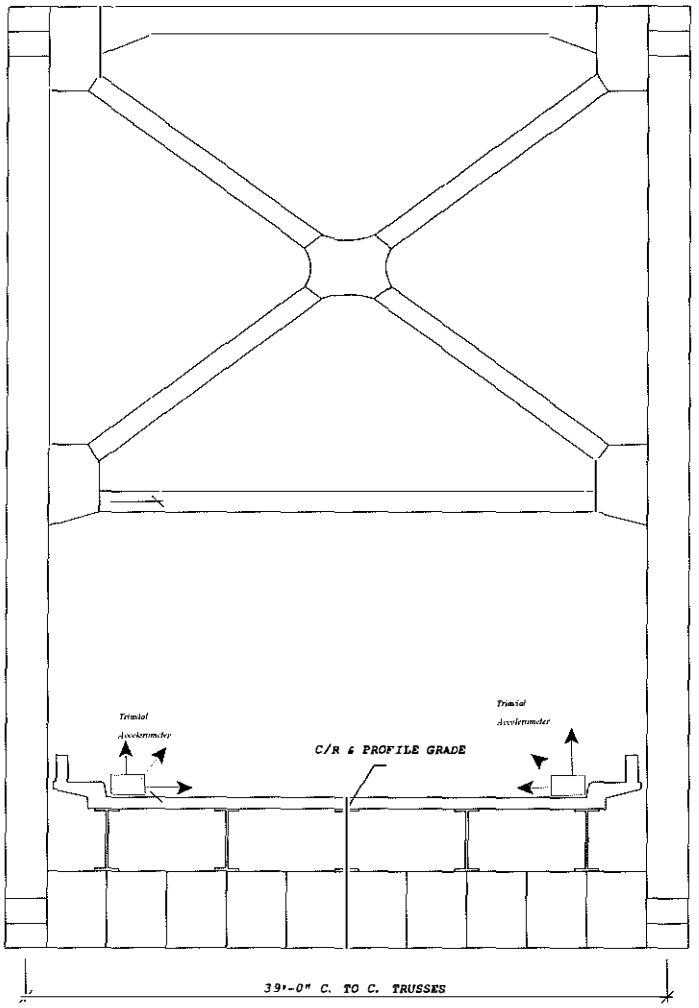

TYPICAL SECTION THRU TRUSS

Figure 3.1c Accelerometer positions on the deck

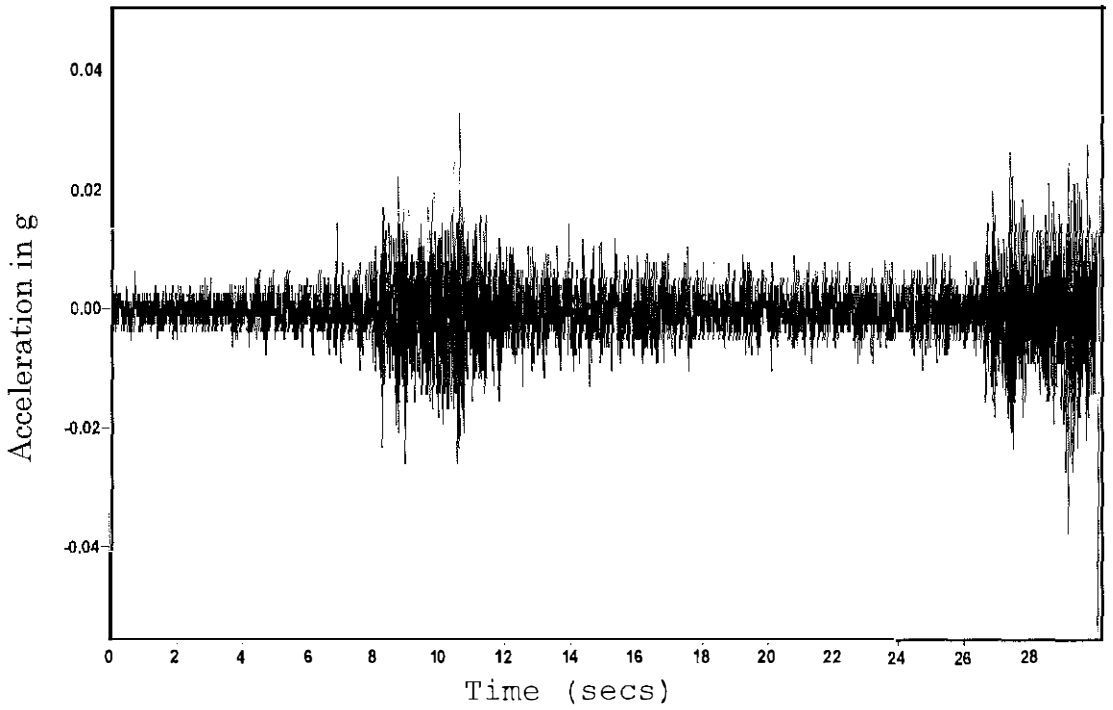

Figure 3.2a Transverse Acceleration-Time History from Field Testing at Moving Station 6

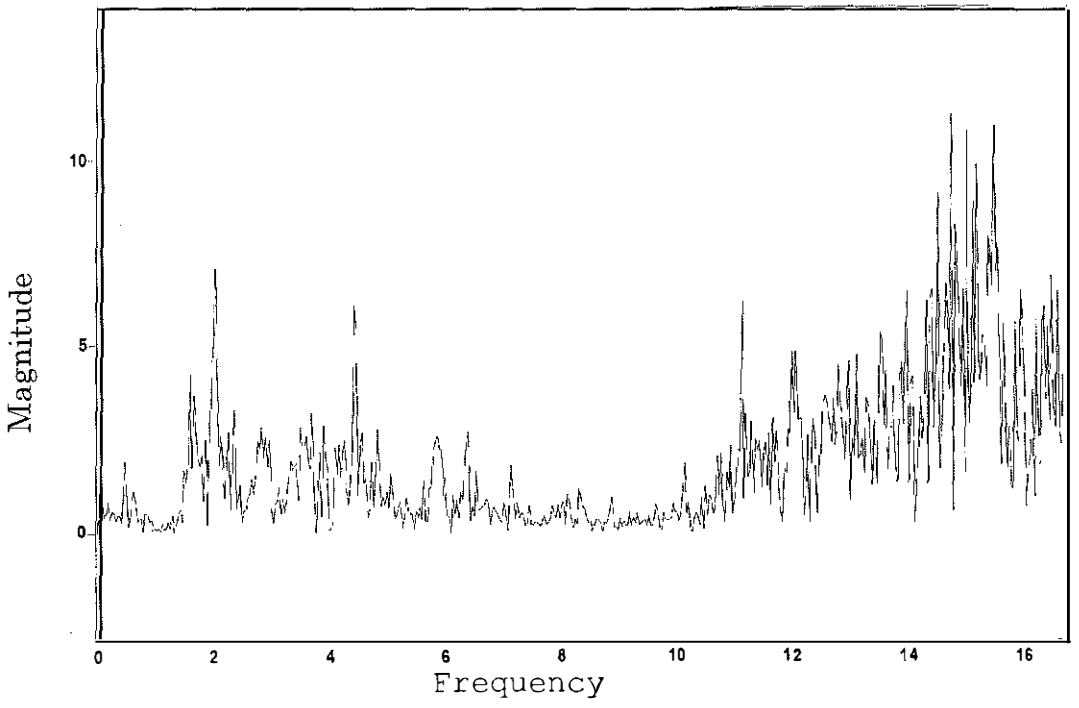

Figure 3.2b FFT of Transverse Acceleration-Time History at Moving Station 6

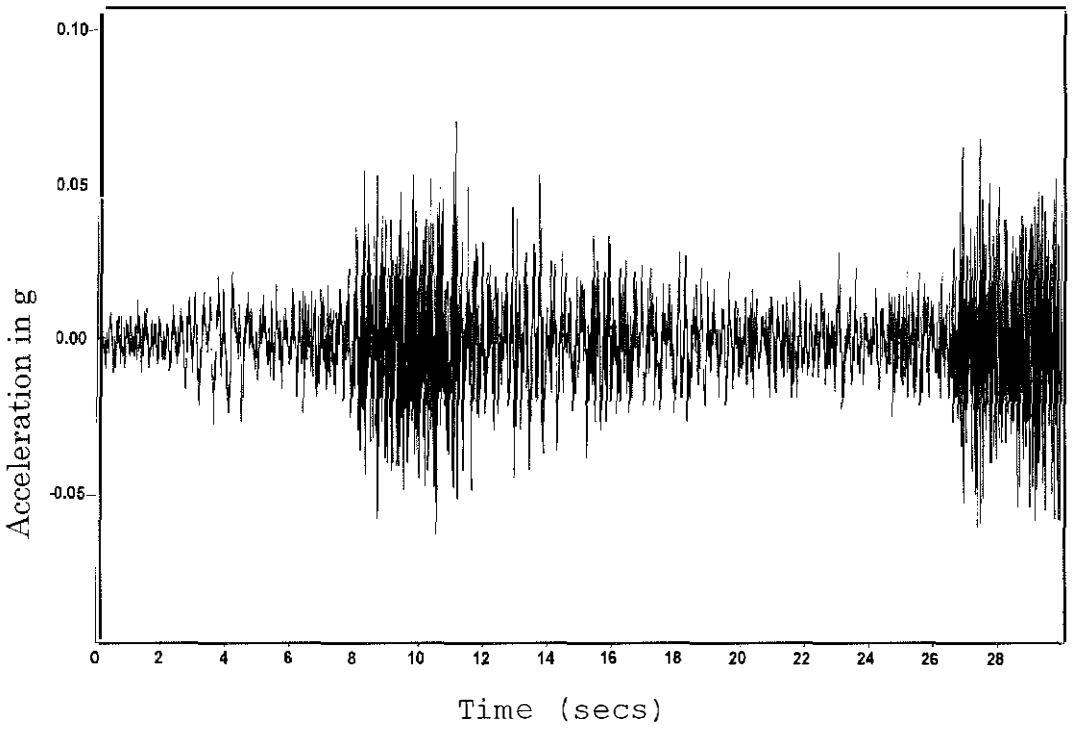

Figure 3.2c Vertical Acceleration-Time History from Field Testing at Moving Station 6

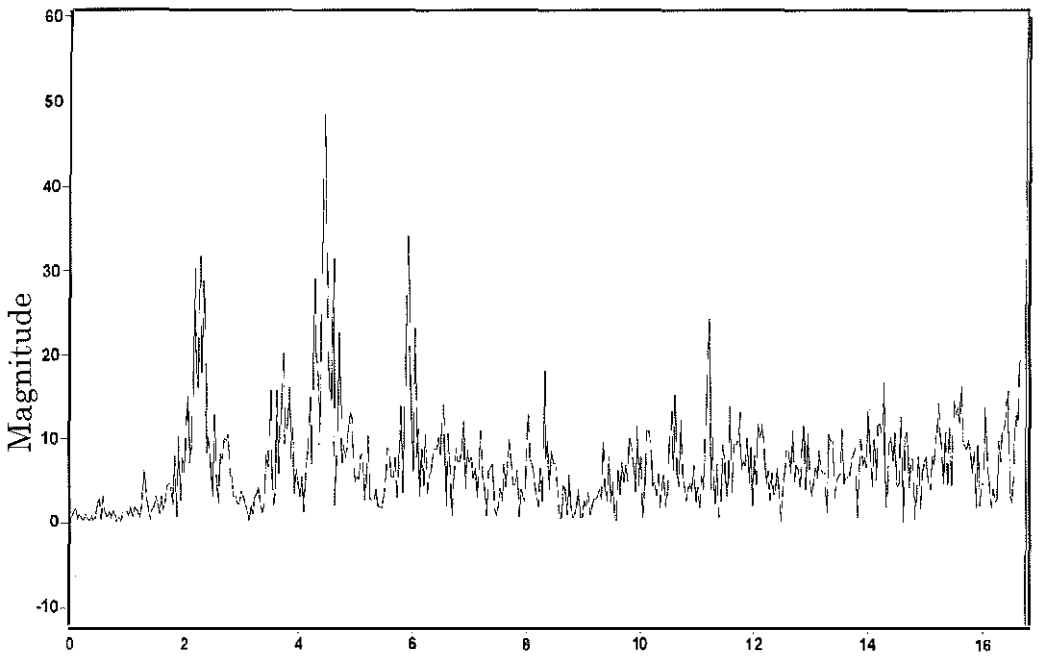

Figure 3.2d FFT of Vertical Acceleration-Time History at Moving Station 6

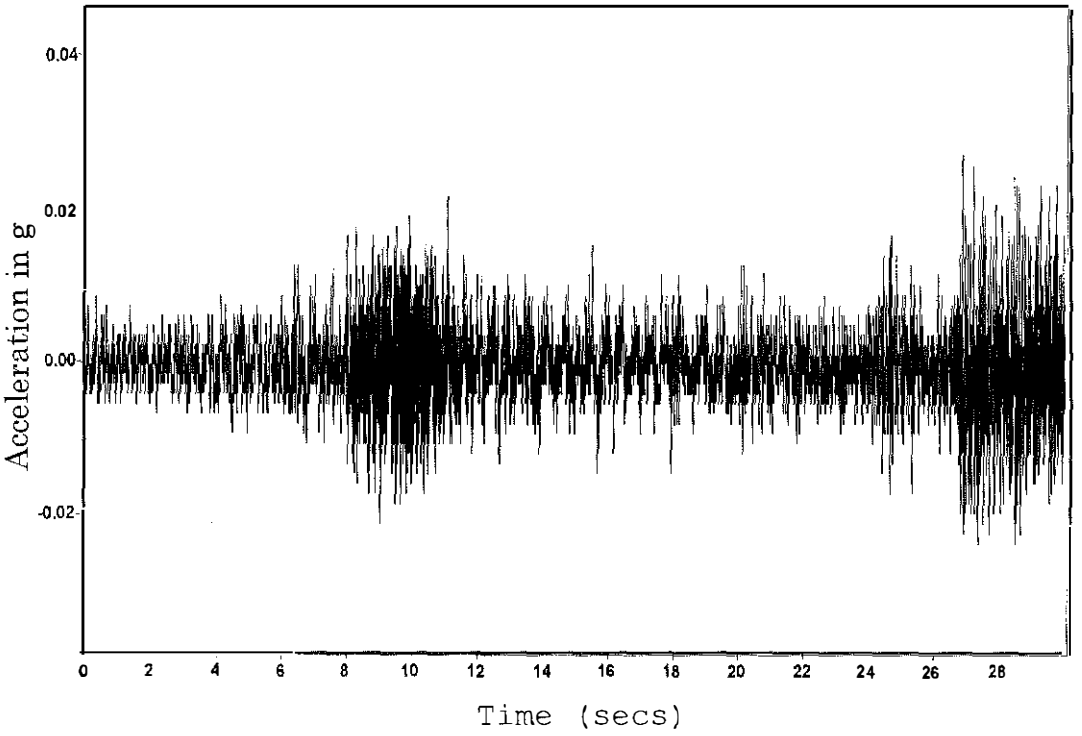

Figure 3.2e Longitudinal Acceleration-Time History from Field Testing at Moving Station 6

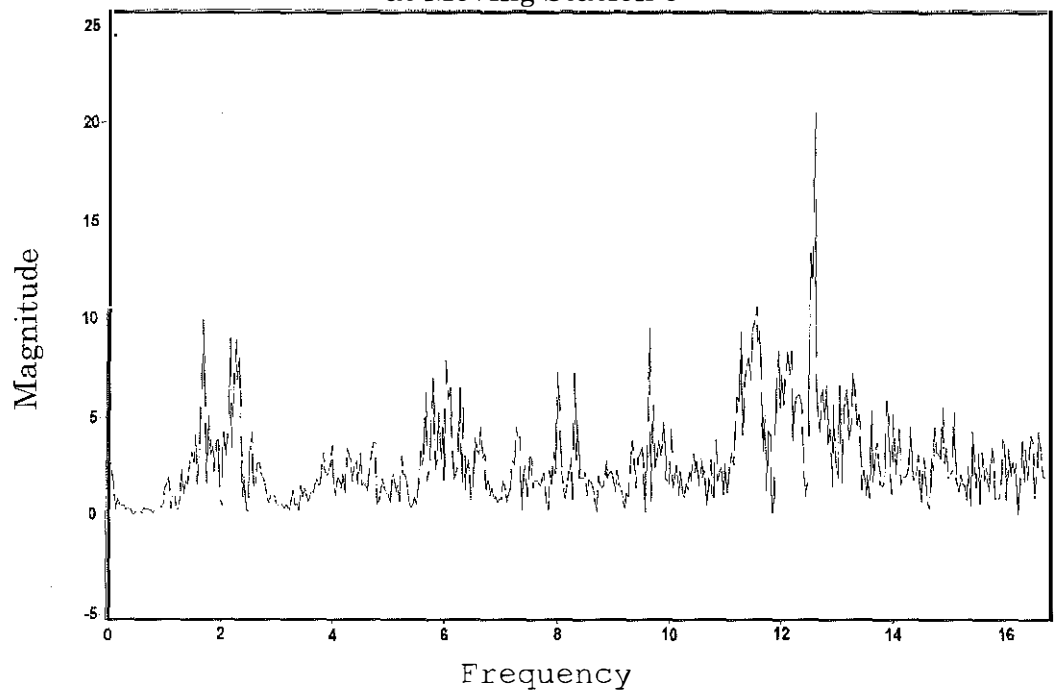

Figure 3.2f FFT of Longitudinal Acceleration-Time History at Moving Station 6

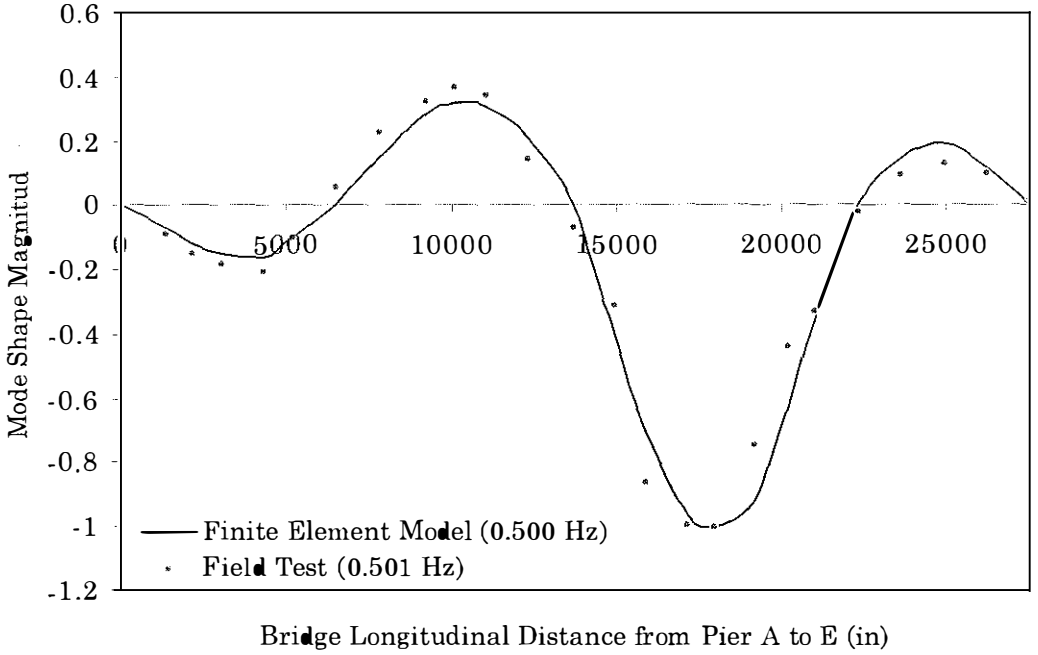

Figure 3.3a First Transverse Mode

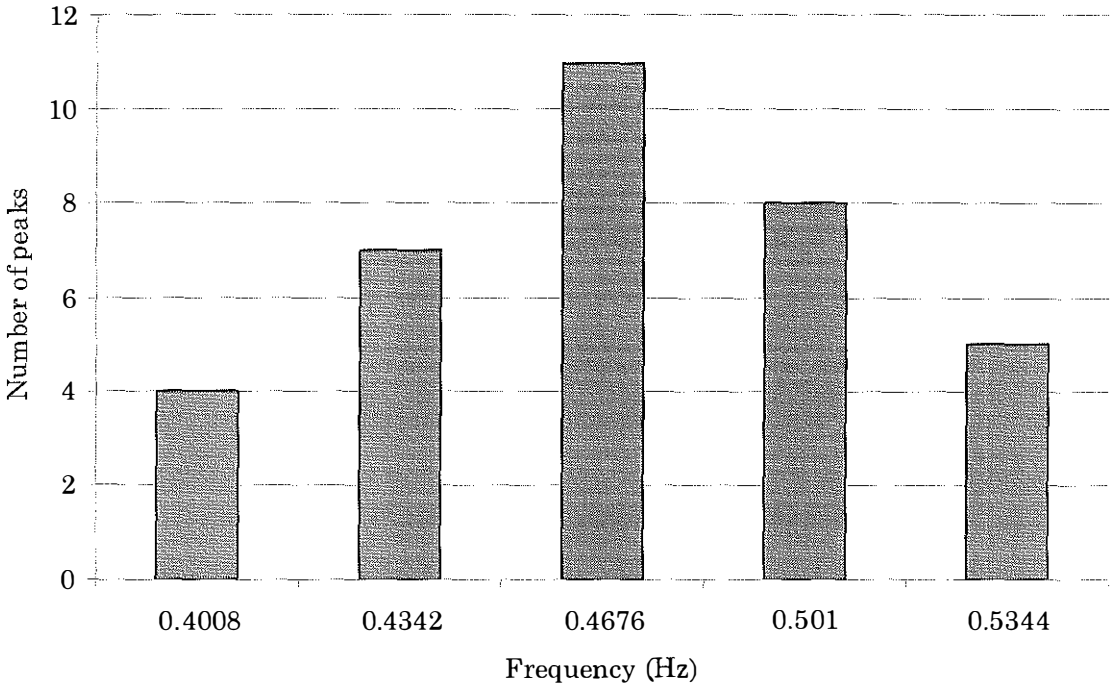

Figure 3.3b Peak Comparison for the First Transverse Mode

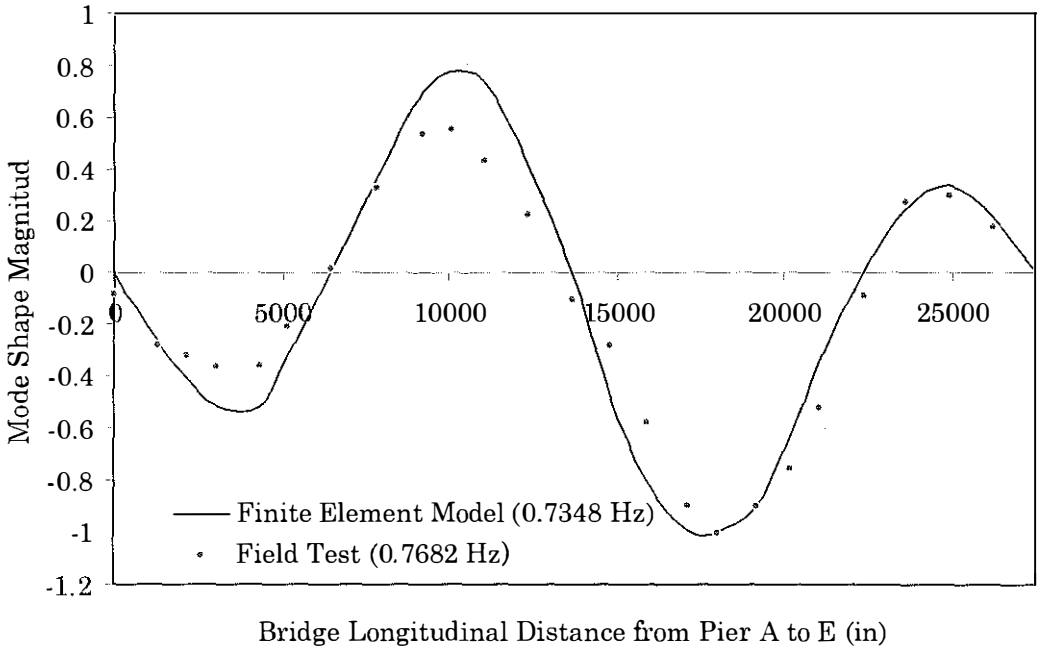

Figure 3.4a First Vertical Mode

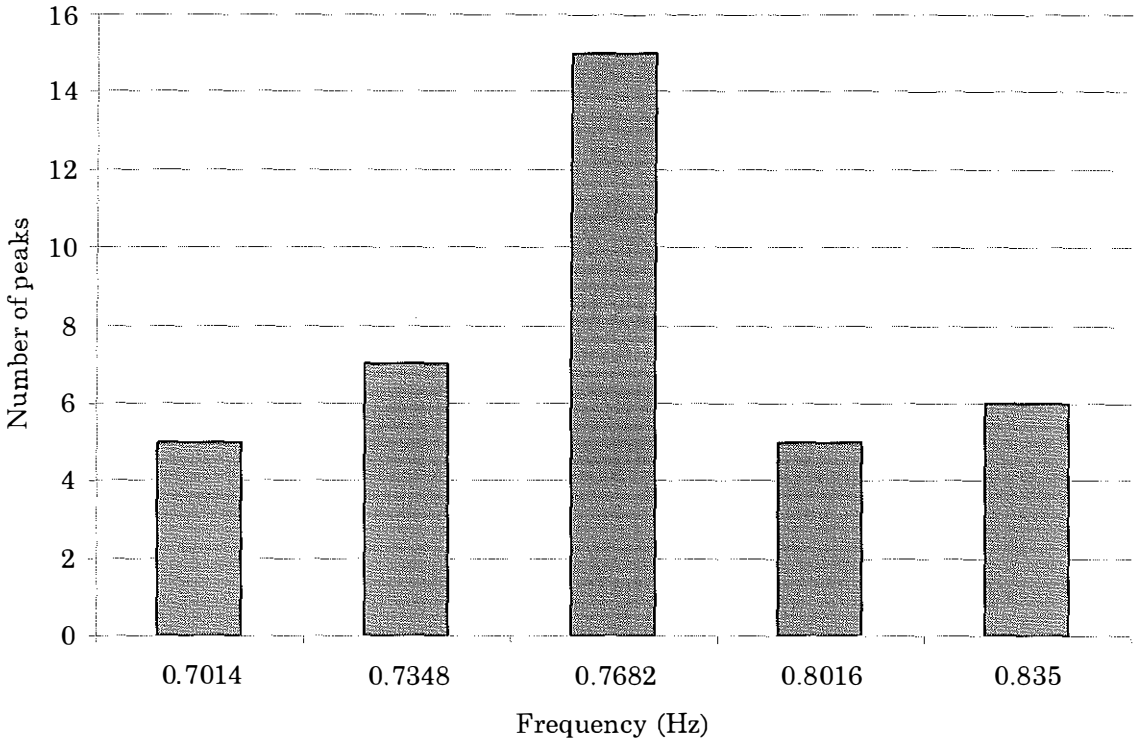

Figure 3.4b Peak Comparison for the First Vertical Mode

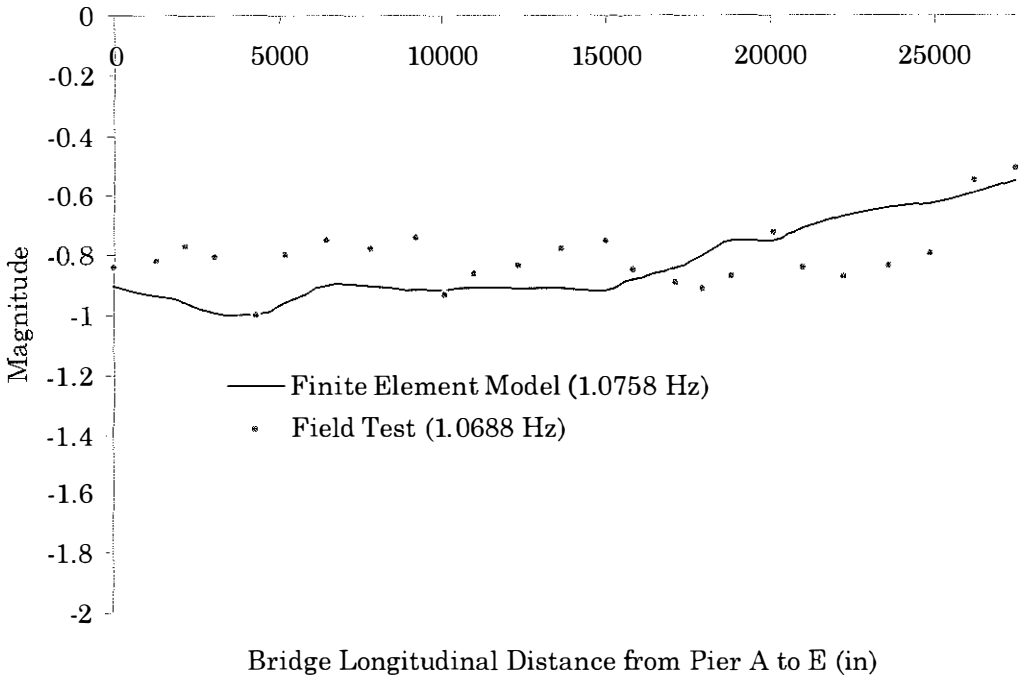

Figure 3.5a First Longitudinal Mode

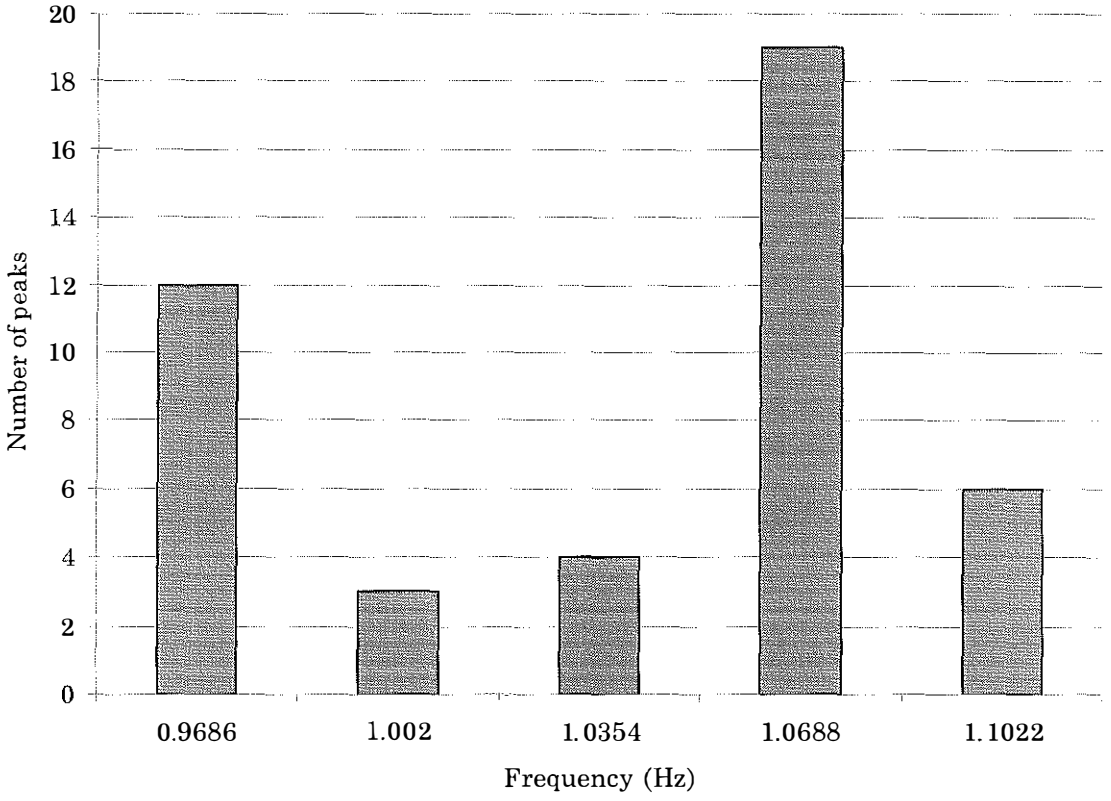

Figure 3.5b Peak Comparison for the First Longitudinal Mode

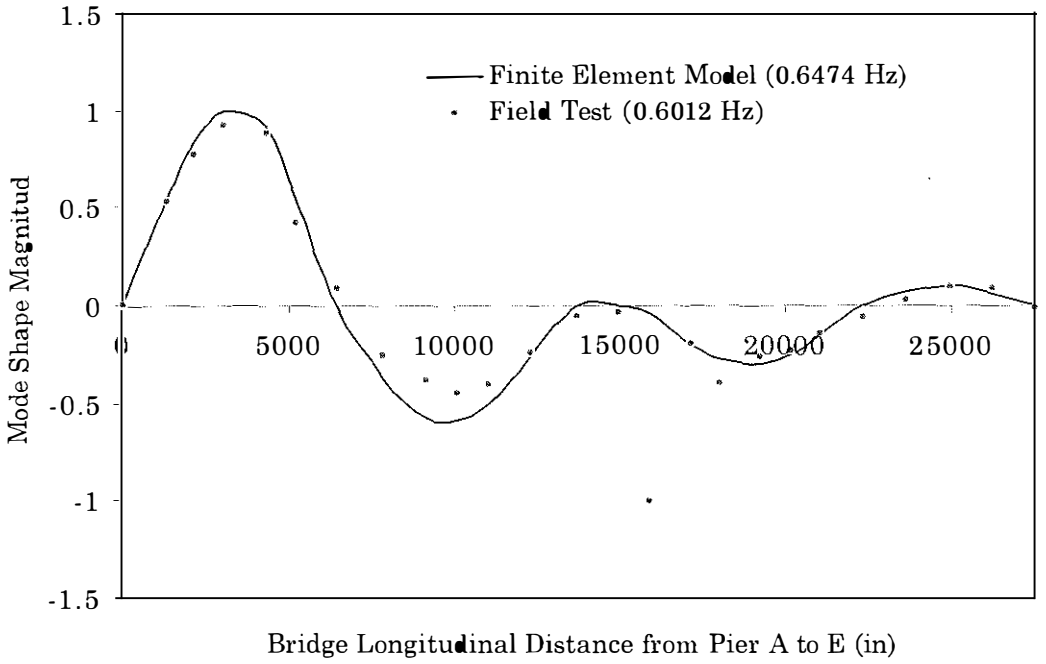

Figure 3.6a Second Transverse Mode

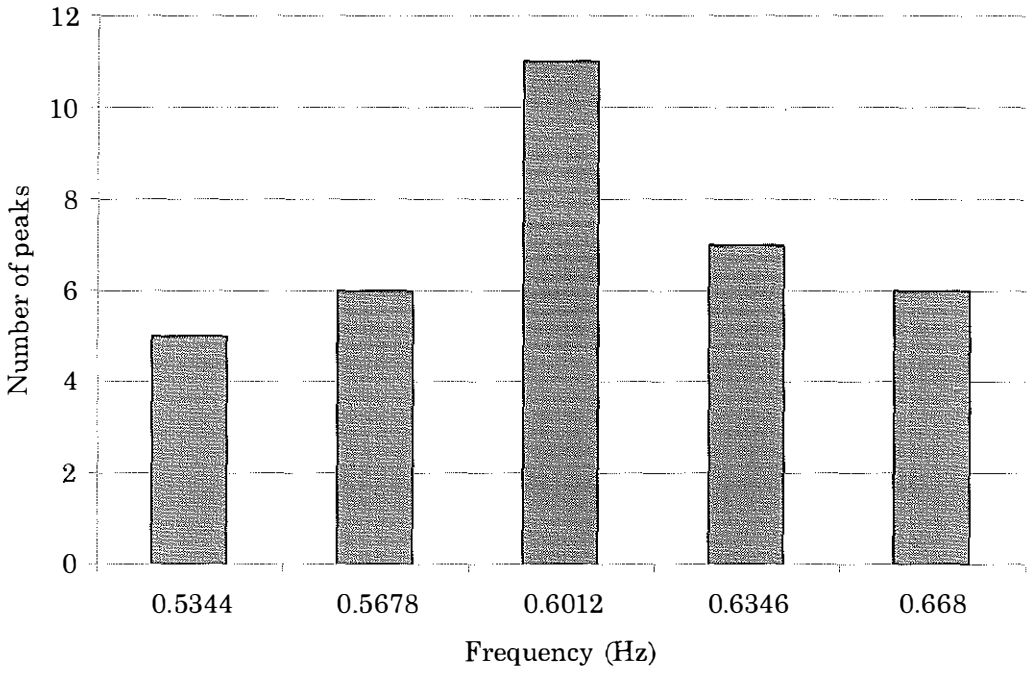

Figure 3.6b Peak Comparison for the Second Transverse Mode

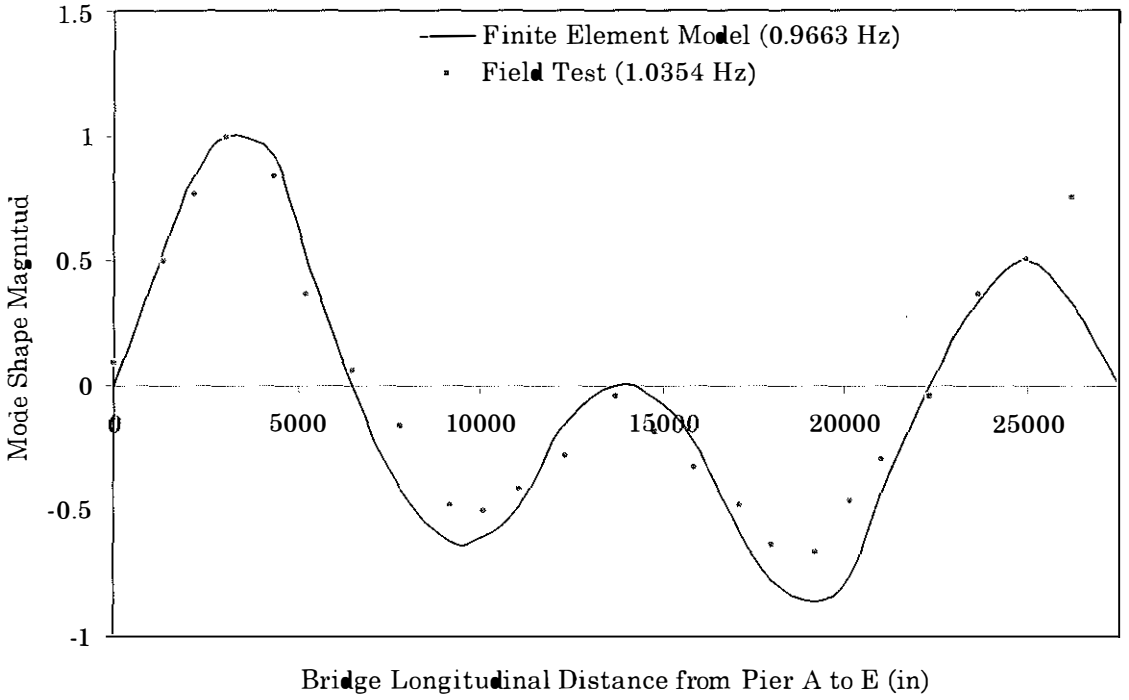

Figure 3.7a Second Vertical Mode

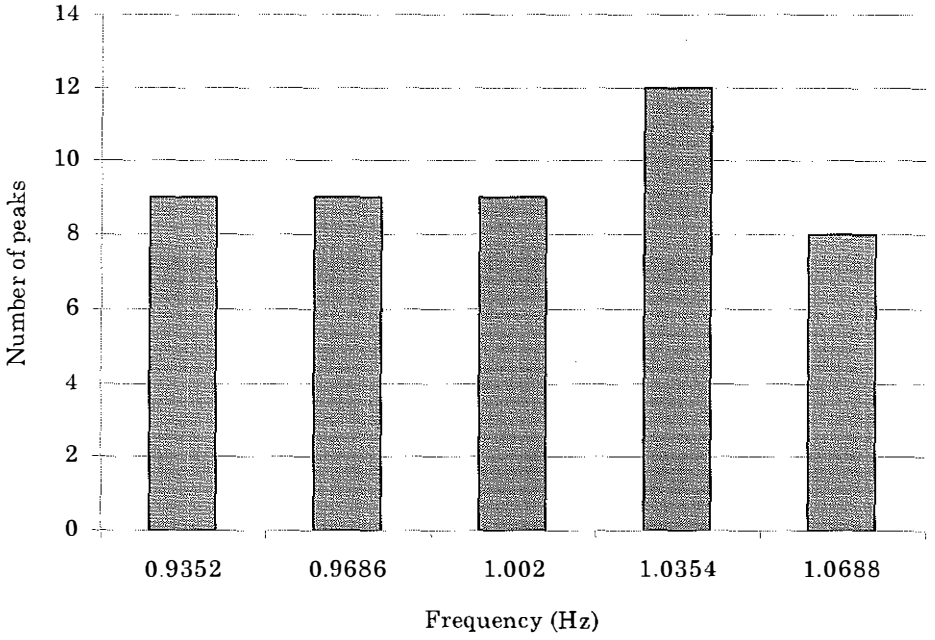

Figure 3.7b Peak Comparison for the Second Vertical Mode

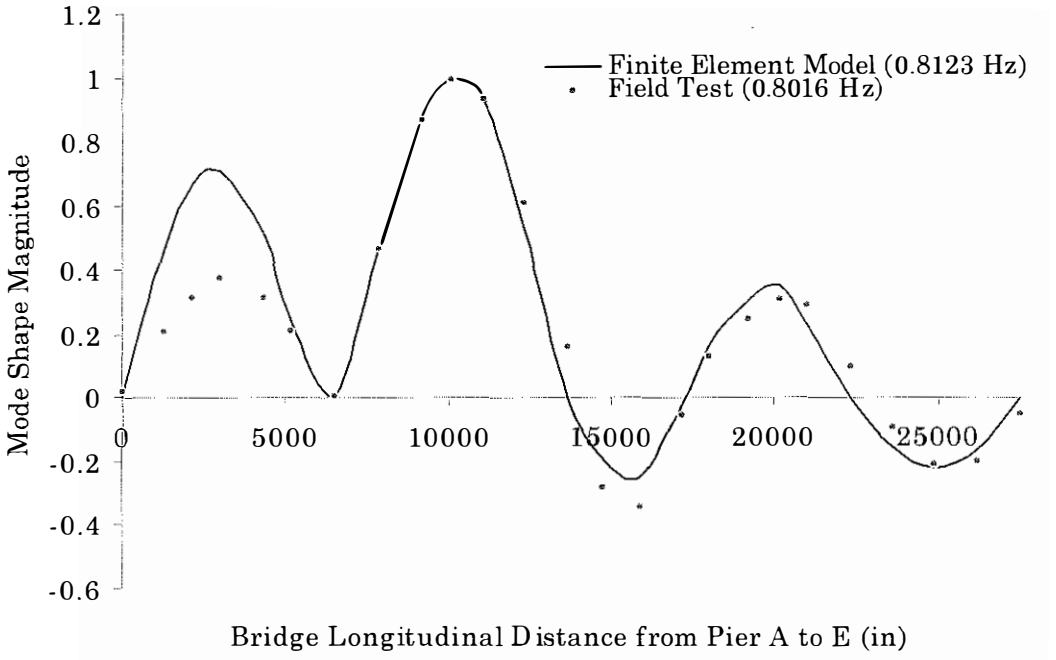

Figure 3.8a Third Transverse Mode

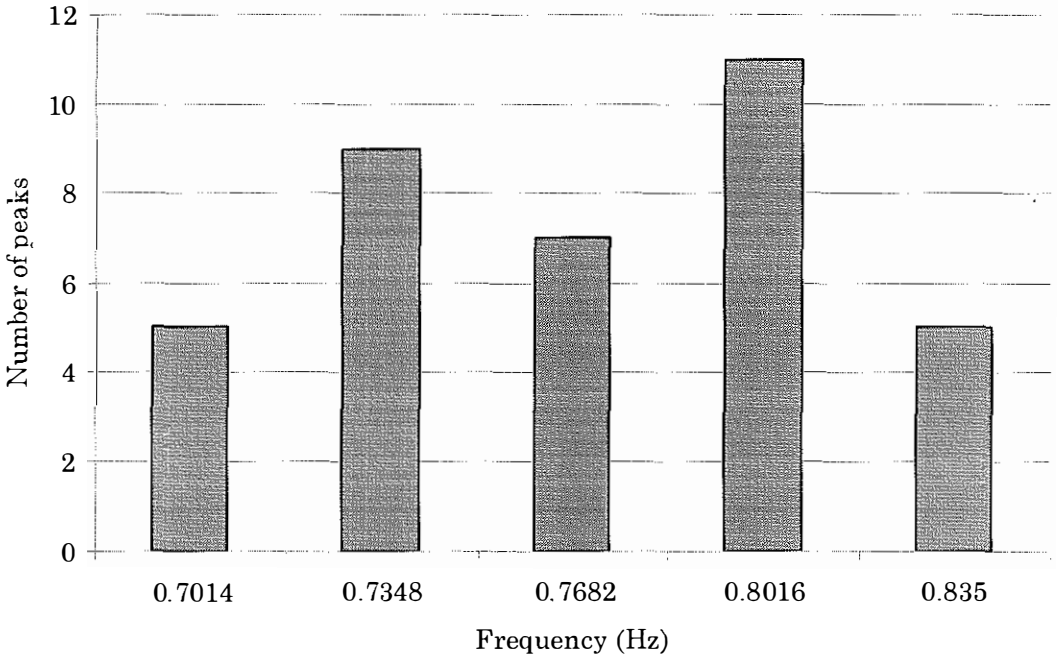

Figure 3.8b Peak Comparison for the Third Transverse Mode

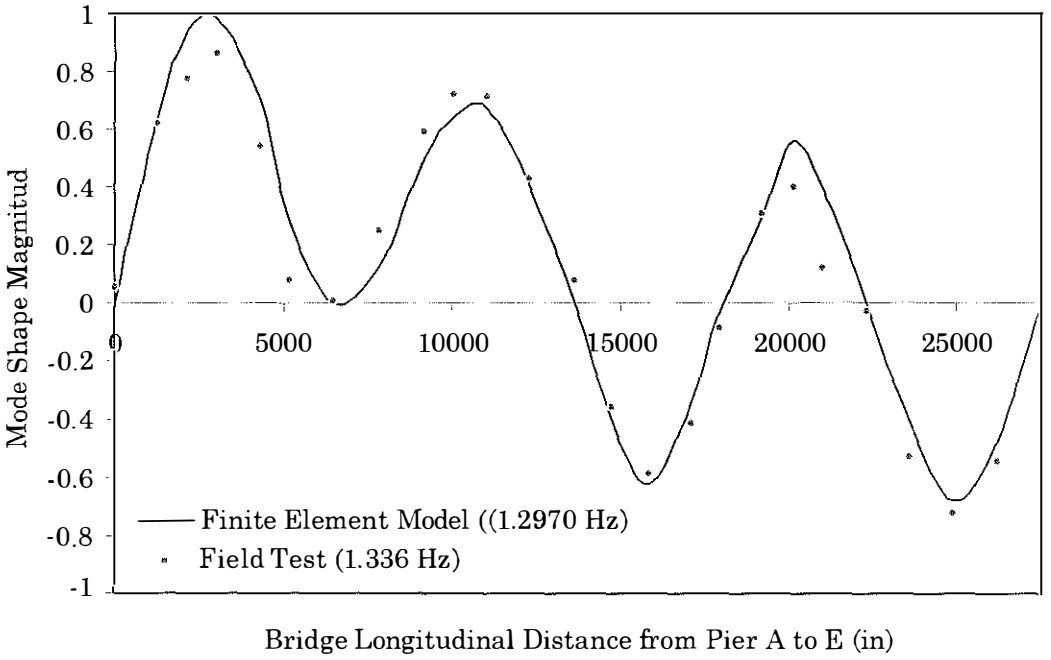

Figure 3.9a Third Vertical Mode

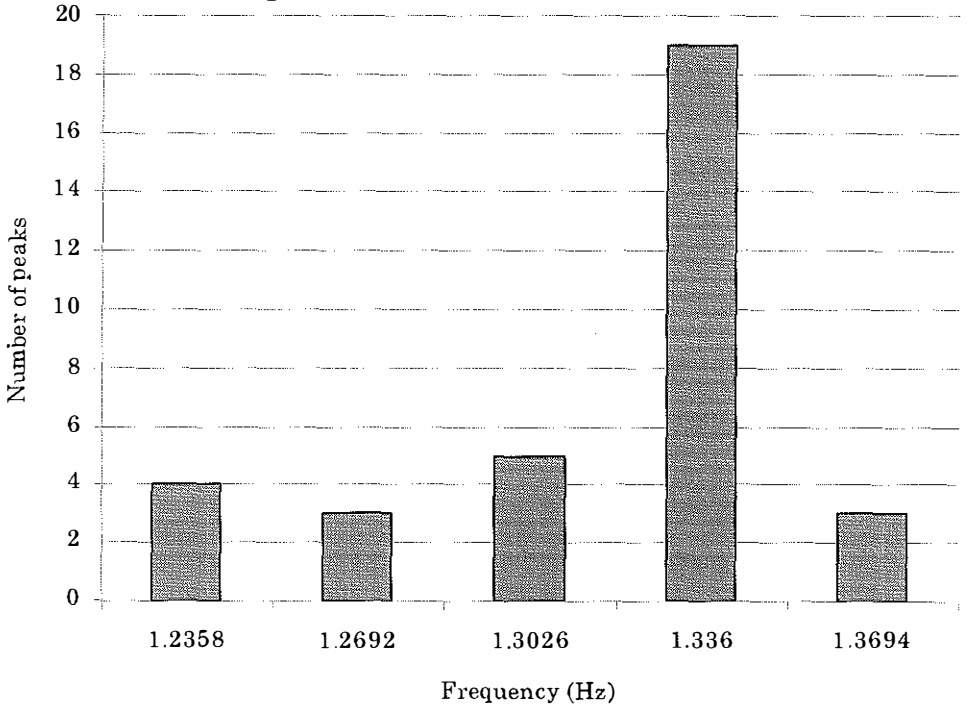

Figure 3.9b Peak Comparison for the Third Vertical Mode

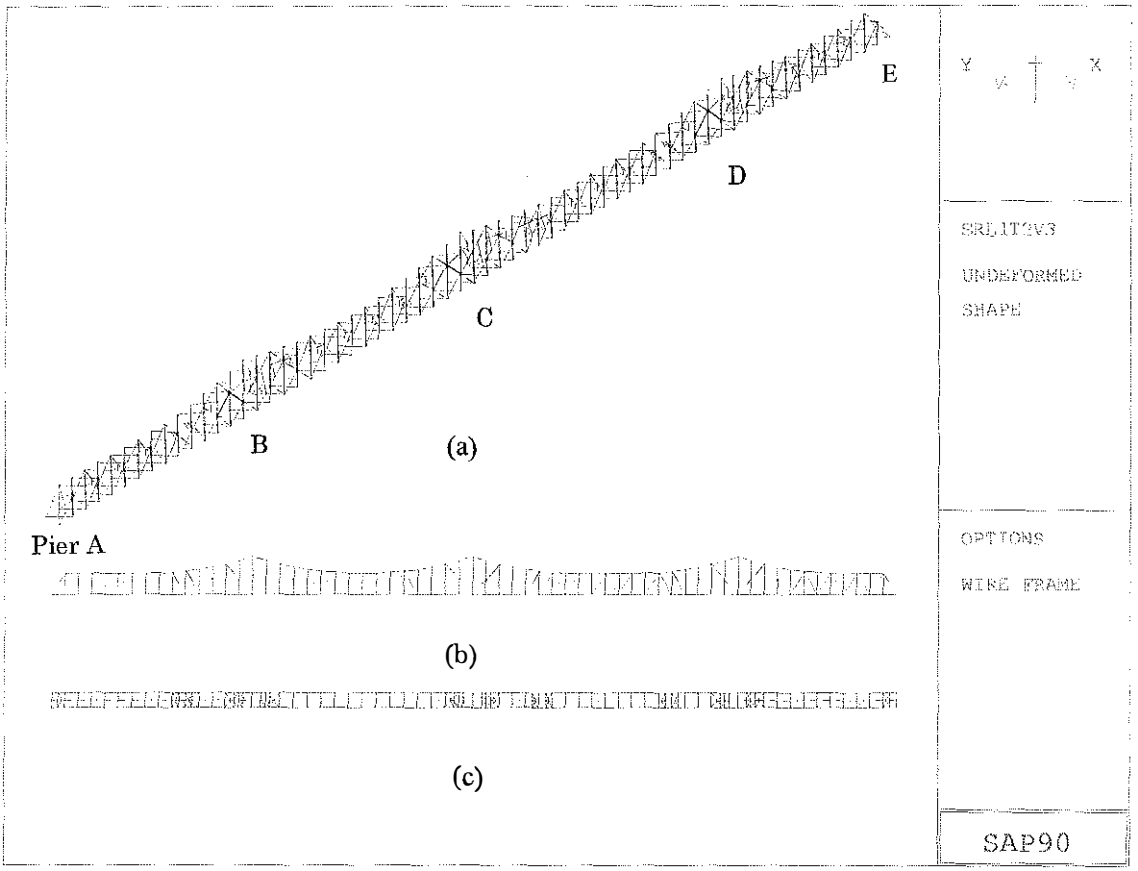

Figure 4.1 3D Finite Element Model of the US41 Southbound Bridge
(a) Isometric View, (b) Elevation View, and (c) Plan View

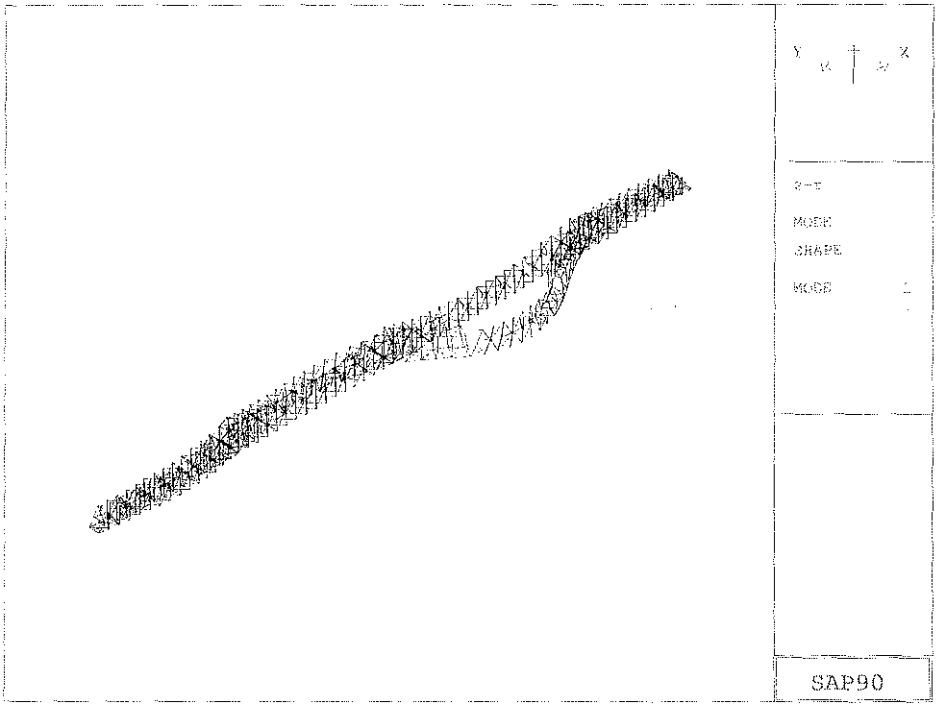

(a)

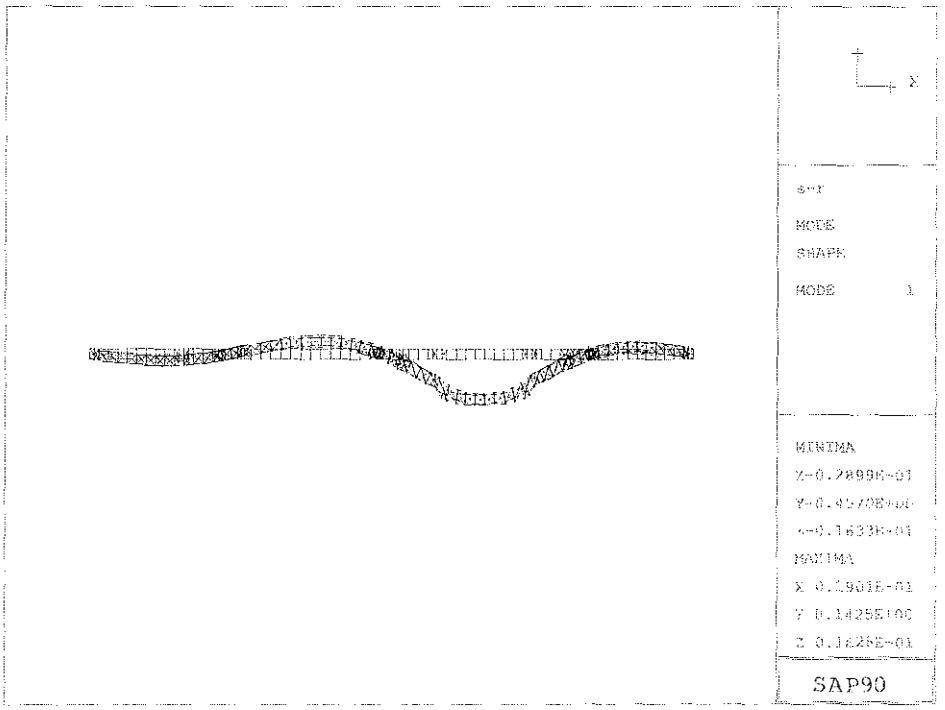

(b)

Figure 4.2 Mode Shape of the Fundamental Frequency (0.50 Hz)
(a) Isometric View, and (b) Plan View

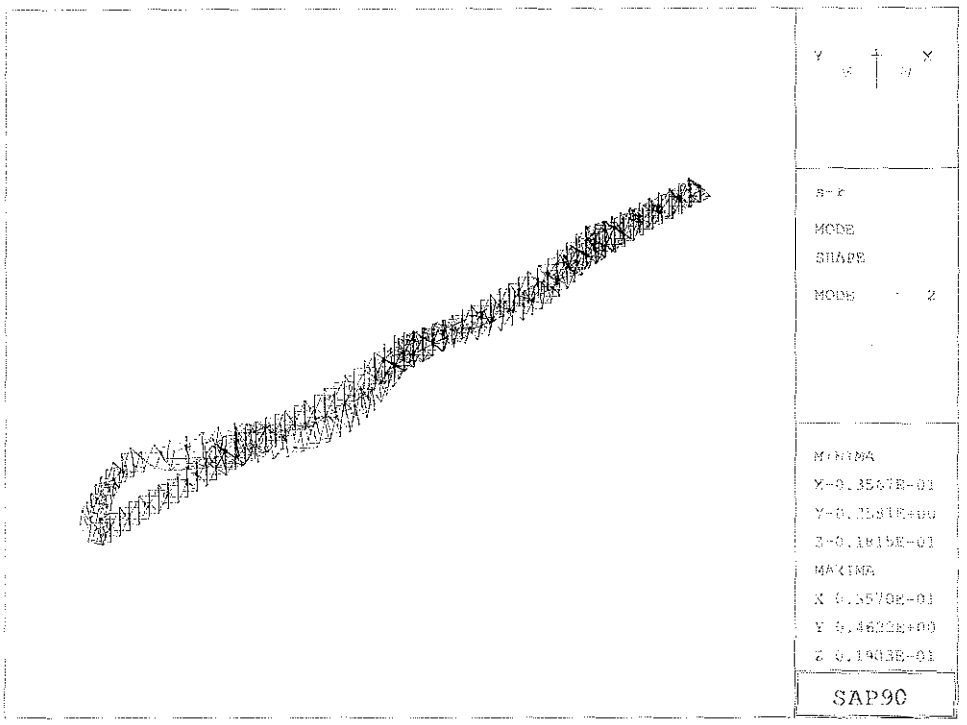

(a)

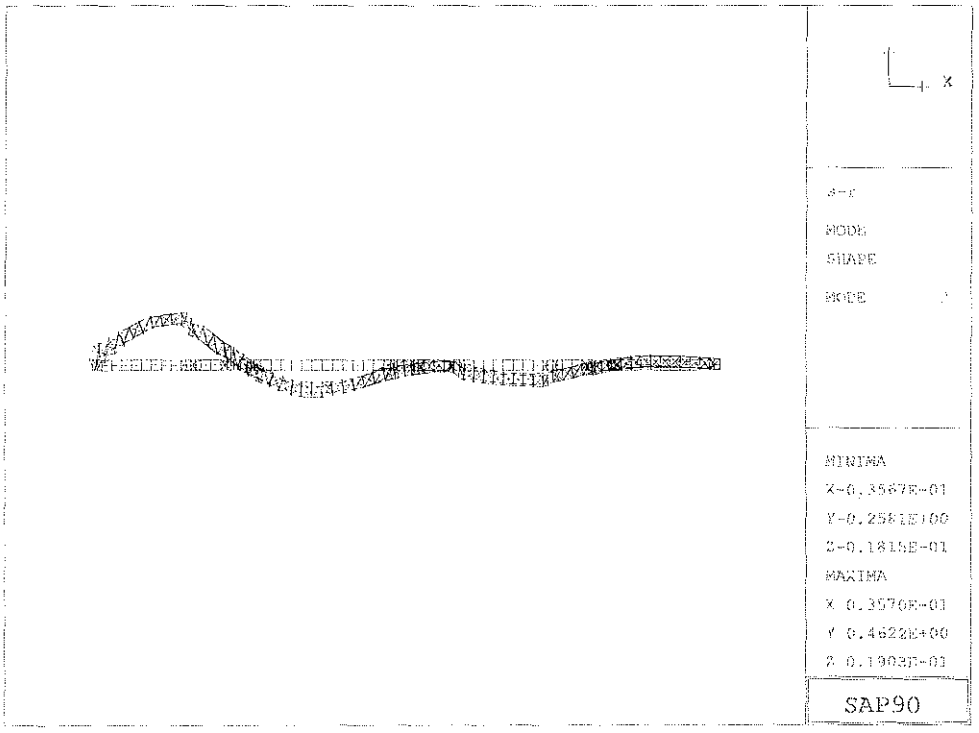

(b)

Figure 4.3 Mode Shape of the Second Natural Frequency (0.65 Hz)
(a) Isometric View, and (b) Plan View

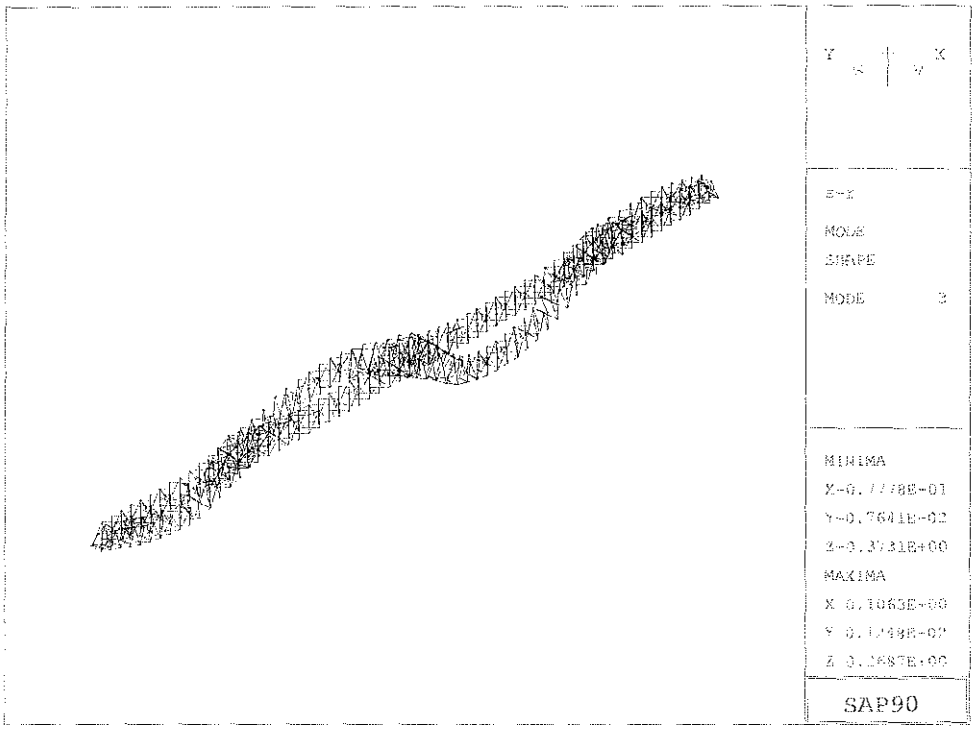

(a)

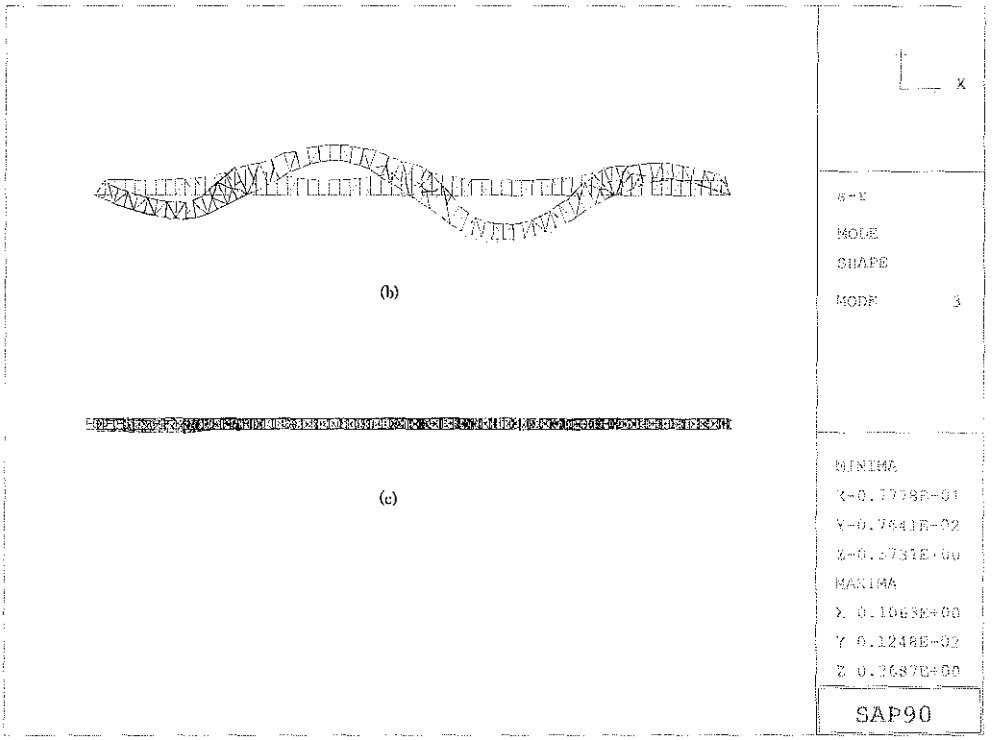

Figure 4.4 Mode Shape of the Third Natural Frequency (0.73 Hz)
(a) Isometric View, (b) Elevation View, and (c) Plan View

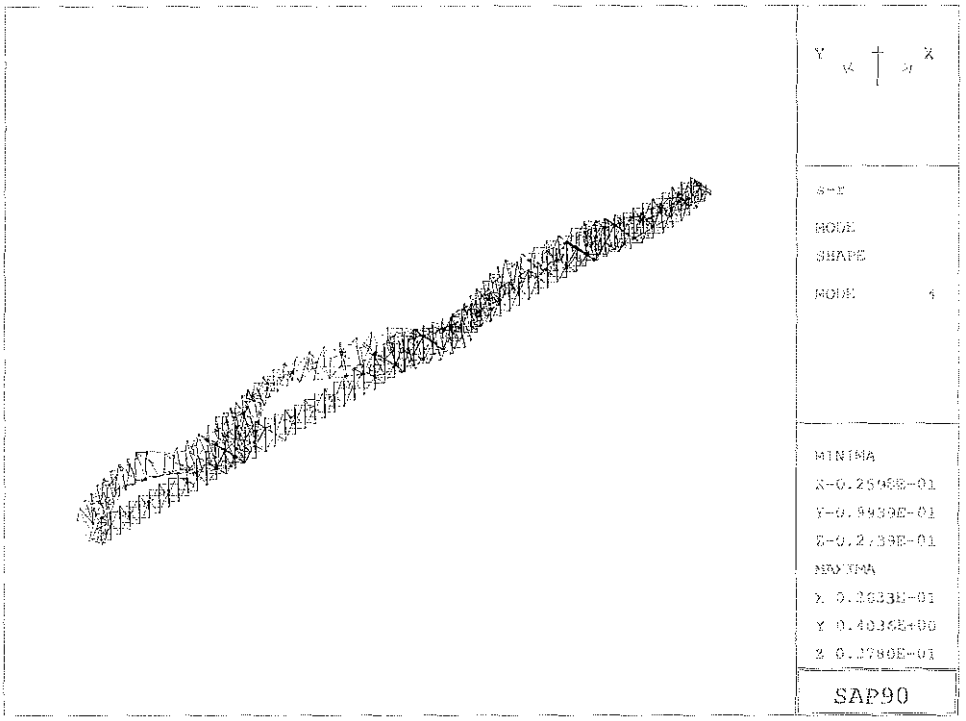

Figure 4.5 Mode Shape of the Fourth Natural Frequency (0.81 Hz)

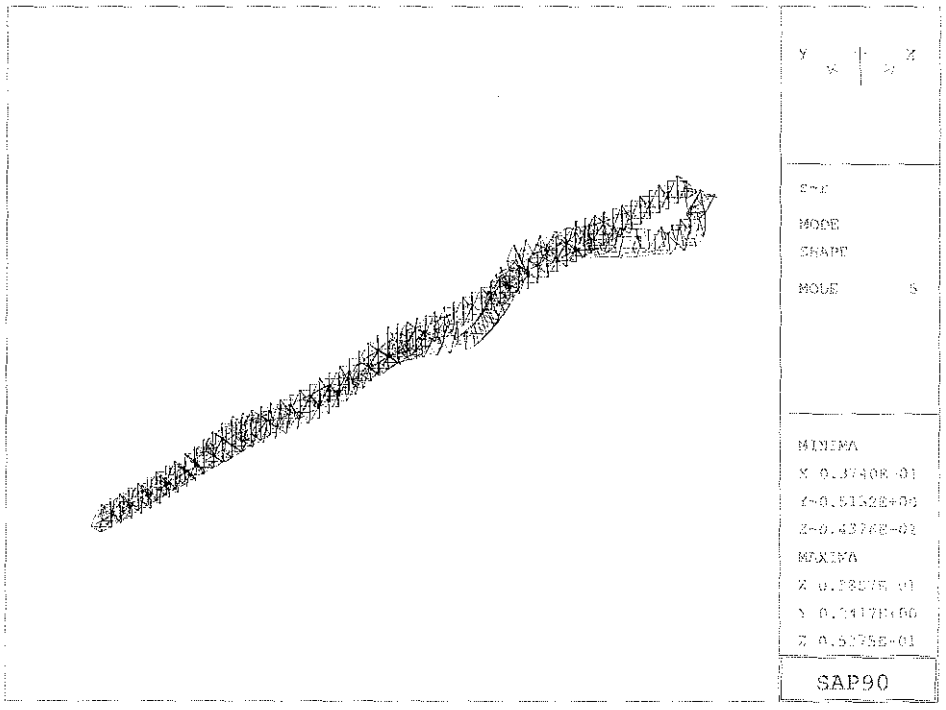

(a)

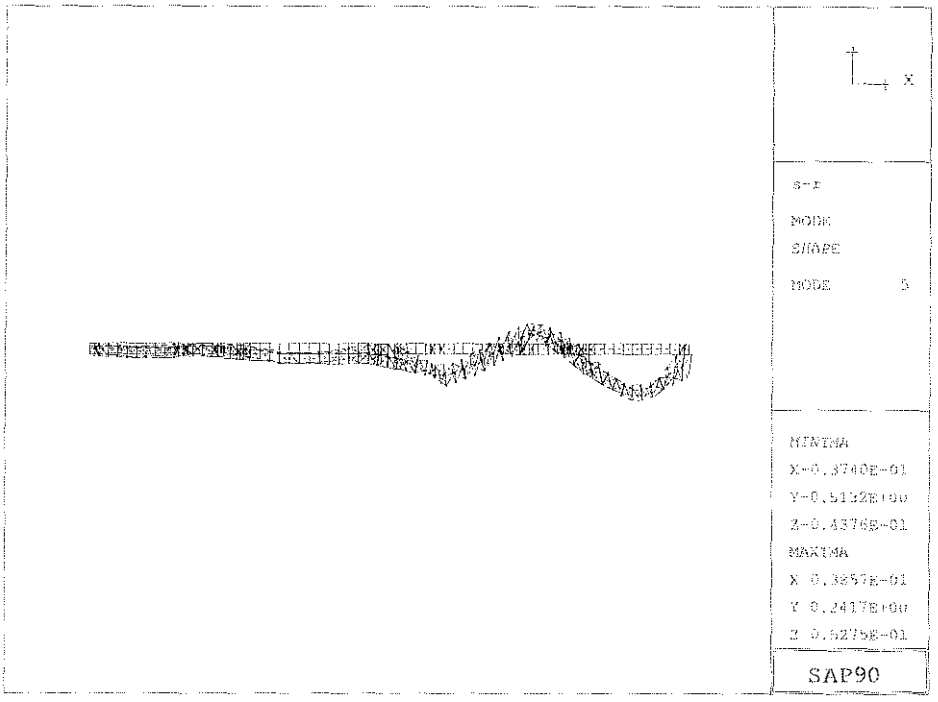

(b)

Figure 4.6 Mode Shape of the Fifth Natural Frequency (0.95 Hz)
(a) Isometric View, and (b) Plan View

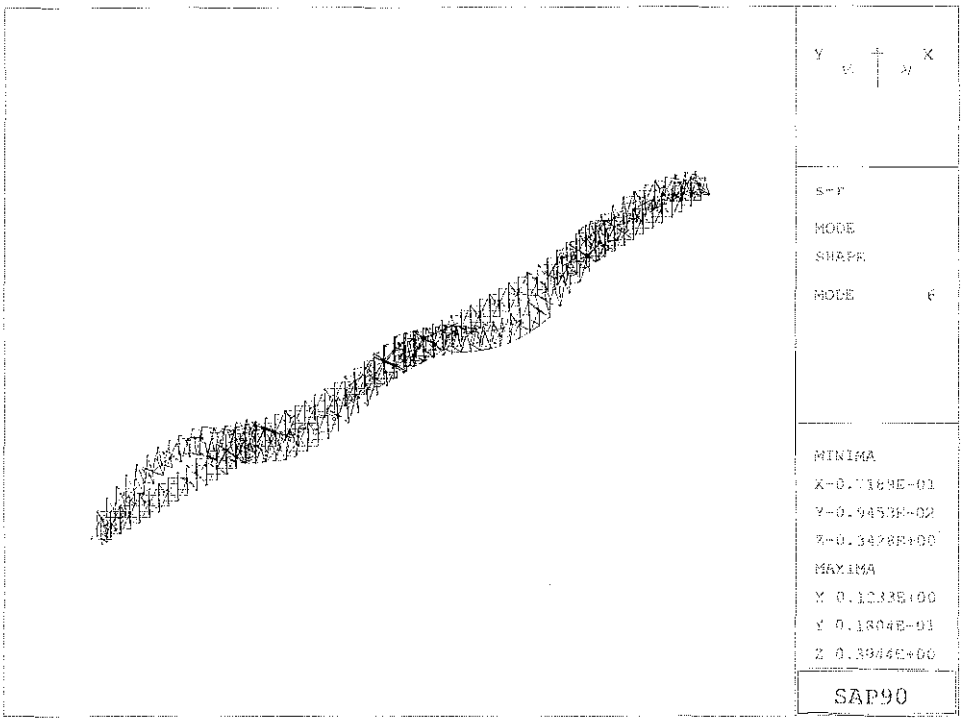

(a)

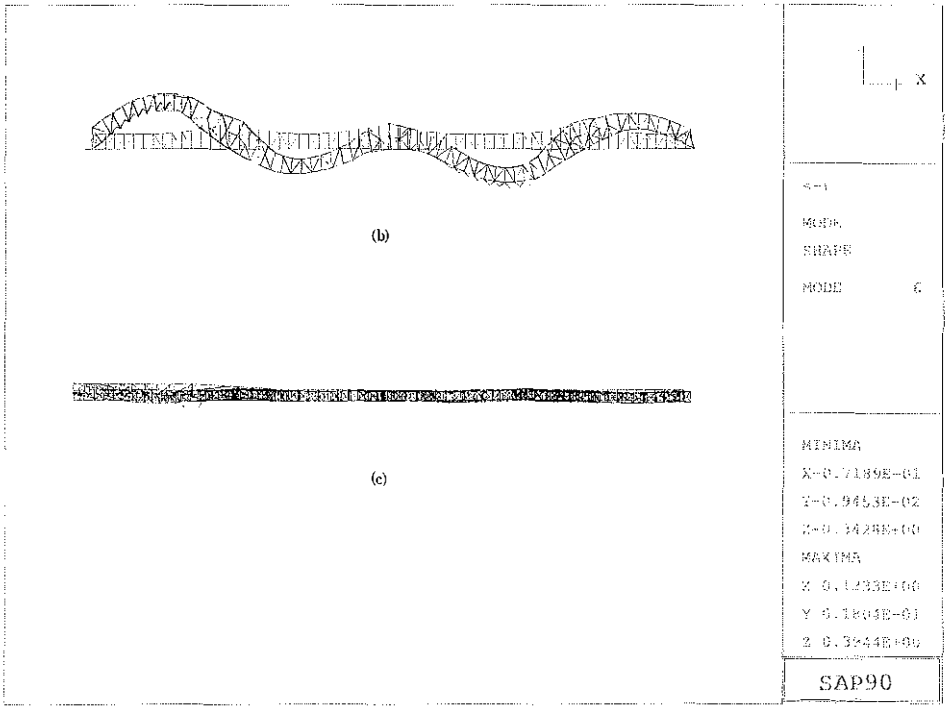

Figure 4.7 Mode Shape of the Sixth Natural Frequency (0.97 Hz)
(a) Isometric View, (b) Elevation View, and (c) Plan View

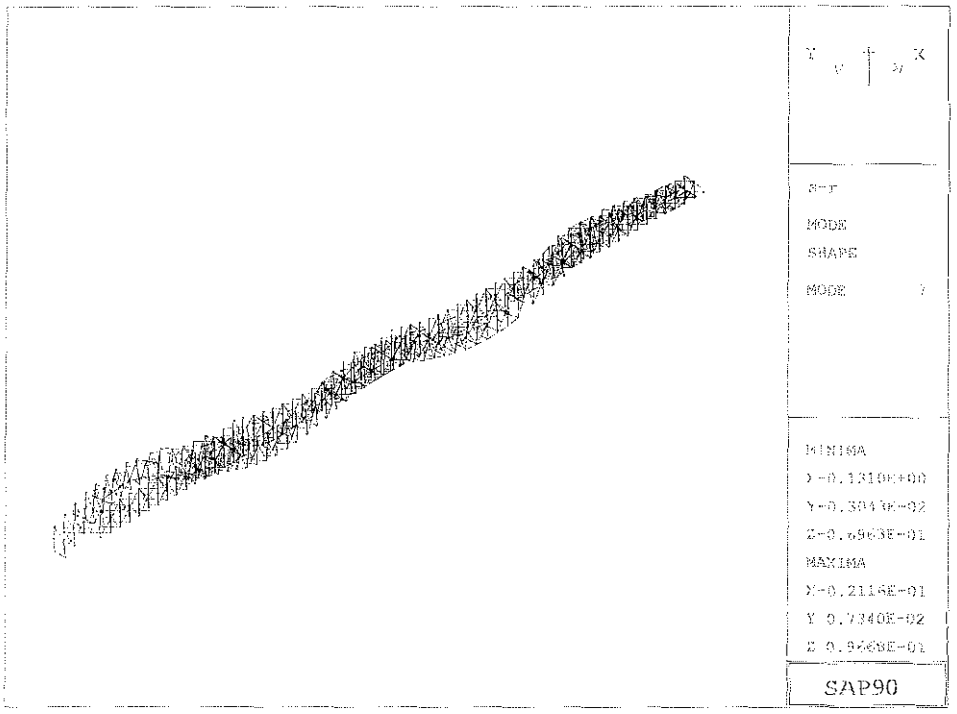

(a)

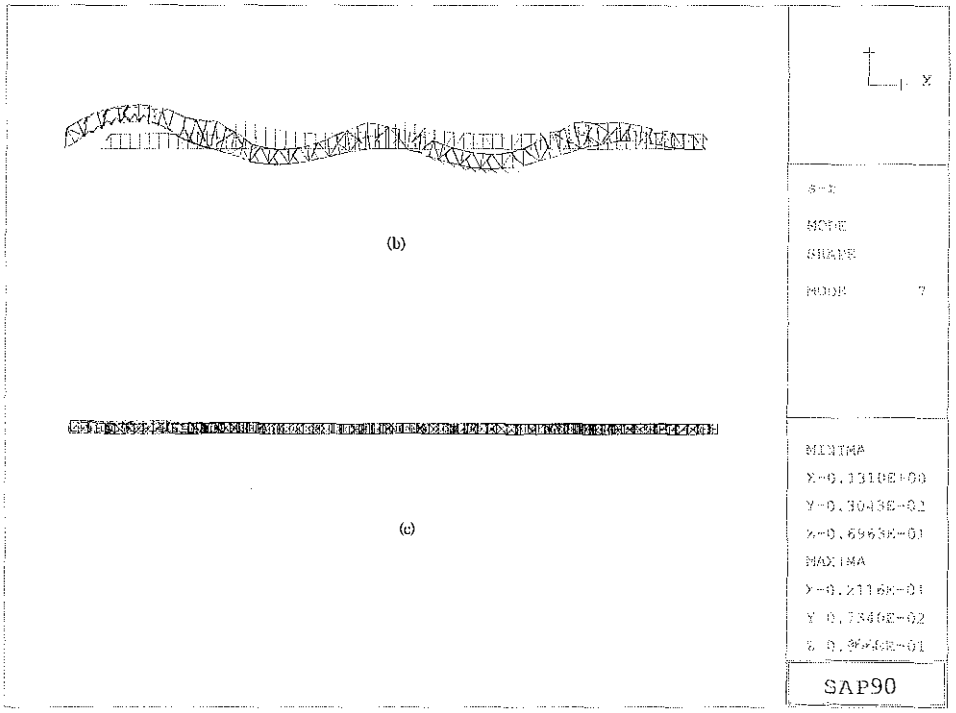

Figure 4.8 Mode Shape of the Seventh Natural Frequency (1.08 Hz)
(a) Isometric View, (b) Elevation View, and (c) Plan View

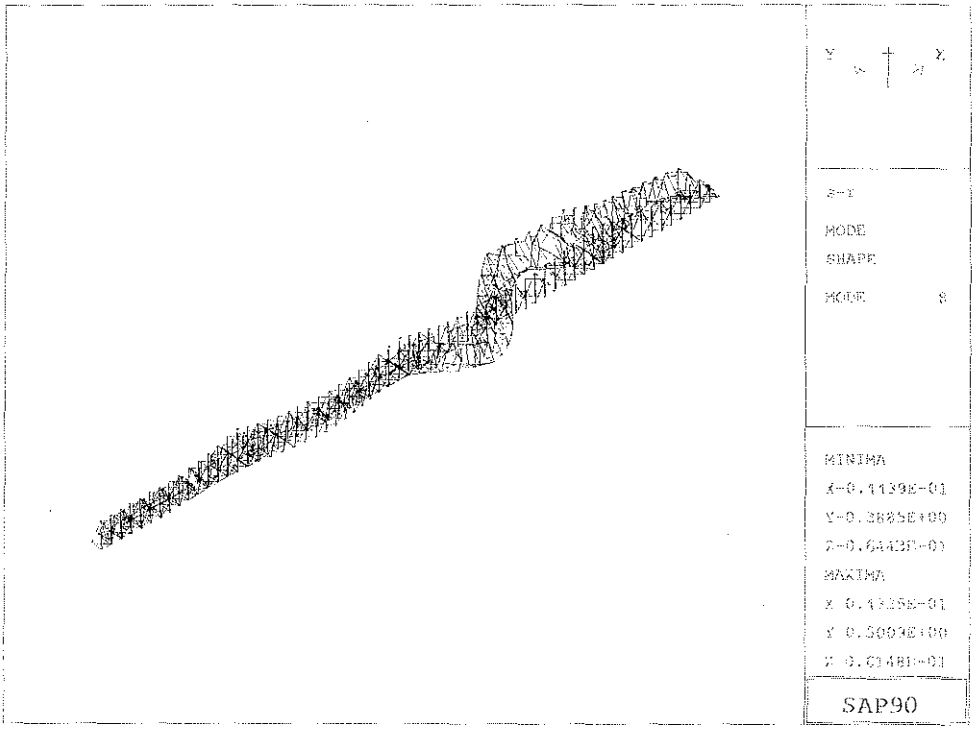

(a)

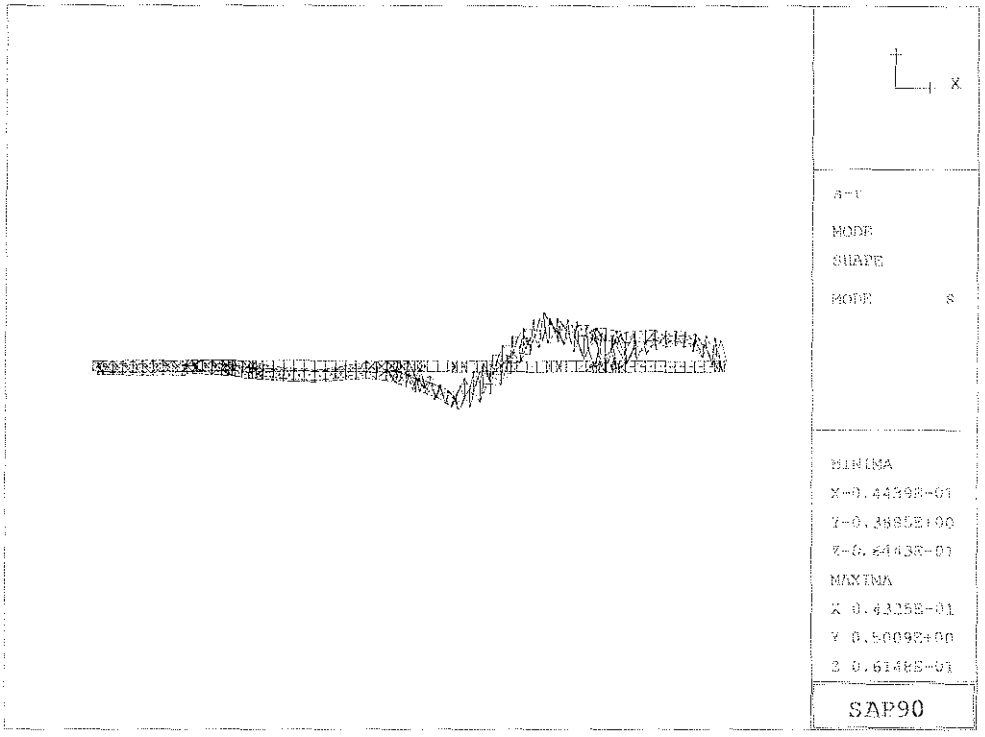

(b)

Figure 4.9 Mode Shape of the Eighth Natural Frequency (1.11 Hz)
(a) Isometric View, and (b) Plan View

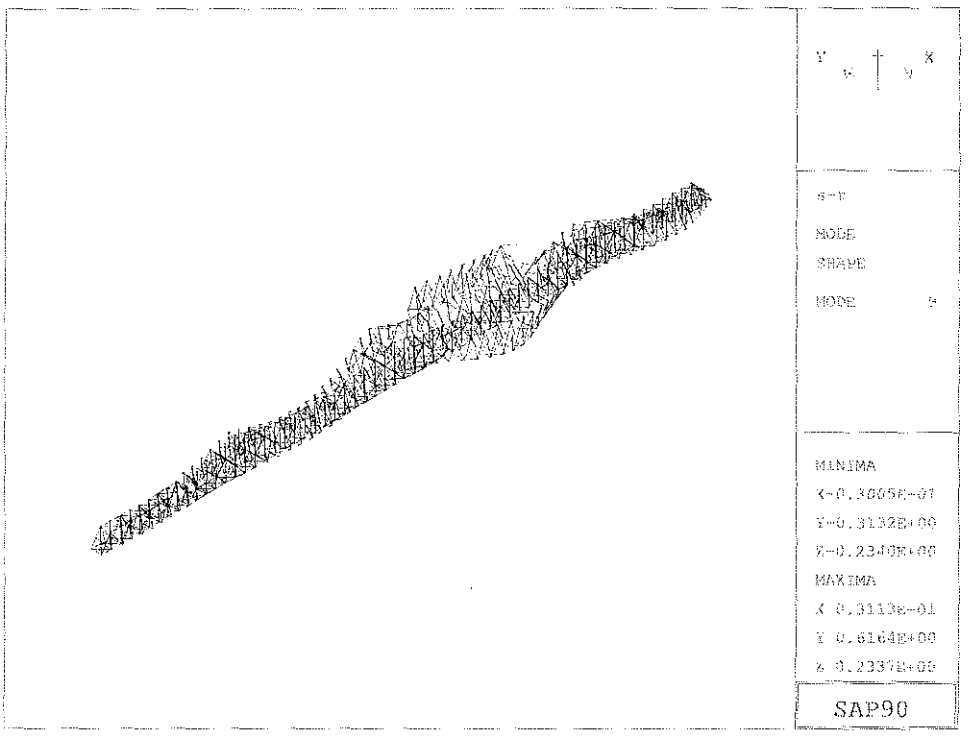

(a)

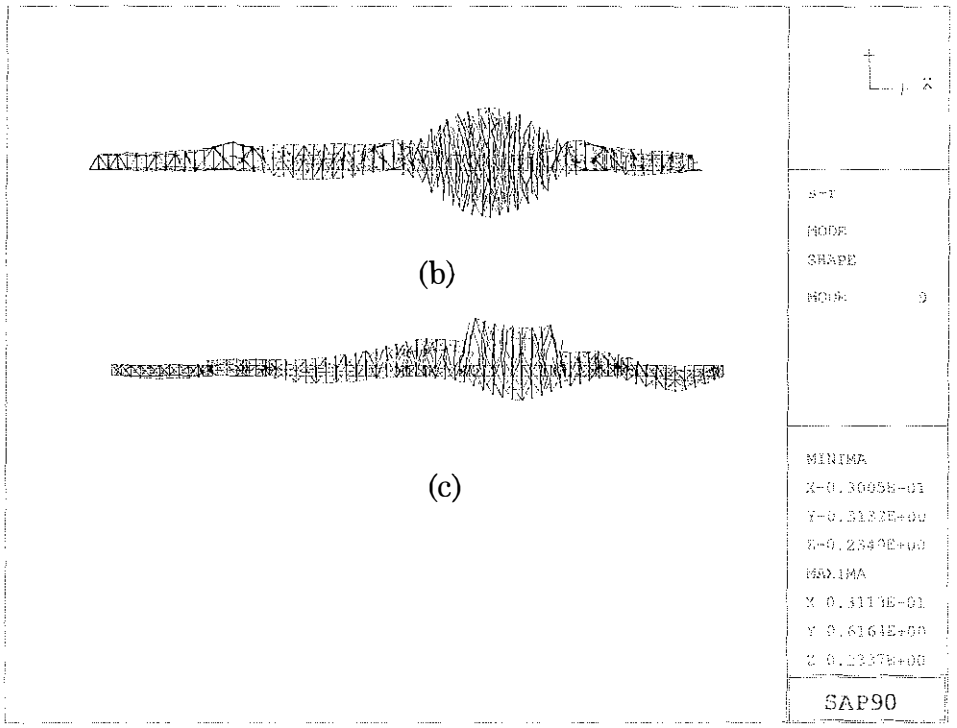

(b)

(c)

Figure 4.10 Mode Shape of the Ninth Natural Frequency (1.21 Hz)
(a) Isometric View, (b) Elevation View, and (c) Plan View

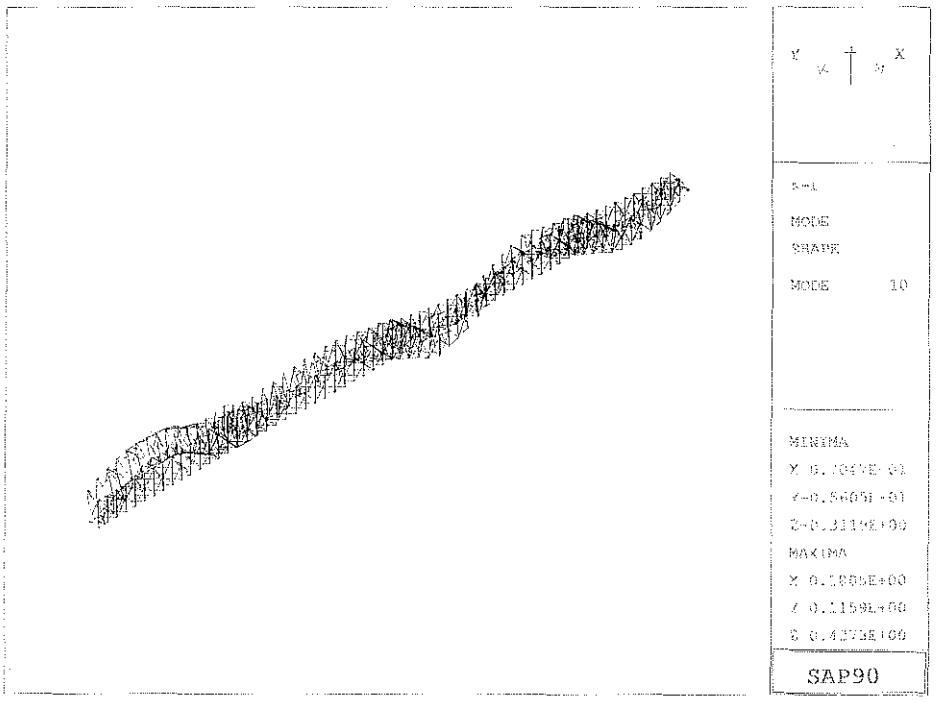

(a)

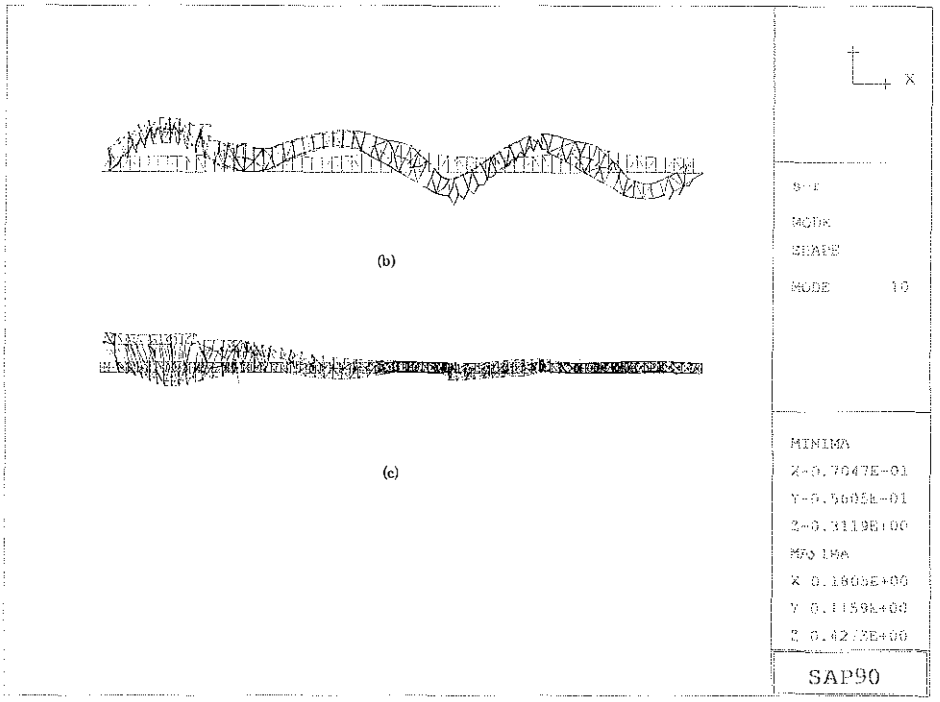

Figure 4.11 Mode Shape of the Tenth Natural Frequency (1.30 Hz)
(a) Isometric View, (b) Elevation View, and (c) Plan View

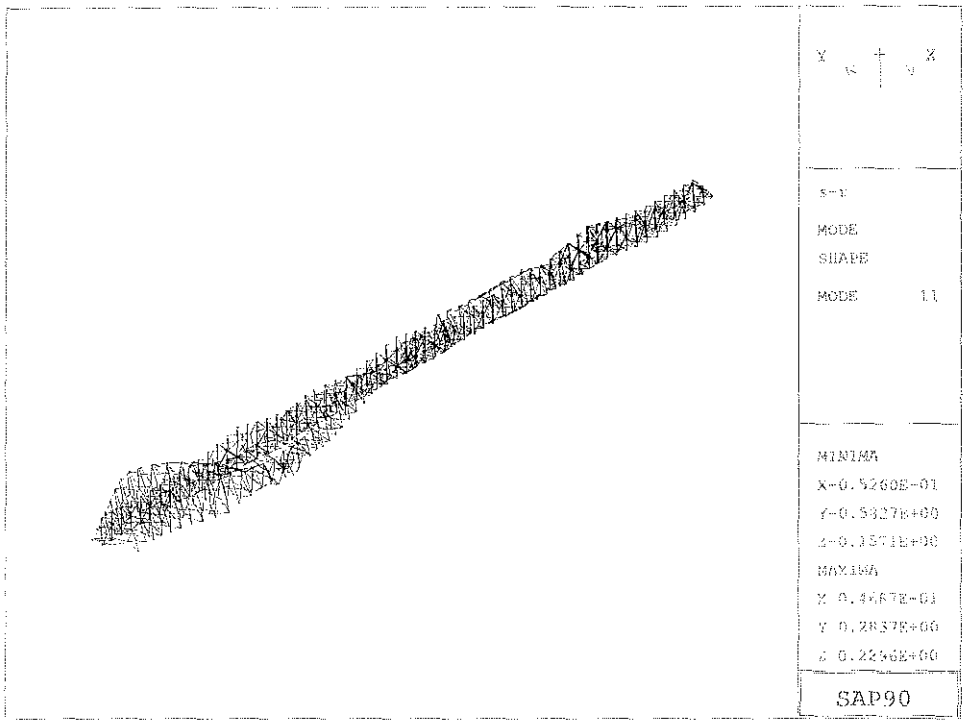

(a)

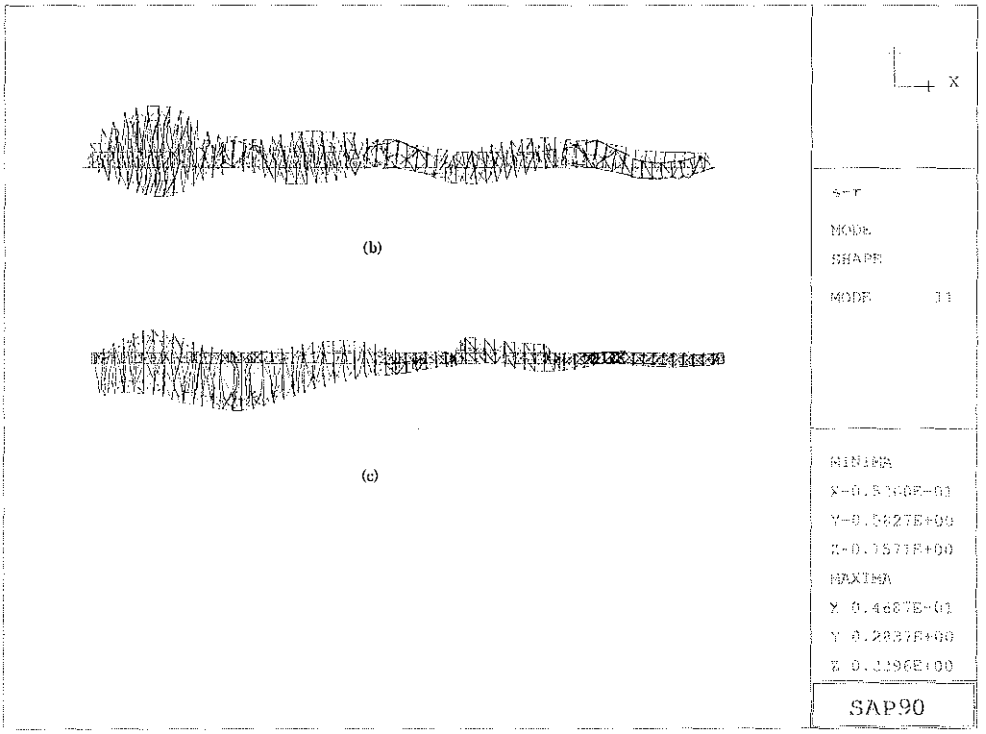

Figure 4.12 Mode Shape of the 11th Natural Frequency (1.36 Hz)
(a) Isometric View, (b) Elevation View, and (c) Plan View

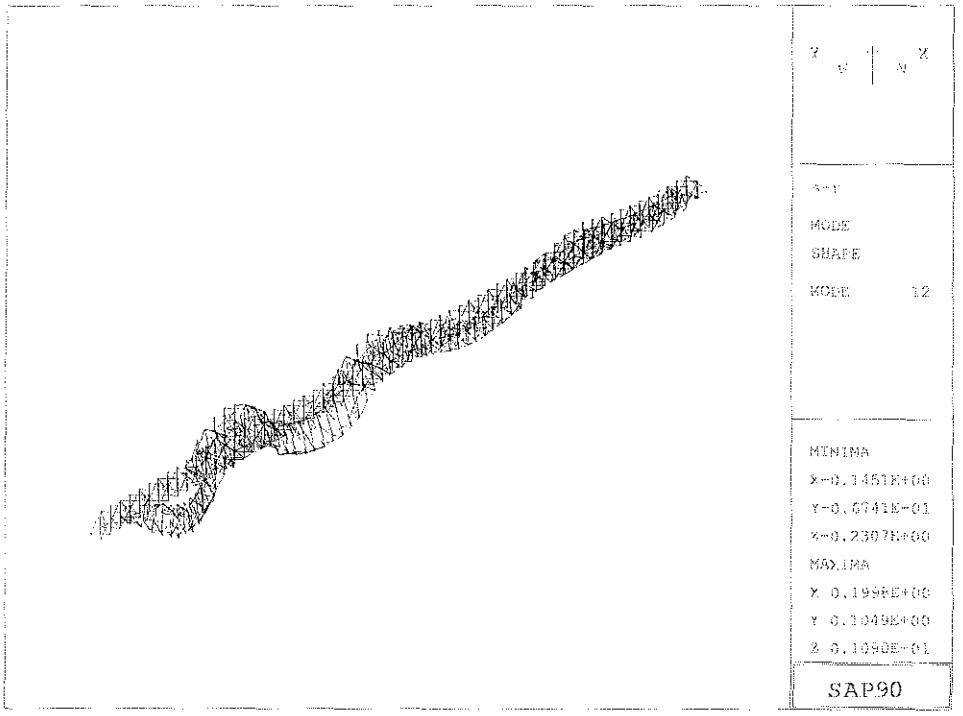

(a)

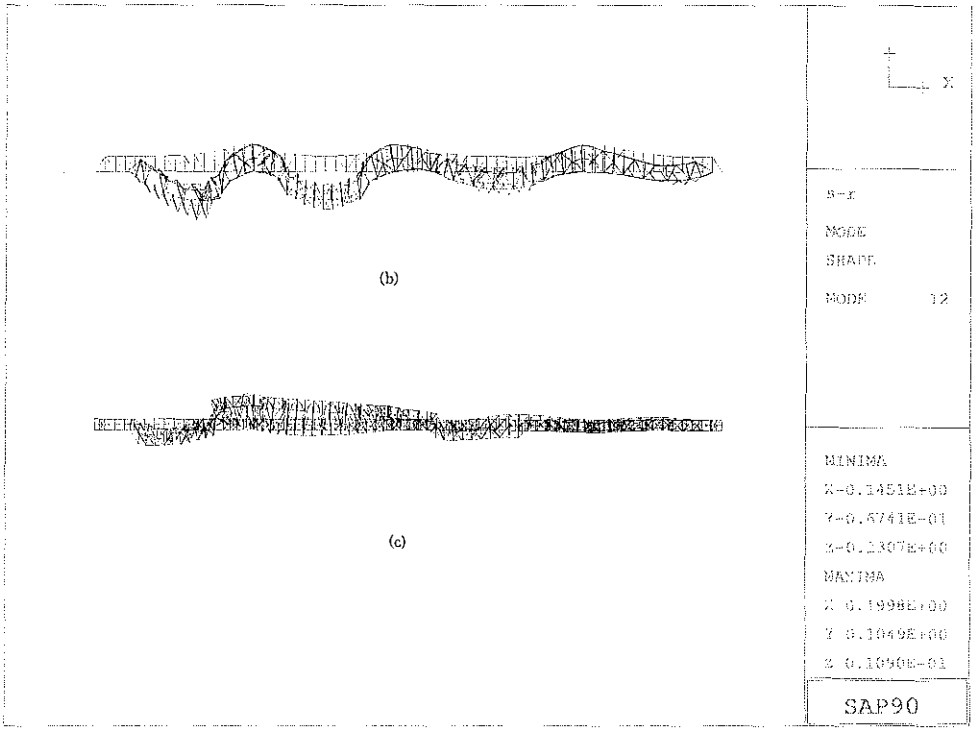

Figure 4.13 Mode Shape of the 12th Natural Frequency (1.43 Hz)
(a) Isometric View, (b) Elevation View, and (c) Plan View

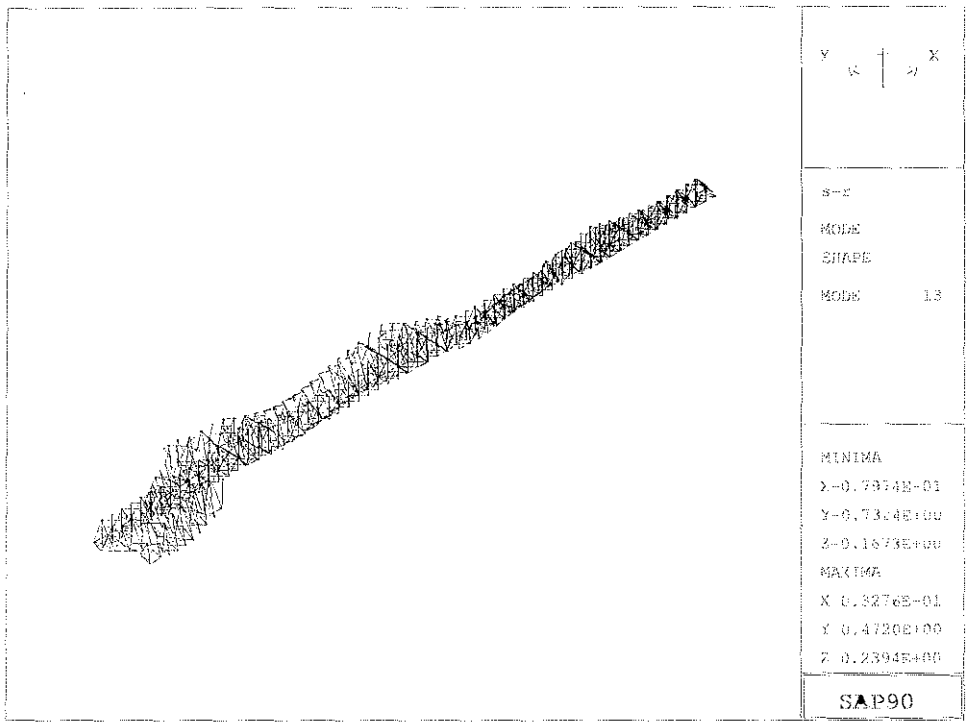

(a)

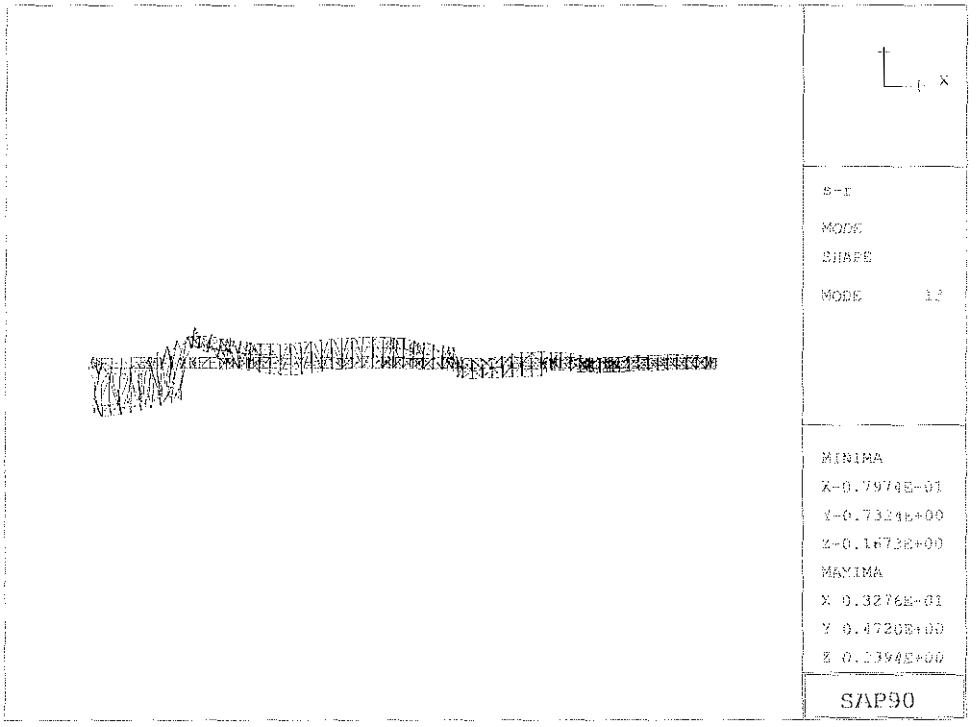

(b)

Figure 4.14 Mode Shape of the 13th Natural Frequency (1.47 Hz)
(a) Isometric View, and (b) Plan View

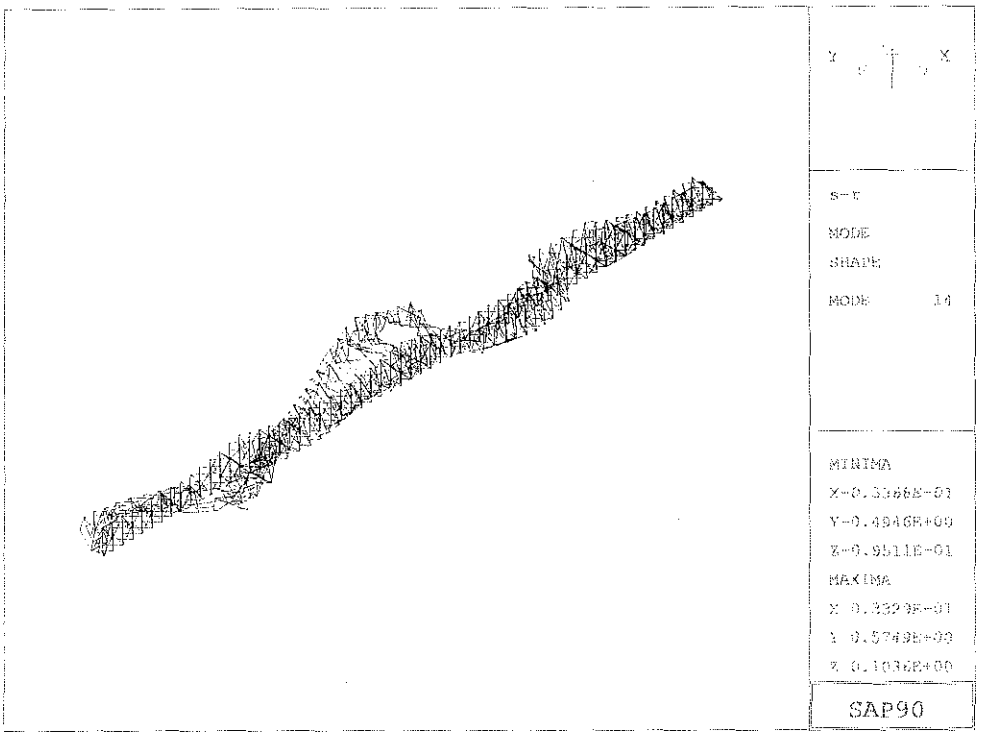

(a)

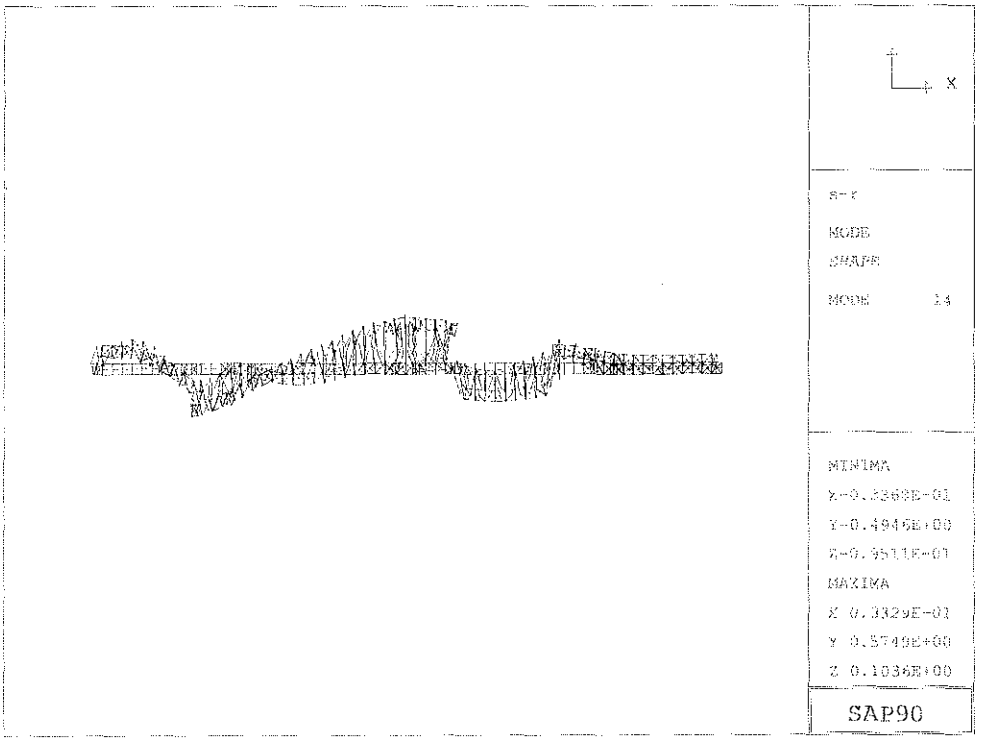

(b)

Figure 4.15 Mode Shape of the 14th Natural Frequency (1.56 Hz)
(a) Isometric View, and (b) Plan View

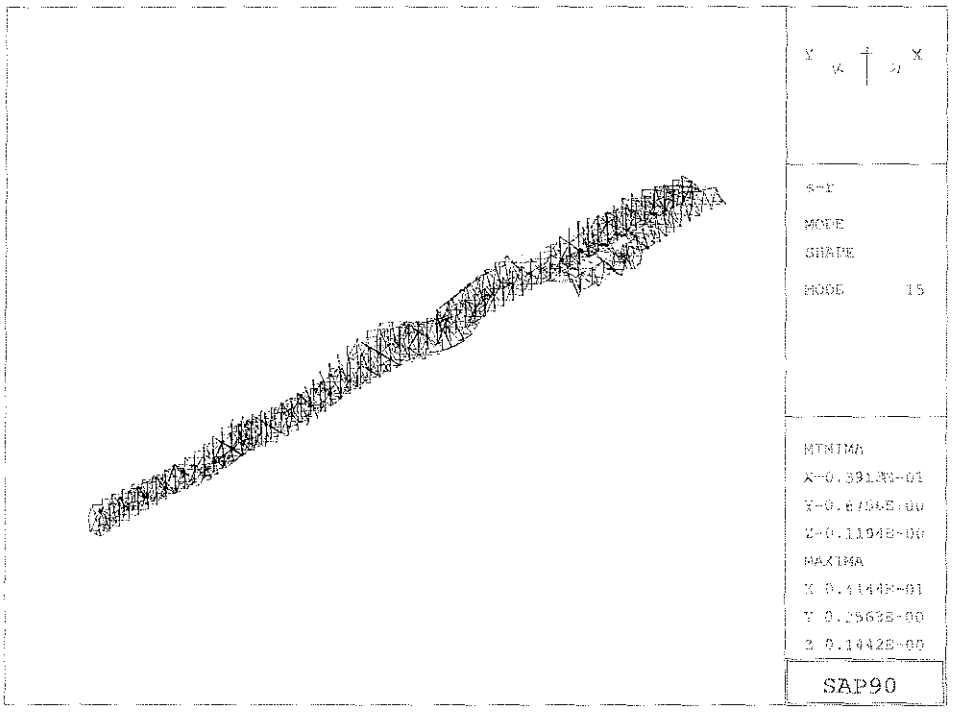

(a)

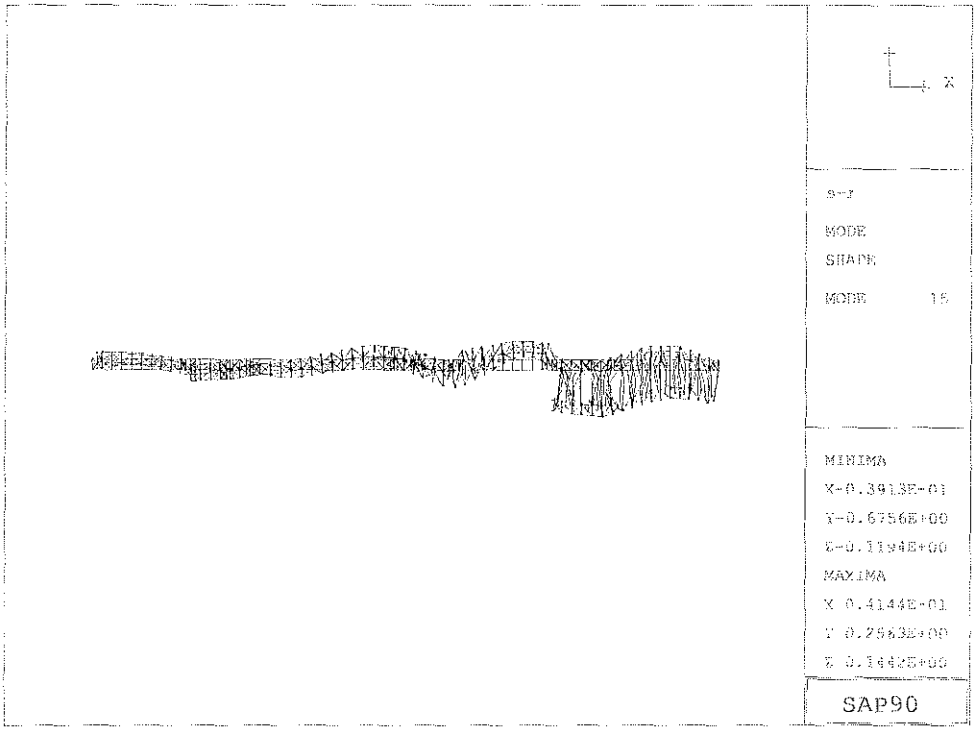

(b)

Figure 4.16 Mode Shape of the 15th Natural Frequency (1.57 Hz)
(a) Isometric View, and (b) Plan View

Figure 5.1 Time-history and Response spectra identification map for the Commonwealth of Kentucky

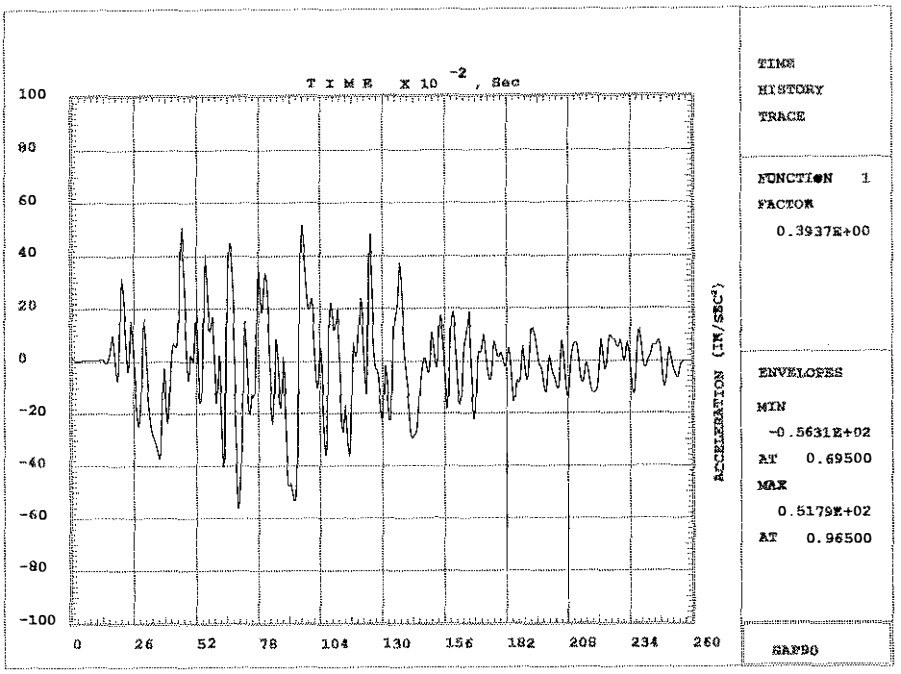

Figure 5.2 Acceleration-Time History of the Horizontal Component of the 50-year Earthquake

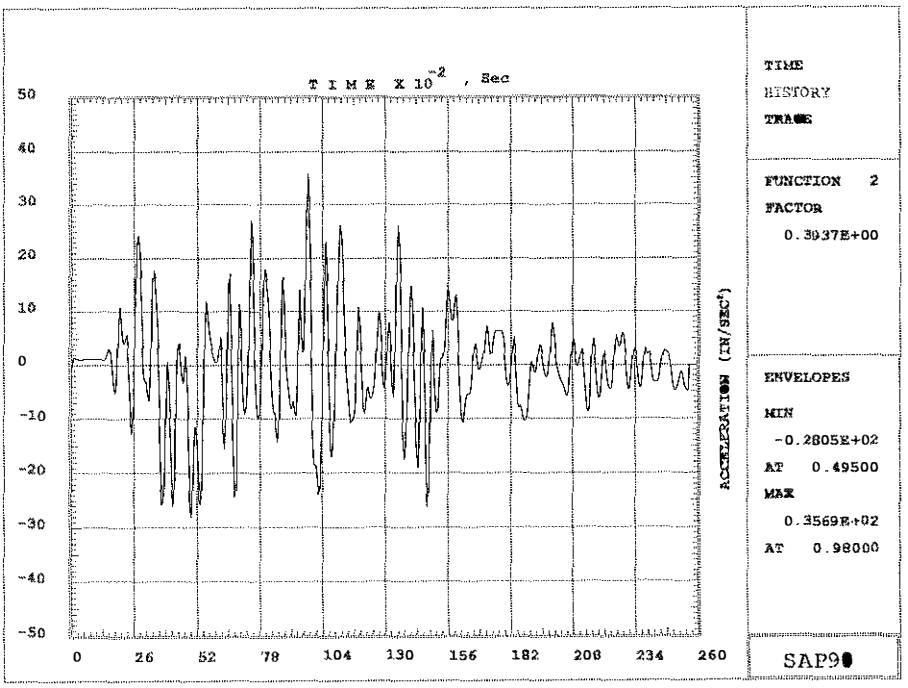

Figure 5.3 Acceleration-Time History of the Vertical Component of the 50-year Earthquake

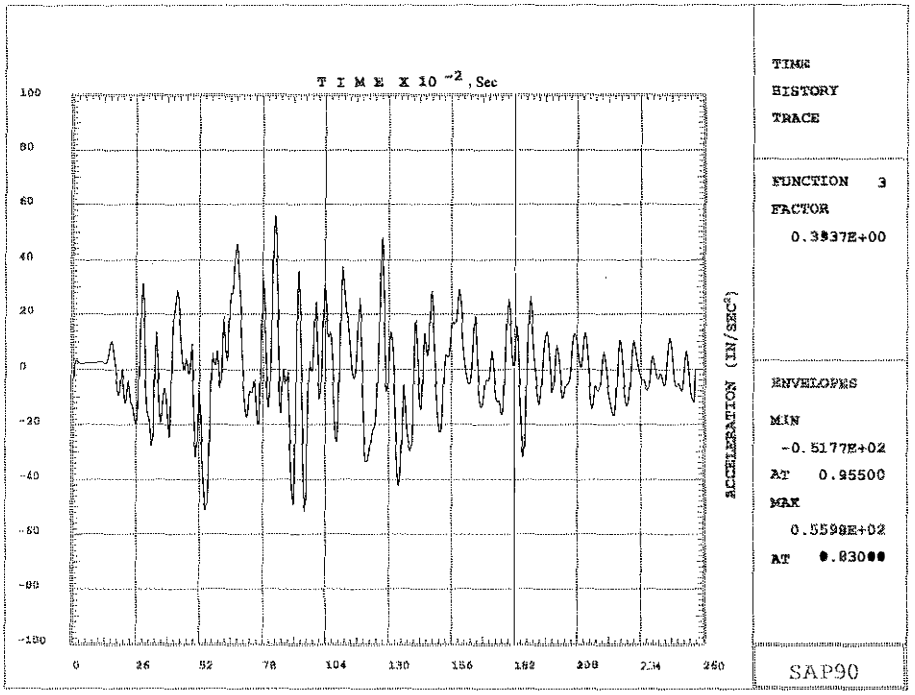

Figure 5.4 Acceleration-Time History of the Transverse Component of the 50-year Earthquake

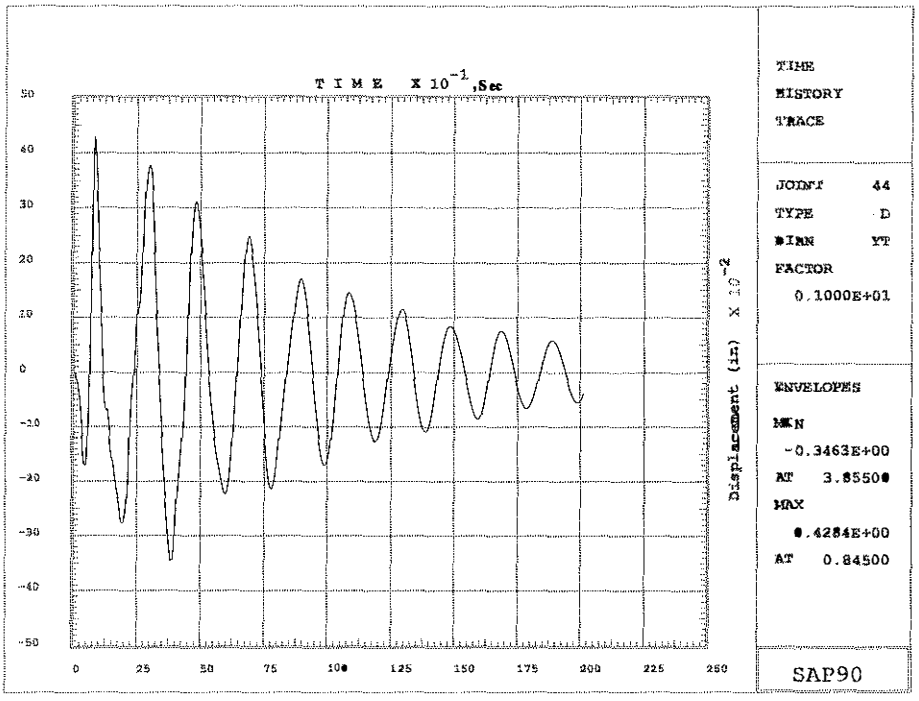

Figure 5.5 Displacement-Time History in the Transverse Direction at Node 44 under L1T2V3 Excitation Case

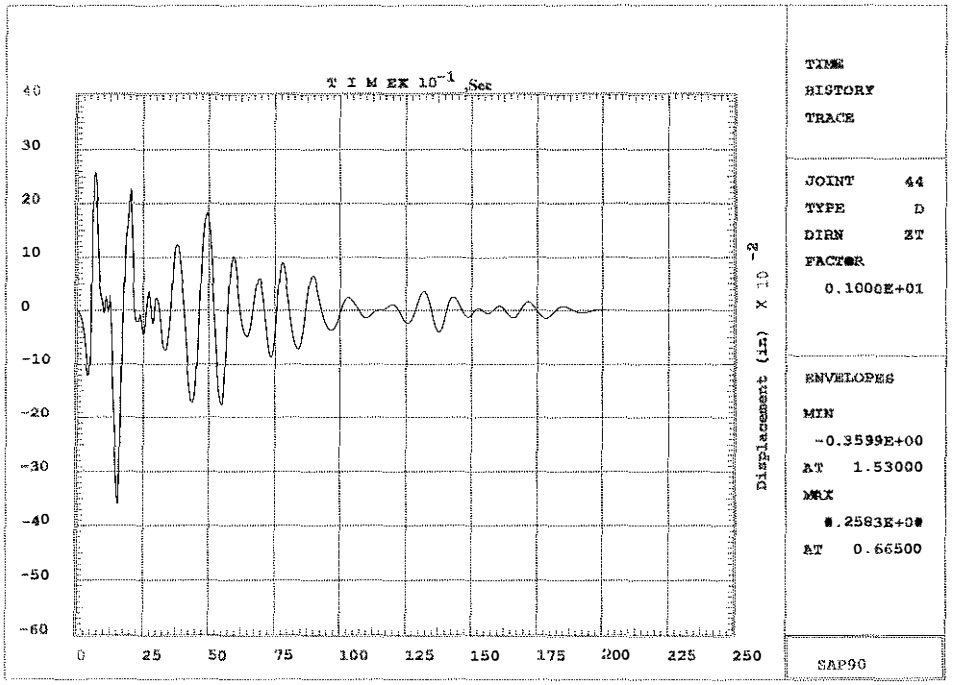

Figure 5.6 Displacement-Time History in the Vertical Direction at Node 44 under L1T2V3 Excitation Case

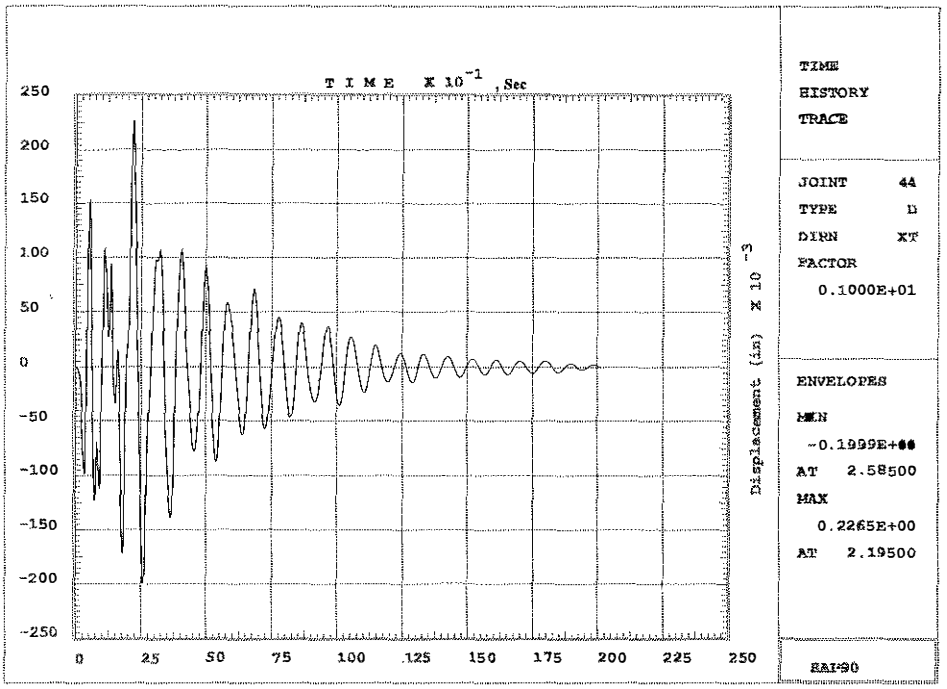

Figure 5.7 Displacement-Time History in the Longitudinal Direction at Node 44 under L1T2V3 Excitation Case

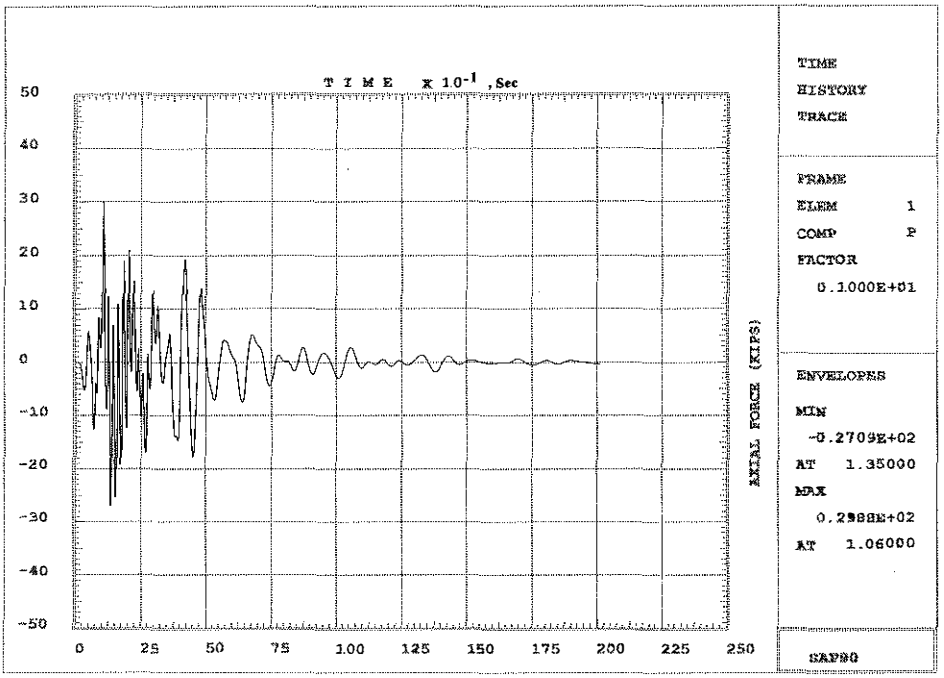

Figure 5.8 Axial Force-Time History of Member 1 under the L1T2V3 Excitation Case

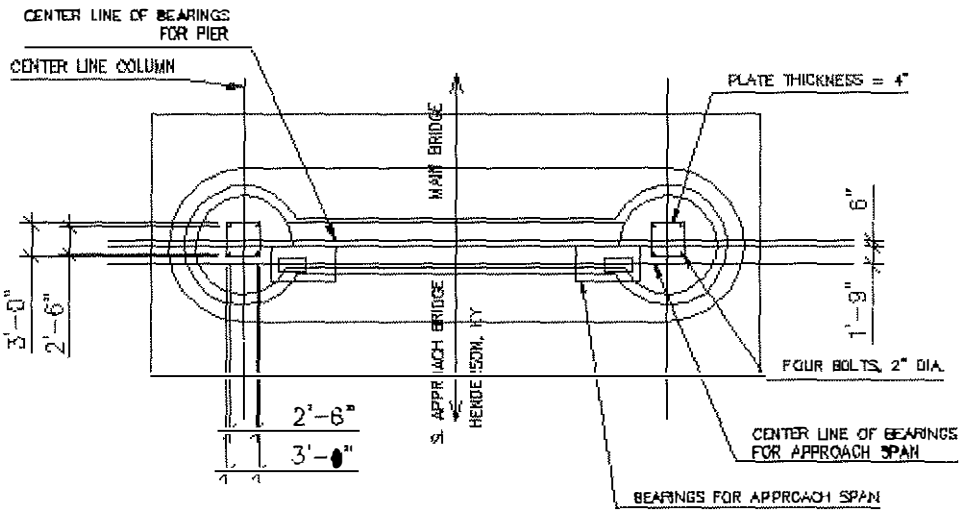

Note: 1. Assuming that the existing bolts are in good condition, additional minimum shear capacity of anchor bolts required = 1125 kips

2. Alternate retrofit would be to replace the existing bearings with seismic isolation bearings

Figure 5-9 Minimum Required Shear Capacity (V_{req}) to be Provided by Additional Anchor Bolts at Bearings of the Pier A on the US41 Southbound Main Bridge

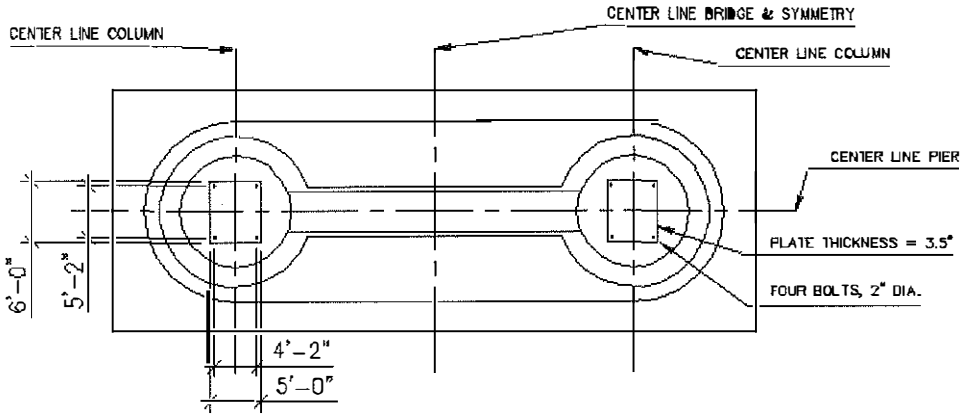

Note: 1. Assuming that the existing bolts are in good condition, additional minimum shear capacity of anchor bolts required = 560 kips

2. Alternate retrofit would be to replace the existing bearings with seismic isolation bearings

Figure 5-10 Minimum Required Shear Capacity (V_{req}) to be Provided by Additional Anchor Bolts at Bearings of the Pier B on the US41 Southbound Main Bridge

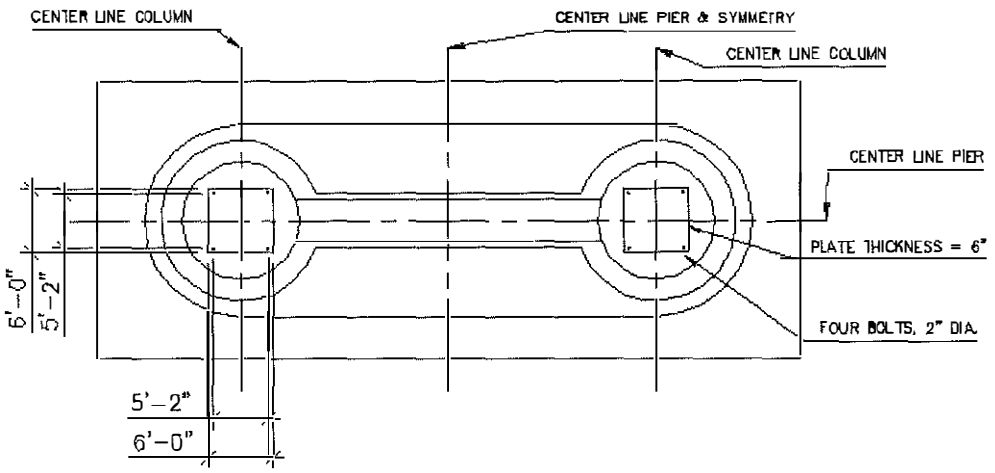

Note: 1. Assuming that the existing bolts are in good condition, additional minimum shear capacity of anchor bolts required = 635 kips

2. Alternate retrofit would be to replace the existing bearings with seismic isolation bearings

Figure 5-11 Minimum Required Shear Capacity (V_{req}) to be Provided by Additional Anchor Bolts at Bearings of the Pier C on the US41 Southbound Main Bridge

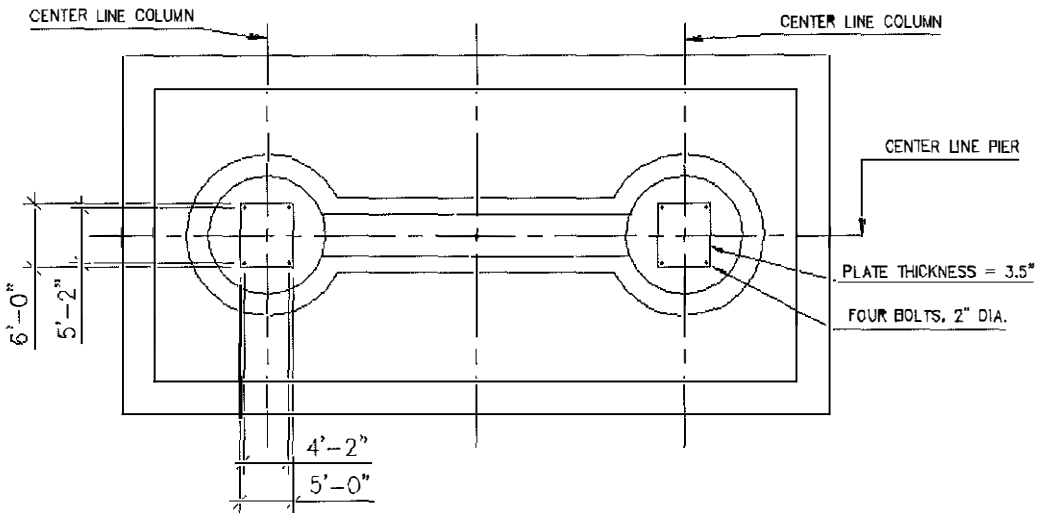

Note: 1. Assuming that the existing bolts are in good condition, additional minimum shear capacity of anchor bolts required = 1795 kips

2. Alternate retrofit would be to replace the existing bearings with seismic isolation bearings

Figure 5-12 Minimum Required Shear Capacity (V_{req}) to be Provided by Additional Anchor Bolts at Bearings of the Pier D on the US41 Southbound Main Bridge

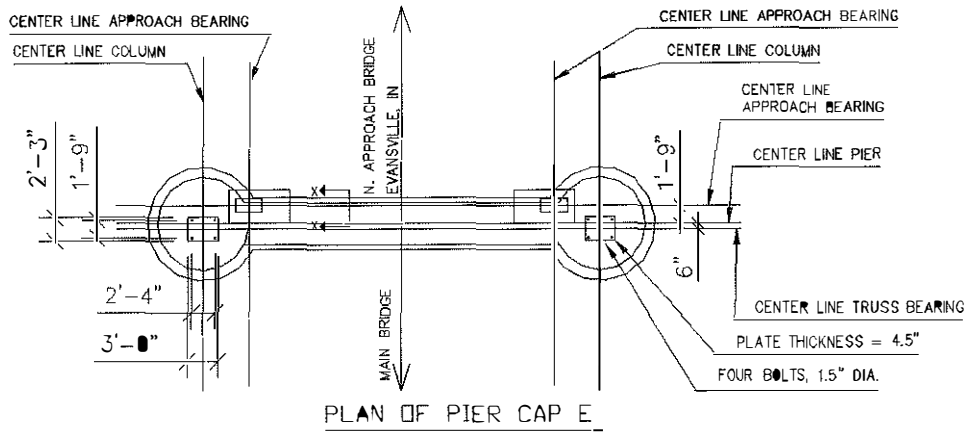

Note: 1. Assuming that the existing bolts are in good condition, additional minimum shear capacity of anchor bolts required = 1925 kips

2. Alternate retrofit would be to replace the existing bearings with seismic isolation bearings

Figure 5-13 Minimum Required Shear Capacity (V_{req}) to be Provided by Additional Anchor Bolts at Bearings of the Pier E on the US41 Southbound Main Bridge

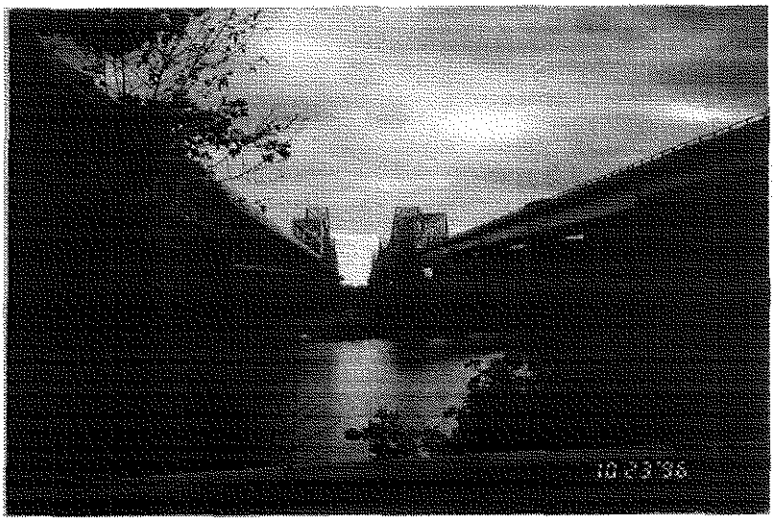

Figure 6.1a Evansville, IN Approach Bridge
(Southbound on Rightside)

Figure 6.1b Henderson, KY Approach Bridge

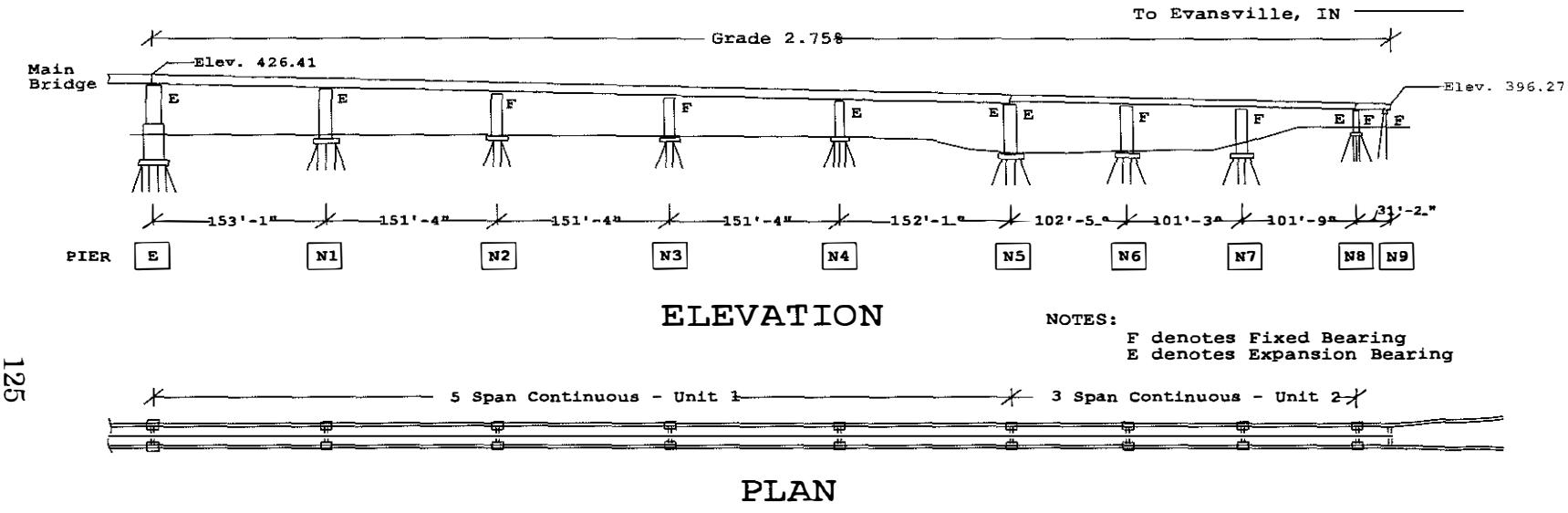

Figure 6.2 Plan and Elevation Views of the Evansville, IN Approach on the US41 Southbound Bridge

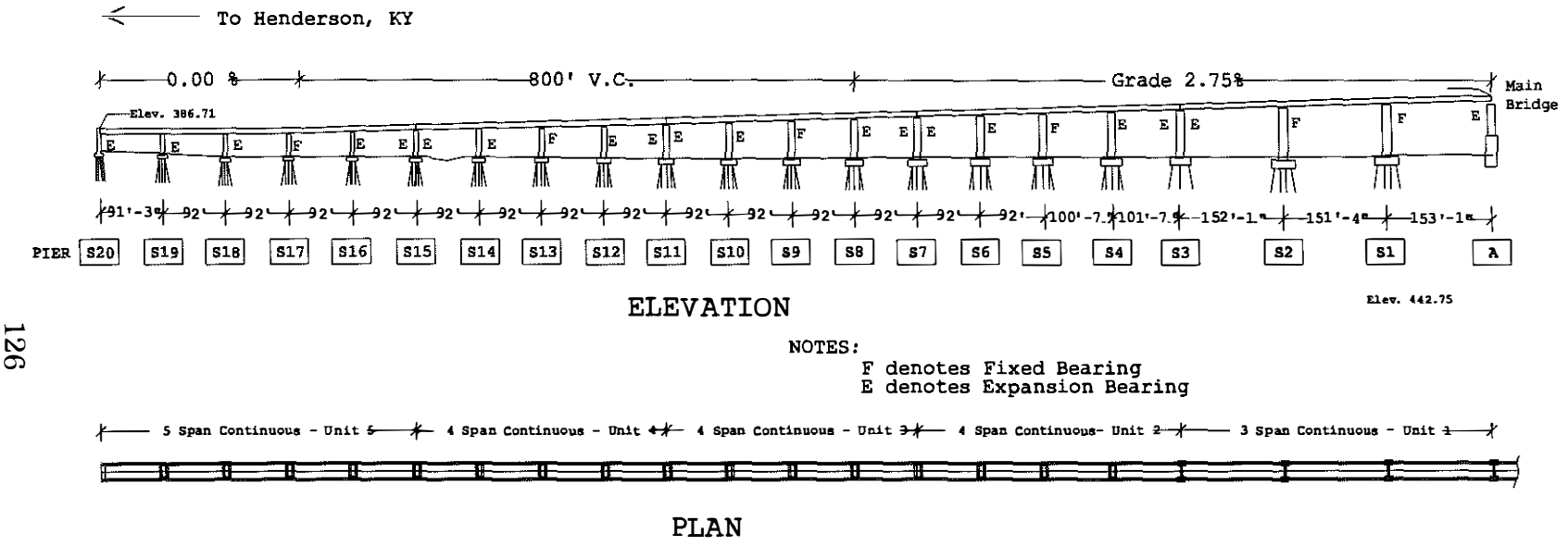

Figure 6.3 Plan and Elevation Views of Henderson, KY Approach of the US41 Southbound Bridge

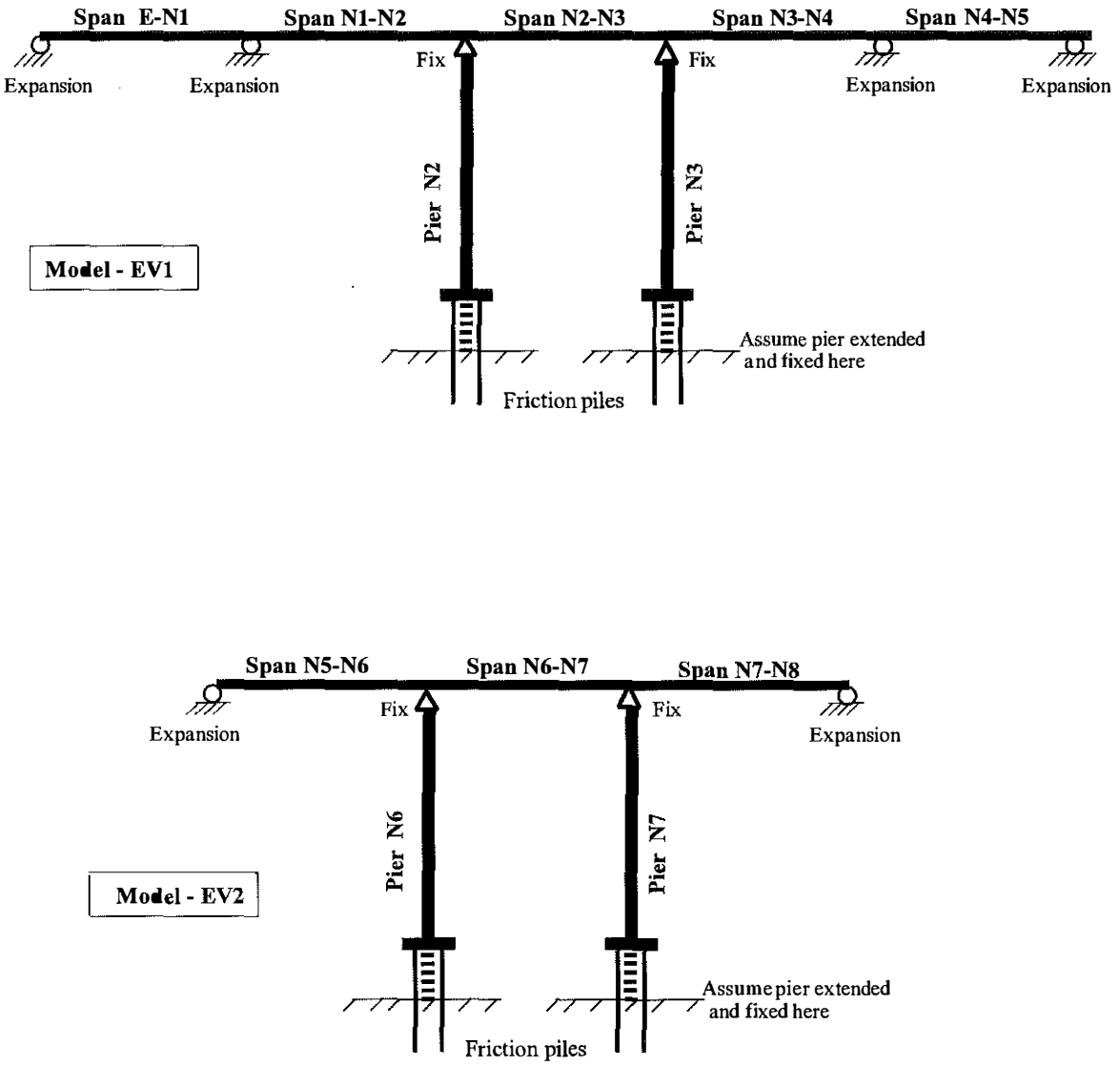

Figure 6.4 Single Degree of Freedom System Models for Evansville, IN Approach

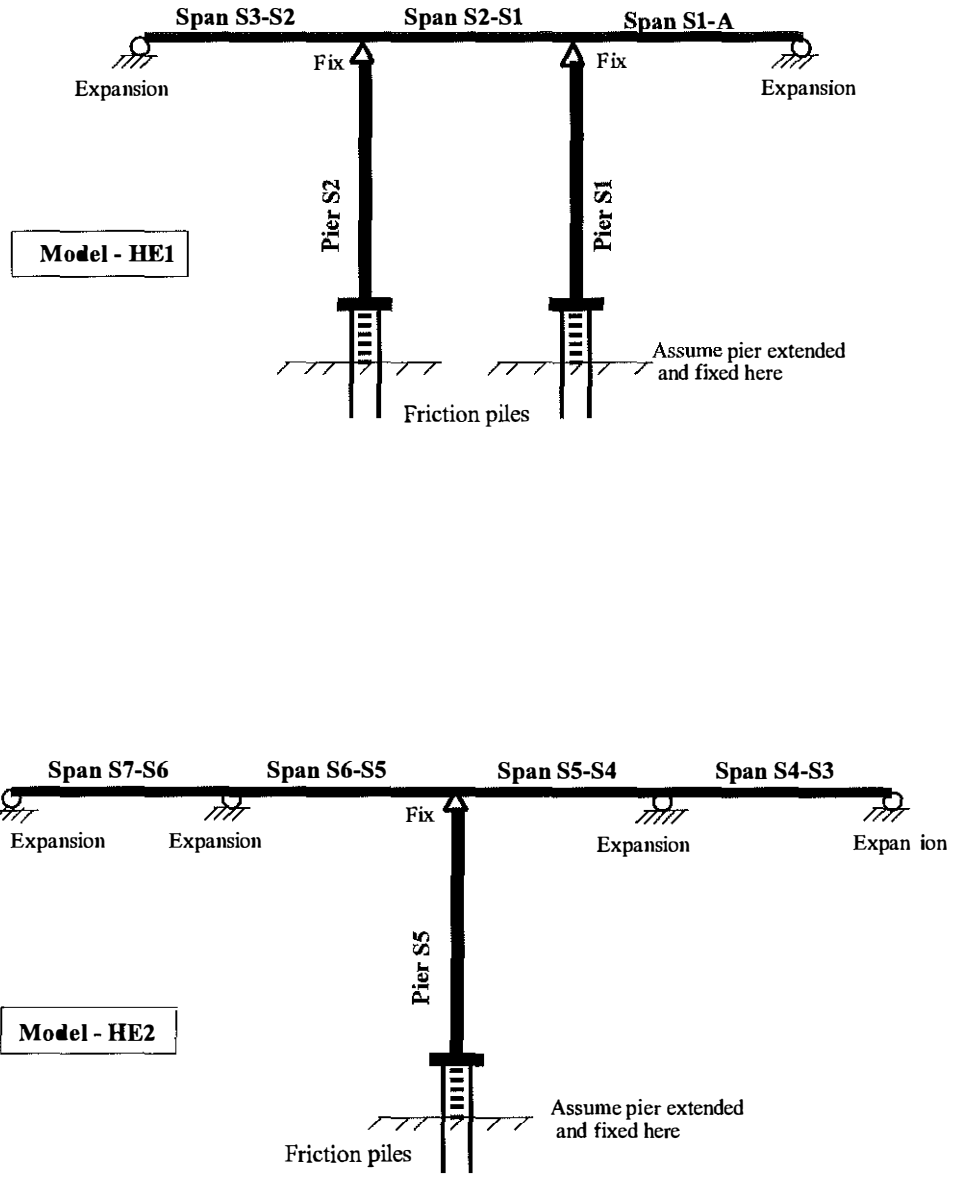

Figure 6.5 Single Degree of Freedom System Models for Henderson, KY Approach

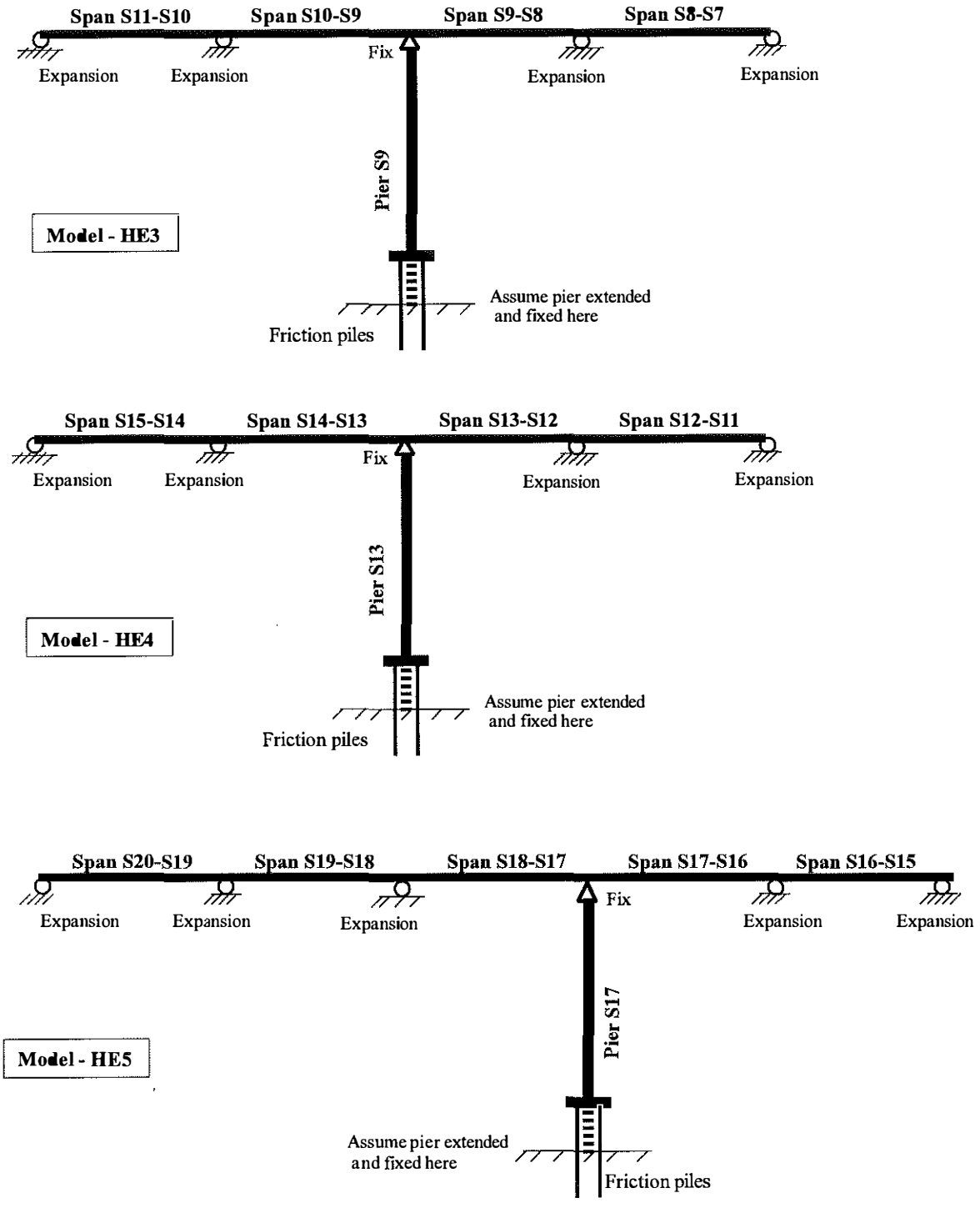

Figure 6.5 (Cont'd) Single Degree of Freedom System Models for Henderson, KY Approach

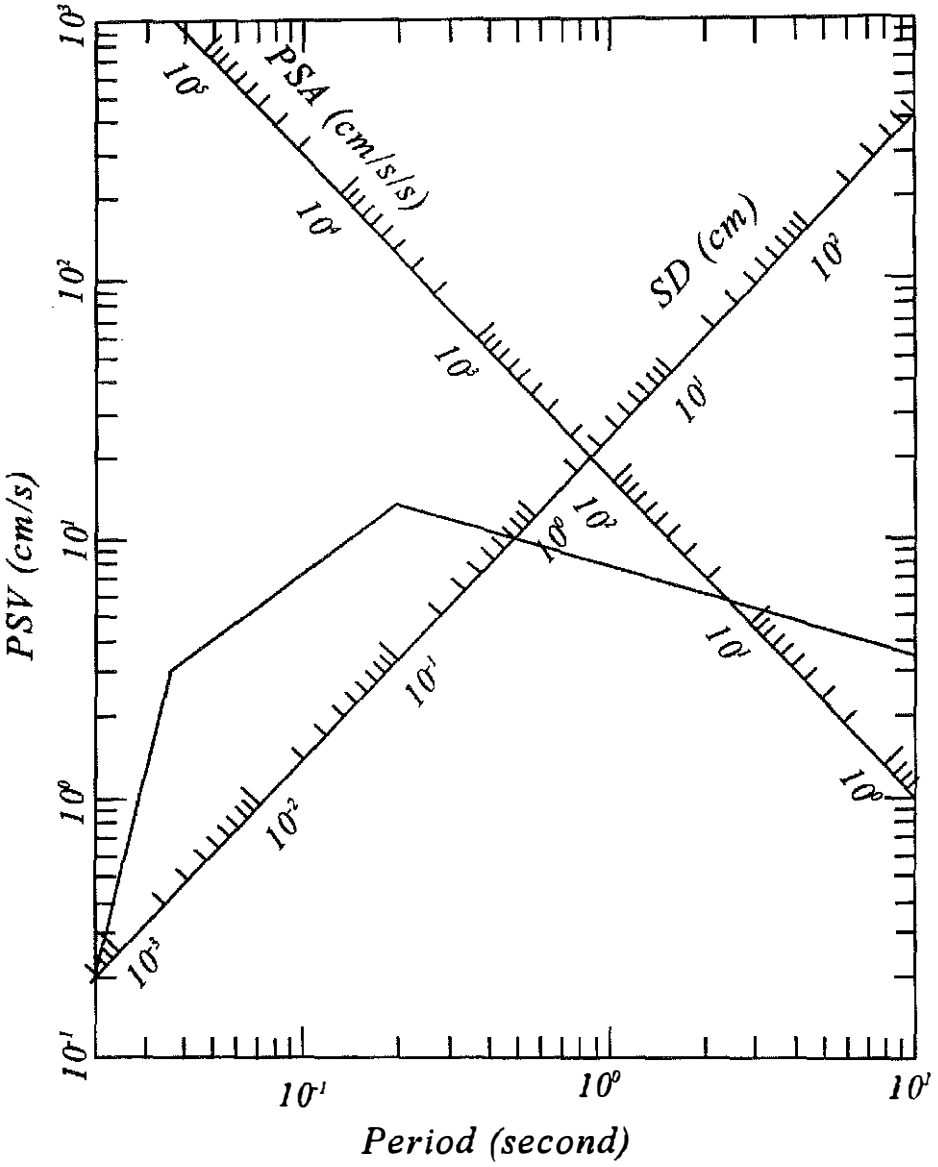

Figure 6.6 Response Spectra for the 50-year Event for Henderson, KY (0.15g-2 from Fig. 5.1); Damping = 5%

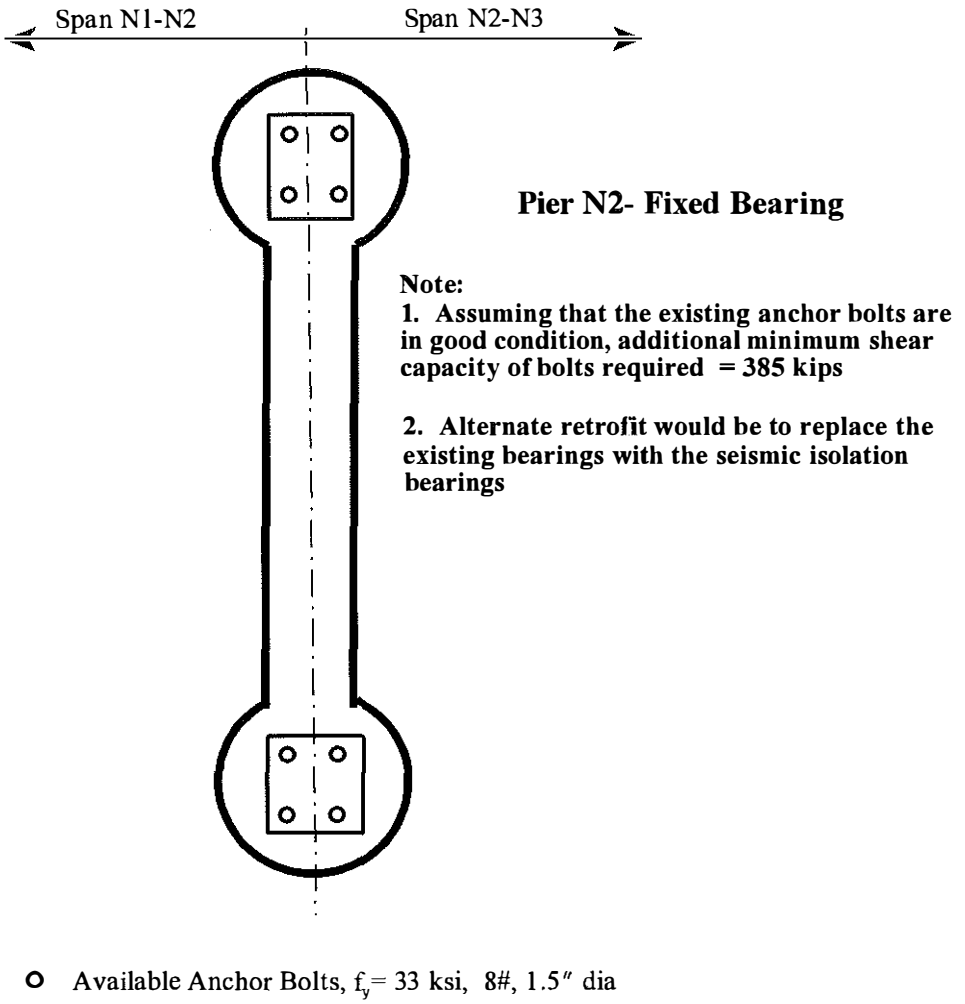

Figure 6.7 Minimum Required Shear Capacity (V_{req}) to be Provided by Additional Anchor Bolts at Bearings of the Pier N2 on the Evansville, IN Approach on the US41 Southbound Bridge

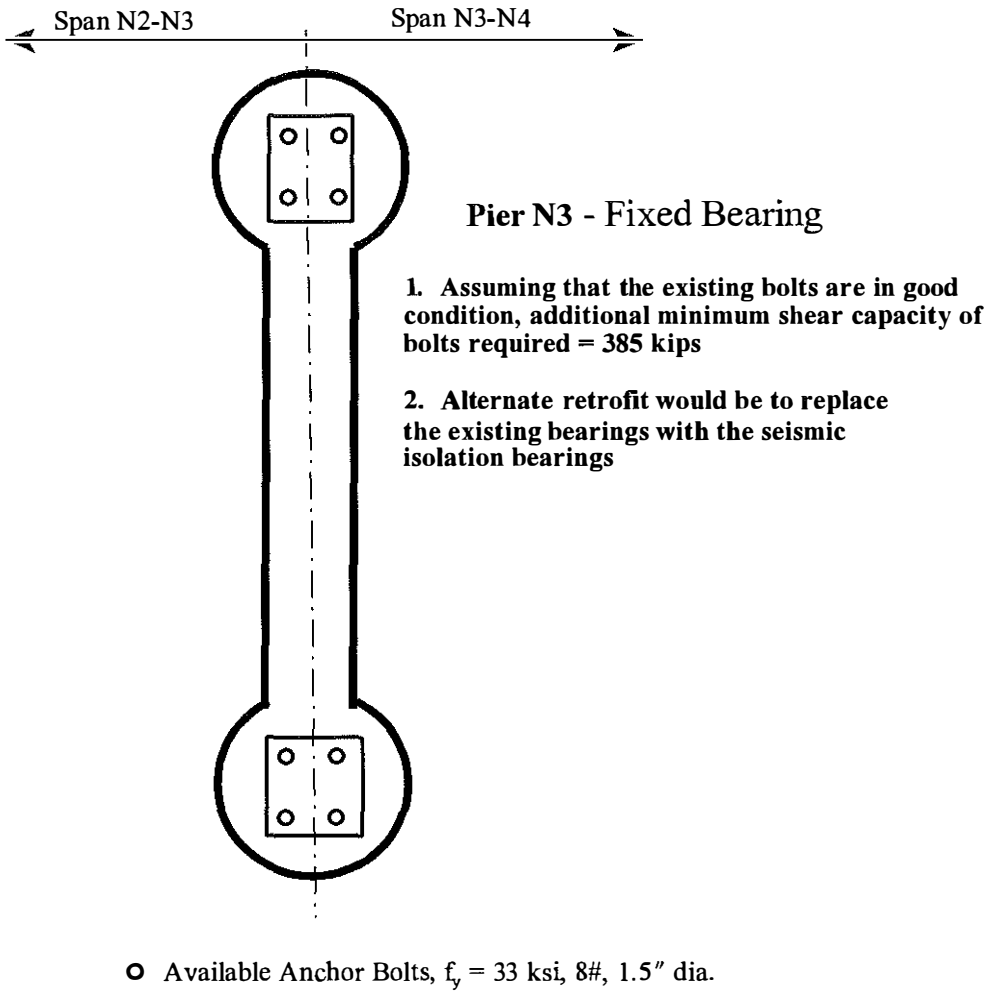

Figure 6.8 Minimum Required Shear Capacity (V_{req}) to be Provided by Additional Anchor Bolts at Bearings of the Pier N3 on the Evansville, IN Approach on the US41 Southbound Bridge

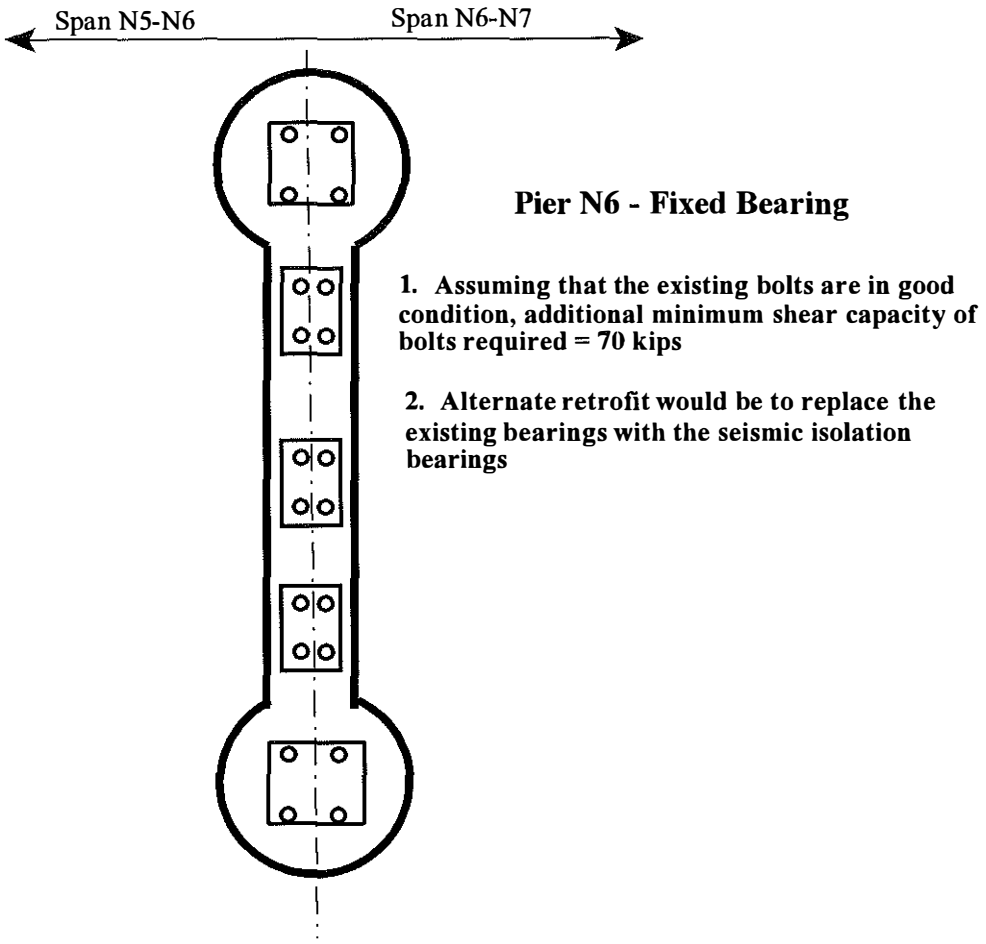

Figure 6.9 Minimum Required Shear Capacity (V_{req}) to be Provided by Additional Anchor Bolts at Bearings of the Pier N6 on the Evansville, IN Approach on the US41 Southbound Bridge

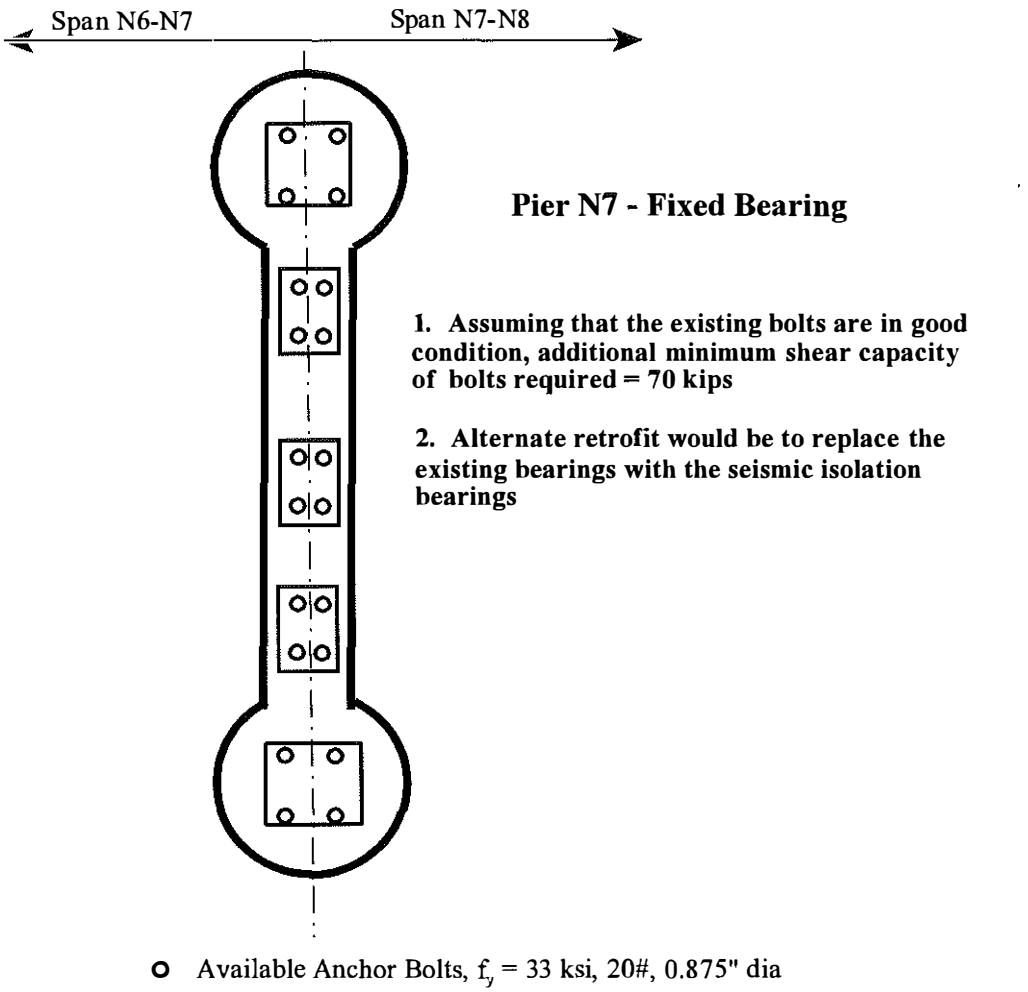

Figure 6.10 Minimum Required Shear Capacity (V_{req}) to be Provided by Additional Anchor Bolts at Bearings of the Pier N7 on the Evansville, IN Approach on the US41 Southbound Bridge

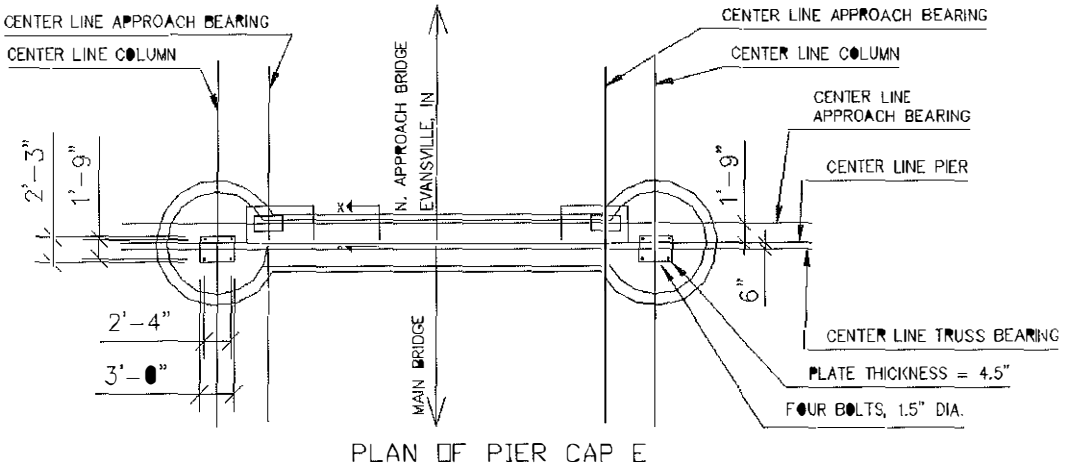

PLAN OF PIER CAP E

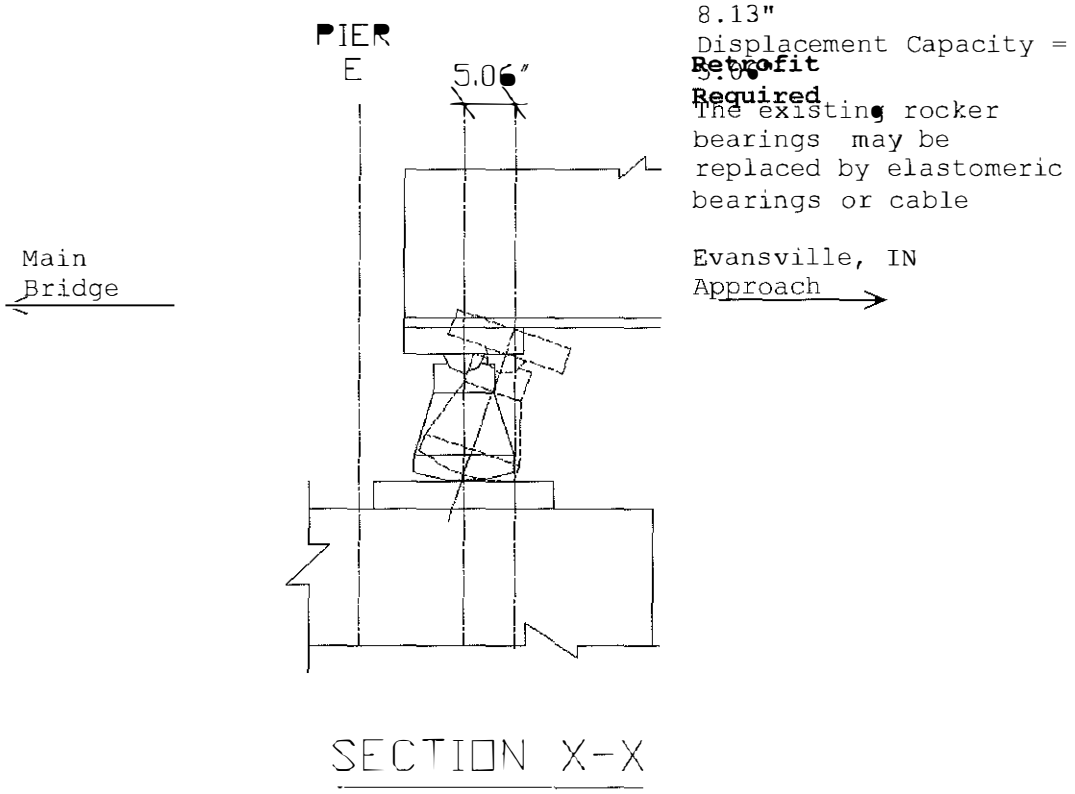

SECTION X-X

Figure 6-11 Proposed Retrofit Measure for the Expansion Bearings at Pier E on the Evansville, IN Approach, US 41 Southbound Bridge

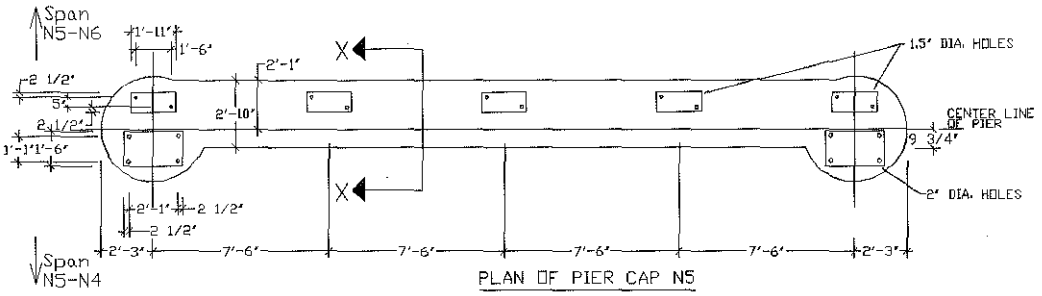

Displacement Demand = 8.13"
Displacement Capacity = 5.06"

Retrofit Required

The existing rocker bearings may be replaced with elastomeric bearings or cable restrainers may be

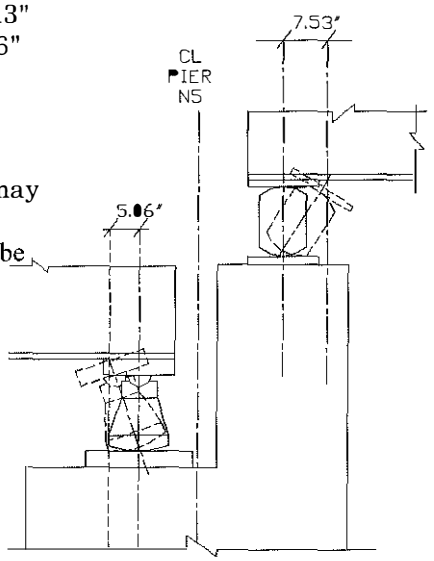

Displacement Demand = 6.02"
Displacement Capacity = 7.53"

No Retrofit Required

SECTION X-X

Figure 6-12 Proposed Retrofit Measure for the Expansion Bearings at Pier N5 on the Evansville, IN Approach, US 41 Southbound Bridge

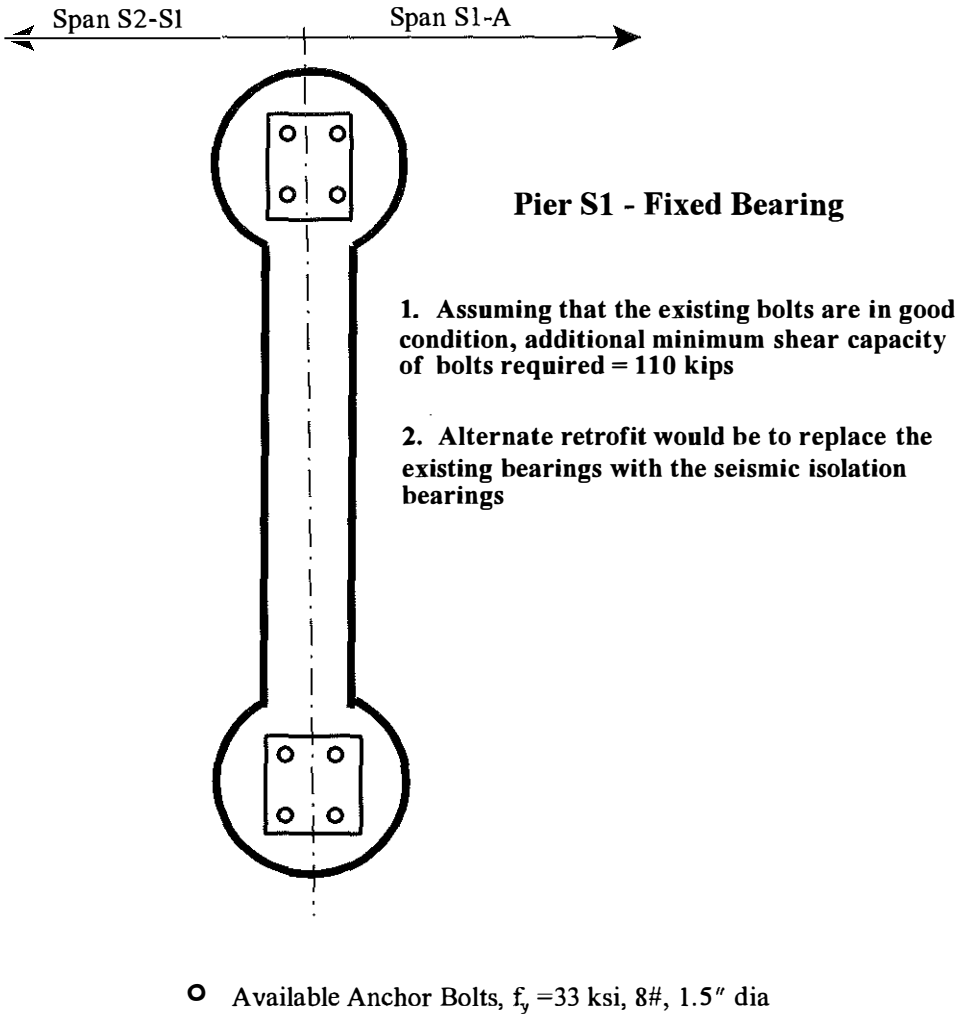

Figure 6.13 Minimum Required Shear Capacity (V_{req}) to be Provided by Additional Anchor Bolts at Bearings of the Pier S1 on the Henderson, KY Approach on the US41 Southbound Bridge

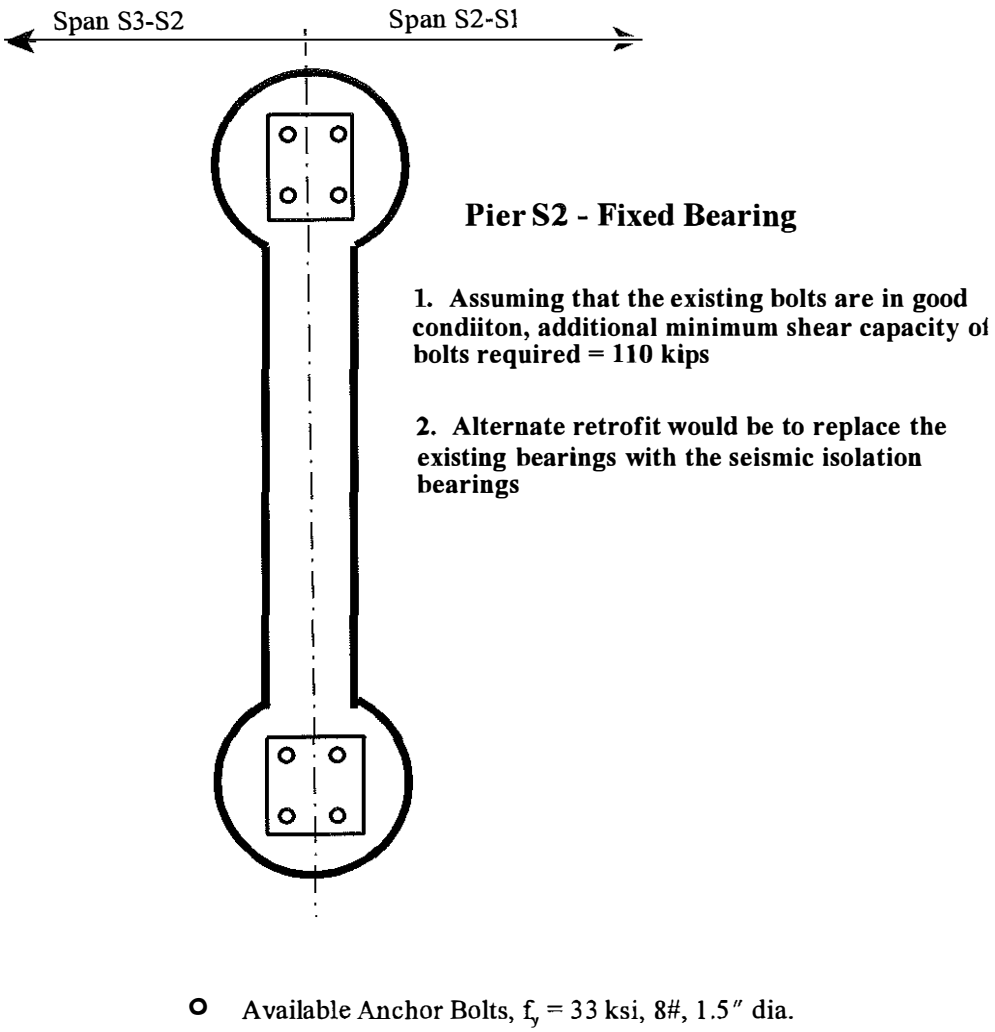

Figure 6.14 Minimum Required Shear Capacity (V_{req}) to be Provided by Additional Anchor Bolts at Bearings of the Pier S2 on the Henderson, KY Approach on the US41 Southbound Bridge

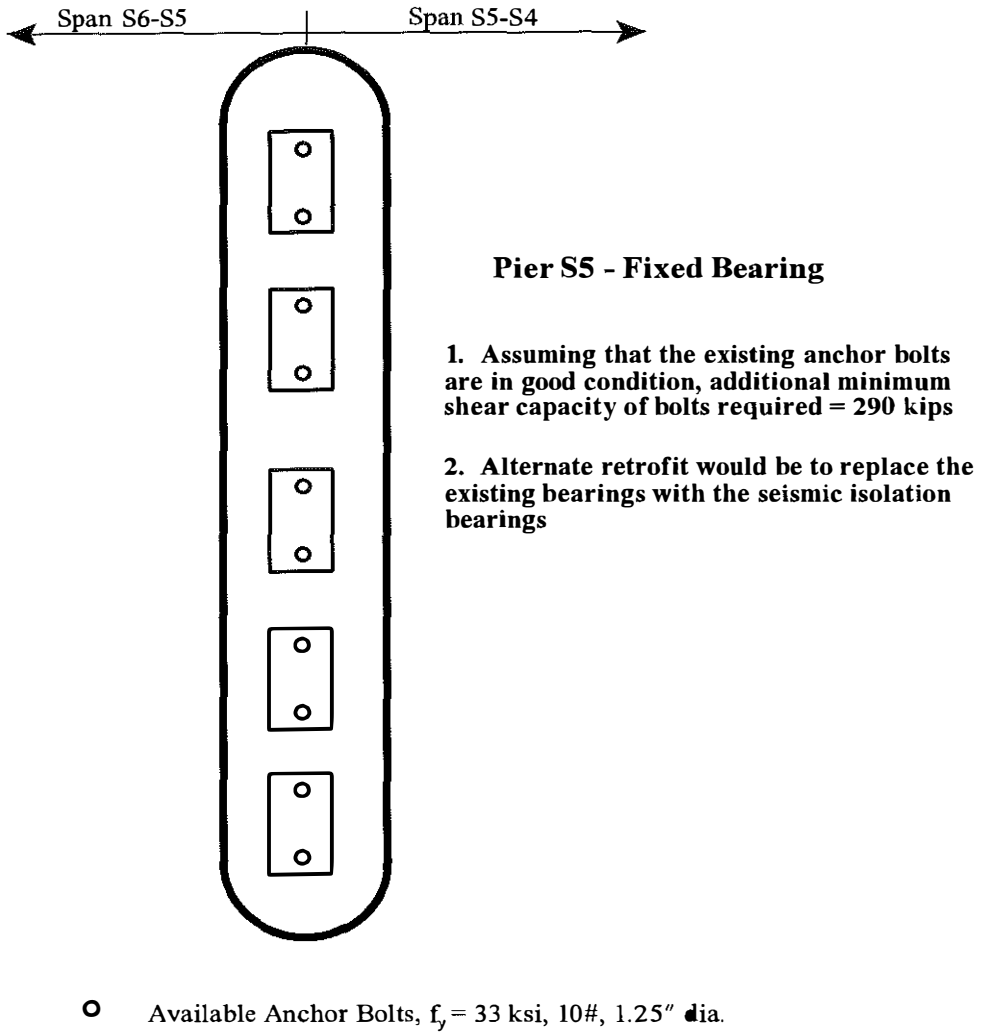

Figure 6.15 Minimum Required Shear Capacity (V_{req}) to be Provided by Additional Anchor Bolts at Bearings of the Pier S5 on the Henderson, KY Approach on the US41 Southbound Bridge

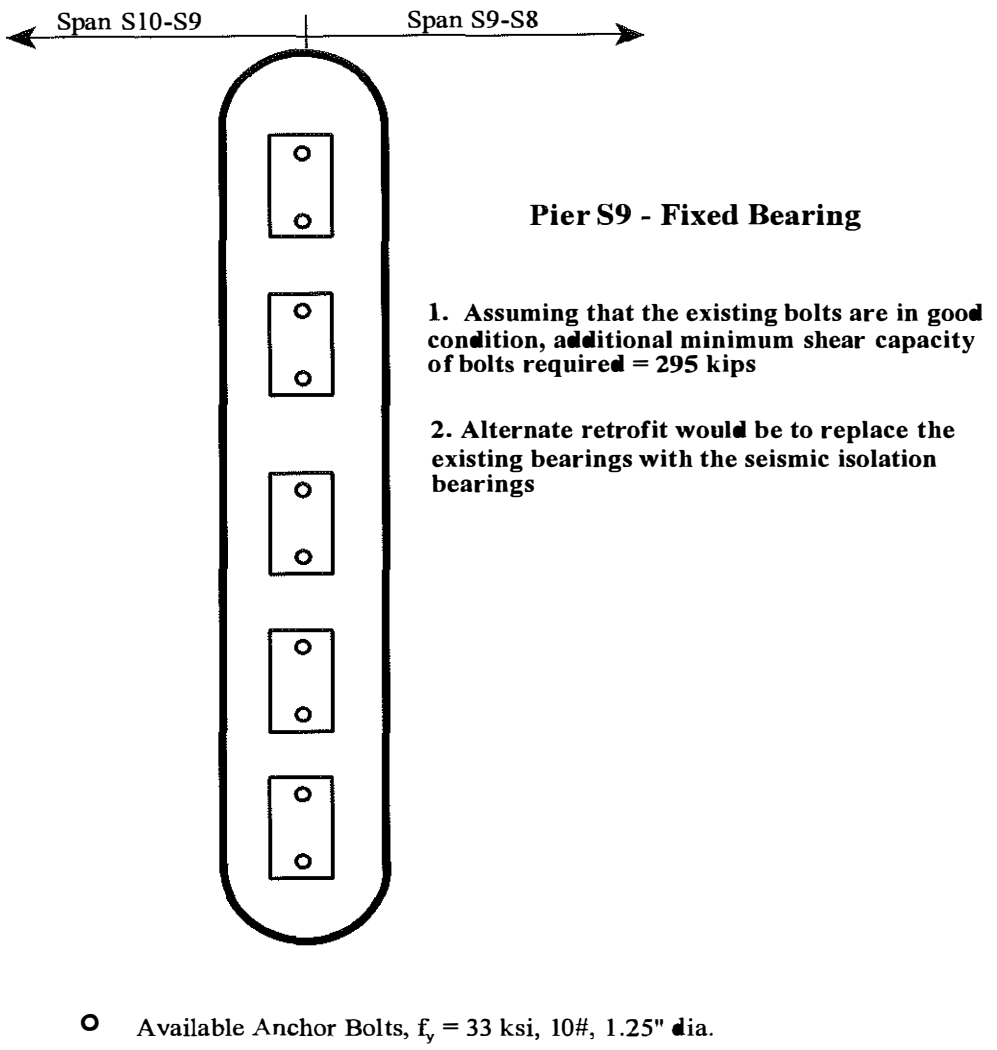

Figure 6.16 Minimum Required Shear Capacity (V_{req}) to be Provided by Additional Anchor Bolts at Bearings of the Pier S9 on the Henderson, KY Approach on the US41 Southbound Bridge

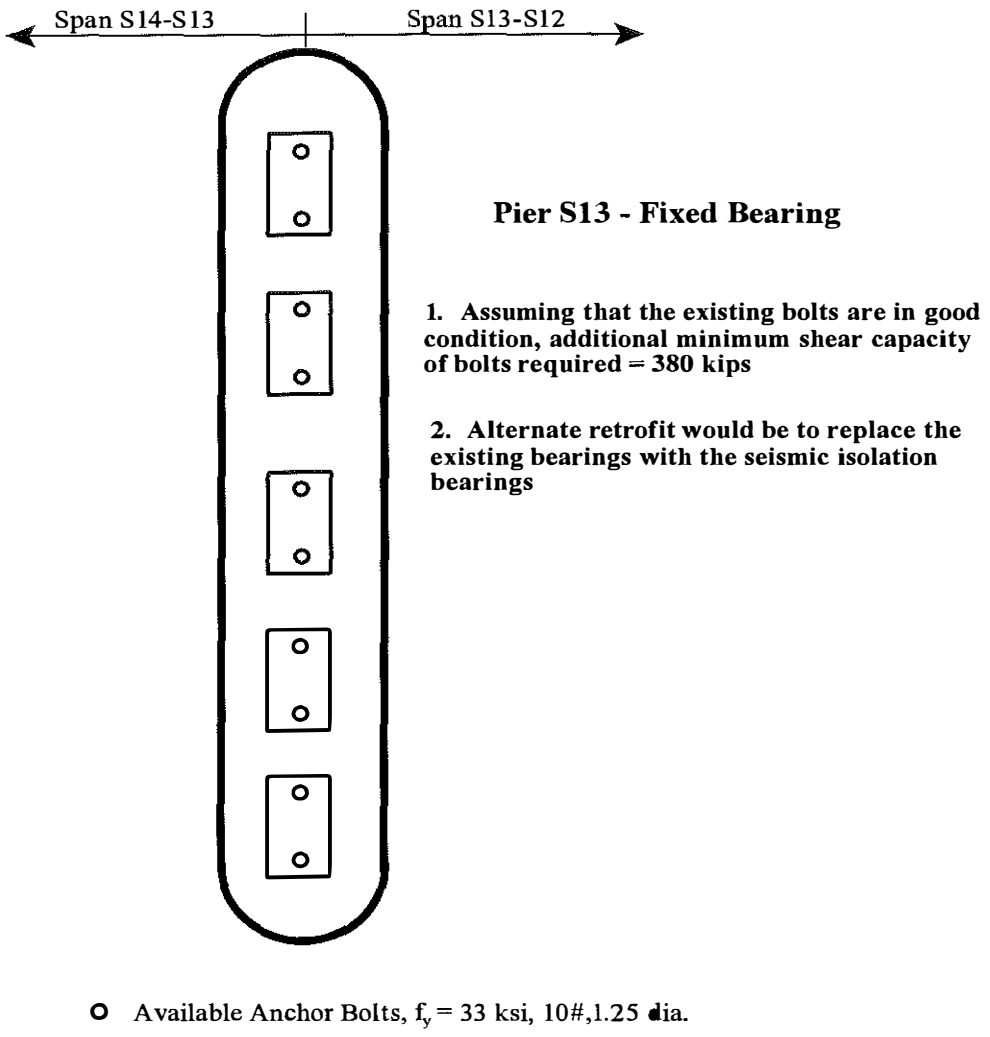

Figure 6.17 Minimum Required Shear Capacity (V_{req}) to be Provided by Additional Anchor Bolts at Bearings of the Pier S13 on the Henderson, KY Approach on the US41 Southbound Bridge

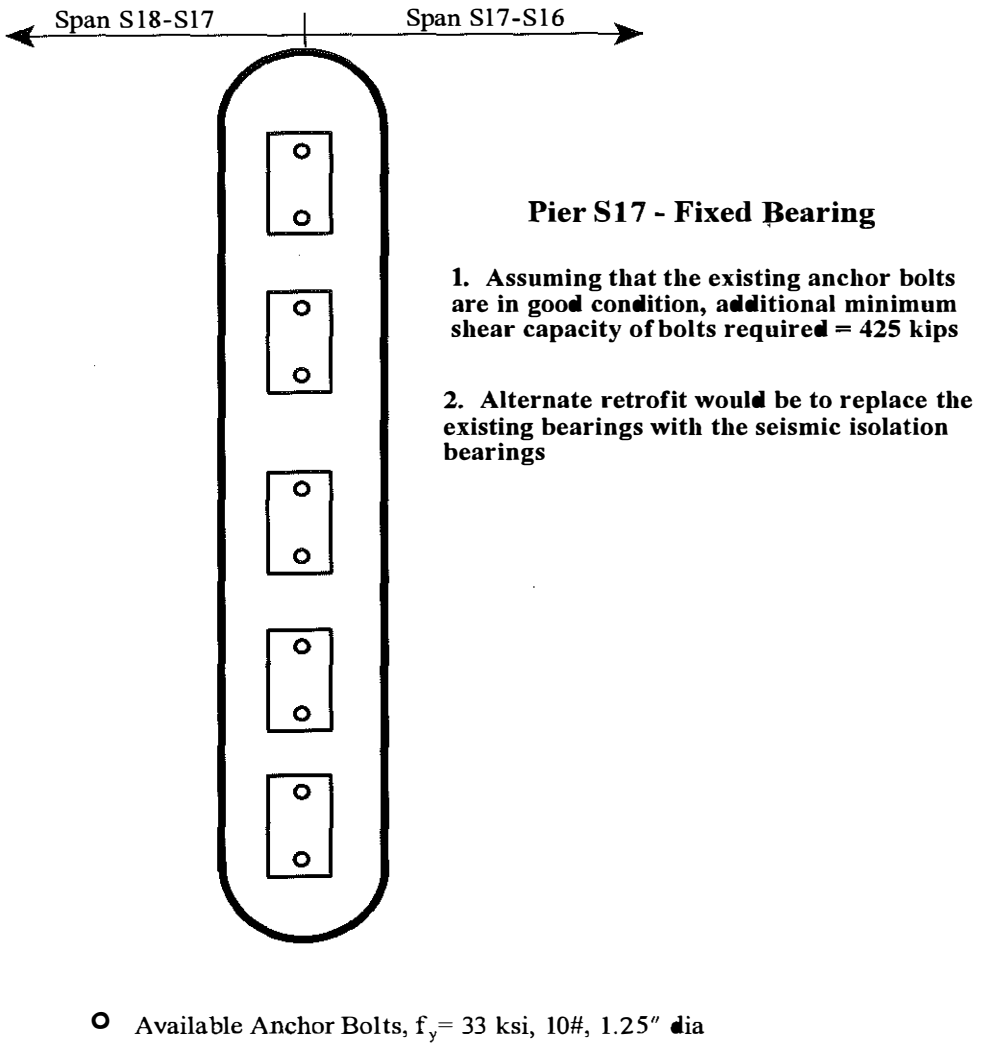

Figure 6.18 Minimum Required Shear Capacity (V_{req}) to be Provided by Additional Anchor Bolts at Bearings of the Pier S17 on the Henderson, KY Approach on the US41 Southbound Bridge

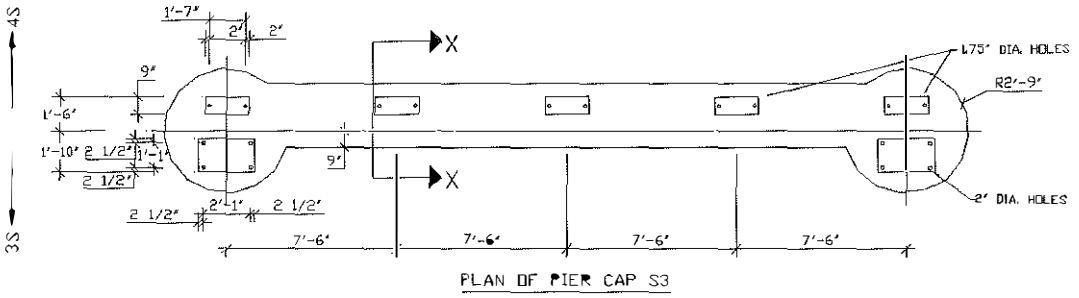

PLAN OF PIER CAP S3

Displacement Capacity = 8.50"
Displacement Demand = 6.41"

Retrofit Not Required

Displacement Capacity = 5.00"
Displacement Demand = 6.17"

Retrofit Required

The existing rocker bearings may be replaced with elastomeric bearings, or cable restrainers may be provided

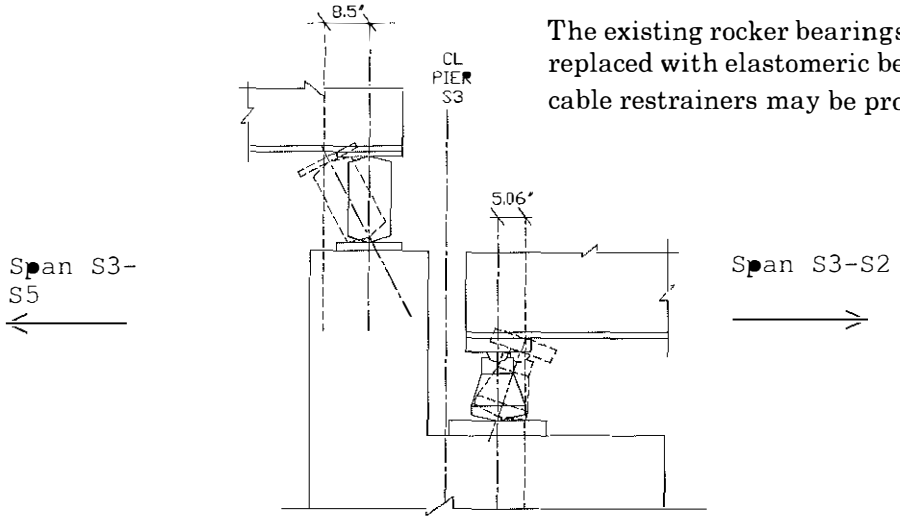

SECTION X-X

Figure 6-19 Proposed Retrofit Measure for the Pier S3 on the Evansville, IN Approach, US 41 Southbound Bridge